MATERIALS SCIENCES CORPORATION

MSC/TFR/804/1114

DEFINITION AND MODELING OF CRITICAL FLAWS
IN GRAPHITE FIBER REINFORCED EPOXY RESIN MATRIX
COMPOSITE MATERIALS

Prepared for:

Naval Air Development Center
Warminster, PA 18974

January 1978

Approved by:

B. Walter Rosen, President

REPORT DOCUMENTATION PAGE		READ INSTRUCTIONS BEFORE COMPLETING FORM
1. REPORT NUMBER NADC-76228-30	2. GOVT ACCESSION NO.	3. RECIPIENT'S CATALOG NUMBER
4. TITLE (and Subtitle) Definition and Modeling of Critical Flaws in Graphite Fiber Reinforced Epoxy Resin Matrix Composite Materials		5. TYPE OF REPORT & PERIOD COVERED Final – Dec. 28, 1976 to Dec. 28, 1977
		6. PERFORMING ORG. REPORT NUMBER MSC/TFR/804/1114
7. AUTHOR(s) R. L. Ramkumar, S. V. Kulkarni and R. B. Pipes		8. CONTRACT OR GRANT NUMBER(s) N62269-77-C-0092
9. PERFORMING ORGANIZATION NAME AND ADDRESS Materials Sciences Corporation Blue Bell Office Campus Blue Bell, PA 19422		10. PROGRAM ELEMENT, PROJECT, TASK AREA & WORK UNIT NUMBERS
11. CONTROLLING OFFICE NAME AND ADDRESS Naval Air Development Center Warminster, PA 18974		12. REPORT DATE January 1978
		13. NUMBER OF PAGES 138
14. MONITORING AGENCY NAME & ADDRESS(if different from Controlling Office)		15. SECURITY CLASS. (of this report) Unclassified
		15a. DECLASSIFICATION/DOWNGRADING SCHEDULE

16. DISTRIBUTION STATEMENT (of this Report)

Approved for Public Release; Distribution is Unlimited.

17. DISTRIBUTION STATEMENT (of the abstract entered in Block 20, if different from Report)

18. SUPPLEMENTARY NOTES

19. KEY WORDS (Continue on reverse side if necessary and identify by block number)

Composite Materials, Nondestructive Testing, Graphite Epoxy, Defect Characterization

20. ABSTRACT (Continue on reverse side if necessary and identify by block number)

A logic for an NDE methodology to quantitatively evaluate the integrity of structural elements is explored. The methodology is based on a simplified analysis to predict flaw criticality and growth, an experimental program to support and verify the analysis, and an NDE technique to use NDI measurements in liaison with the analysis to determine flaw criticality.

DD FORM 1473 1 JAN 73   EDITION OF 1 NOV 65 IS OBSOLETE

Typical flaws are identified and static analyses developed or
presented to predict their growth. A ¶wearout¶ fatigue concept
is incorporated into the static/fatigue model and the concept
of an instability boundary established for every flaw size and
location. An experimental program is outlined to support the
analysis and to measure the specific adhesive surface fracture
energy quantitatively. Acoustic monitoring of the specimens
to detect damage growth and a corresponding vibration analysis
are carried out as a potential NDT and for correlation studies.
Ultrasonic "C" scans are used to ensure quality control and to
determine approximate damage growth rates. The analytical and
experimental results are incorporated into an NDE technique to
quantitatively determine a measure of the residual lifetime and
strength of the structural component. A comparison of these
with a quantified criterion for damage tolerance would estab-
lish flaw criticality through the need, or lack of it, for
mandatory repair.

SUMMARY

A logic for an NDE methodology to quantitatively evaluate the integrity of structural elements is explored. The methodology is based on a simplified analysis to predict flaw criticality and growth, an experimental program to support and verify the analysis, and an NDE technique to use NDI measurements in liaison with the analysis to determine flaw criticality. Typical flaws are identified and static analyses developed or presented to predict their growth. A "wearout" fatigue concept is incorporated into the static/fatigue model and the concept of an instability boundary established for every flaw size and location. An experimental program is outlined to support the analysis and to measure the specific adhesive surface fracture energy quantitatively. Acoustic monitoring of the specimens to detect damage growth and a corresponding vibration analysis are carried out as a potential NDT and for correlation studies. Ultrasonic "C" scans are used to ensure quality control and to determine approximate damage growth rates. The analytical and experimental results are incorporated into an NDE technique to quantitatively determine a measure of the residual lifetime and strength of the structural component. A comparison of these with a quantified criterion for damage tolerance would establish flaw criticality through the need, or lack of it, for mandatory repair.

ACKNOWLEDGMENTS

TABLE OF CONTENTS

TABLE OF CONTENTS (contd.)

LIST OF TABLES

LIST OF TABLES (contd.)

LIST OF FIGURES

LIST OF FIGURES (contd.)

LIST OF FIGURES (contd.)

LIST OF FIGURES (contd.)

INTRODUCTION

In evaluating the integrity of metallic structural elements, nondestructive inspection has focused upon detection of both surface and subsurface flaws and determination of an effective flaw size. Given the flaw size, classical fracture mechanics technology has been employed to predict its rate of growth and the critical length which corresponds to failure of the element. Inherent in this approach is the assumption that microscopic flaws and imperfections grow into macroscopic cracks when the structural element containing the flaw is subjected to a fatigue loading and/or an adverse environment. In addition, the macroscopic isotropy of metallic materials meant that generally initial cracks propagated due to crack-tip tensile stresses normal to the crack plane. For contemporary metallic materials and structures, technology sufficient to detect and assess the criticality of flaws upon component life has been developed. Of course, there continues to be a need to refine nondestructive evaluation techniques and crack growth models.

Fiber-reinforced composite materials are more complex at the macroscopic level than the contemporary, metallic materials. These materials therefore present new problems and challenges, both in flaw detection and in assessing the influence of flaw characteristics upon strength. Also, determination of the influence of a given flaw geometry upon strength and stiffness is considerably more complex than the classical fracture mechanics approach due to the anisotropy of the fiber-reinforced composite materials.

There has been a recent interest in the quantitative evaluation of the damage tolerance of composite structures. Given a composite structural element, it is desired to relate, quantitatively, the existent in situ flaw size and the residual lifetime and the residual strength of the structural element. This will enable definition of regular inspection intervals for the structural element during its service to determine the criticality of the existent flaws.

Various techniques have been used to assure the suitability of a structure for its intended function. Proof-testing to a load level in excess of any expected service load is a possible approach. However, although proof-testing verifies the initial load-bearing capacity of the structural element, it cannot be used to predict the growth of existent flaws with fatigue loading and the effect of this growth on the residual strength and lifetime of the element. Spectrum fatigue loading is an alternate approach which would provide the required lifetime data, but in many cases is prohibitive cost-wise.

The above drawbacks in the conventional experimental procedure indicate the potential advantages of a new methodology which combines analysis with a limited number of experiments to duplicate the response of a flawed structural element to fatigue loading. It is desired to have a procedure which does not require extensive additional testing whenever a new laminate layup is used. The procedure utilized herein is based on the use of nondestructive inspection (NDI) methodology to detect and measure critical flaws. This is supplemented by an analysis to predict the effect of this flaw size on the structural response under given loading conditions. This report describes the analytical and experimental studies to develop such a procedure and to provide data for correlation purposes.

Many types of flaws can exist in a composite structural element. In order to develop the required methodology, a through-the-thickness notch and an interlaminar disbond were chosen as two typical flaws whose effect on the residual strength and the residual lifetime of the structural element was to be studied. For each of these flaws, the following tasks were carried out:

1. Exploring NDI techniques to detect and measure possible strength and service life limiting flaws in graphite fiber reinforced epoxy composites.

-2-

2. Developing an analysis in combination with the supplemental experimental data to quantify the severity of the flaw.

3. Conducting representative fatigue tests and monitoring the growth of the flaw using NDI techniques.

4. Incorporating this into an NDE methodology to predict quantitatively the residual lifetime and the residual strength of the structural element.

5. Carrying out an experiment/analysis correlation study to verify the predictions made by the NDE methodology.

SCOPE OF THE PROBLEM

Defects in fiber-reinforced composite laminated structural components originate during fabrication and during service. Fabrication or "birth defects" may occur during the preparation of the prepreg (improper yarn spacing, broken filaments), laminate layup and cure (matrix voids, resin-rich regions, interlaminar damage), and structural component assembly (improper drilling, machining, potential flaw growth regions such as bolted joints, etc.). Service damage will occur due to a fatigue load spectrum (which is random in nature), impact or FOD (Foreign Object Damage), and environment (UV, moisture, corrosion, lightning, etc.). The various types of flaws that may originate and propagate during the service life of a composite structural component are listed in table 1. These result in a large number of potential failure modes.

The initiation and growth of flaws is dependent upon the imposed loads and the laminate construction. The various types of loads that affect flaw initiation and growth may be categorized as: inplane loads (tensile, compressive, shear, and biaxial); transverse loads; and thermal loads. For all of these loads, it is necessary to consider their stochastic nature. Also, it is necessary to consider environmental effects. The laminate characteristics that influence the flaw growth are the material properties of the individual laminae (dependent on the fiber orientation), the stacking sequence of the layers, the geometry of the laminate, and the location, size, and shape of the flaw.

A knowledge of the various types of flaws that may initiate and grow in a composite structural element and the factors that influence these flaws identifies a problem of enormous complexity. The objective of the present program is to choose representative flaws that are considered critical to composite structures and to develop a methodology by which the damage tolerance of the flawed structure can

-4-

be quantified. The damage tolerance of a flawed composite structural element will be quantified here in terms of the residual strength and the residual modulus of the element when subjected to known service conditions. The objective is met by combining an analysis of the flawed composite structure with an experimental program that supplements the analysis. The undesirable alternative of an extensive experimental program utilizing spectrum fatigue loading would make the cost prohibitive.

In order to arrive at a definition of a critical flaw, it is necessary to formulate analytical and/or semi-empirical models which are capable of predicting the direction and rate of growth and the critical size (at failure) of the different types of flaws such as surface flaws, slit notches through the thickness, and delaminations. Due to the complexity of the problem of failure in composite laminates, it is impossible for a single analytical model to encompass the whole spectrum of fracture and fatigue. A logical initial step is, therefore, to begin with simpler flaw geometries such as a through-the-thickness slit notch and an interlaminar disbond. Based on the analytical and experimental correlation studies and the NDE tests for these flaws, confidence can be developed for similar studies for other flaws.

The slit notch study was chosen because the corresponding analysis to predict the failure modes and loads in a notched laminate due to known service loading conditions was already available at the beginning of the program. The analysis for a composite structure with a delamination at arbitrary locations was developed under the present program and the proposed NDE methodology was demonstrated for this defect in a qualitative manner.

The problem of "critical flaw evaluation" can be summarized as:

(i) Determining <u>what</u> (type of flaw), <u>where</u> (location of the flaw), <u>when</u> (inspection interval), and <u>how</u> (type of NDI technique) to look for flaws.

(ii) Formulating mathematical models, for known loading conditions, to predict in situ critical flaw sizes, modes of failure, residual lifetime, and residual strength for the chosen types of flaw. This is done with the help of supplemental experimental data.

(iii) Using NDI techniques to measure the actual growth of the flaw under service conditions.

(iv) Incorporating (ii) and (iii) into an NDE methodology to quantify the in situ residual strength and residual lifetime.

(v) Carrying out a correlatior study on the NDE predictions.

(vi) Exploring alternative measurement techniques to improve the methodology.

ANALYTICAL METHODOLOGY

The understanding of the damage tolerance of composite structures is a complex problem. A possible method of approach to this problem is to take the design and analysis methods developed for metals and carry them over directly for composites. If the method works, an advance in the state of the art has been obtained at minimum effort. Thus, for both the fatigue and fracture problem of composites, it is reasonable to start by attempting to utilize the methods of fracture mechanics developed for metals. However, one should be prepared to accept the fact that this translation of art may not always be successful. This is because the fracture and fatigue processes in fiber-reinforced laminates are expected to be functions of some of their unique characteristics. These include heterogeneity, statistical variability, microstructural crack growth, and the three-dimensional nature of the stress field.

Several approaches to the predictions of fracture or crack growth in composite materials may be taken; namely, a classical fracture mechanics (CFM) approach applied at a micromechanical level, a classical fracture mechanics approach applied to an effective material on a macromechanical level, or the quasi-heterogeneous minimechanics approach utilized in the earlier studies performed at Materials Sciences Corporation (e.g. ref. 1).

Classical fracture mechanics applied on a micromechanical level is capable of treating a composite as a heterogeneous medium and appears in concept to be a valid approach. However, the extreme complexity of the required analysis places limitations on its practicality. Classical fracture mechanics applied on a macroscopic scale is useful for certain types of problems. The methodology of CFM may be valid when the crack propagation is self-similar. Thus, the scope of this approach is limited because, in many laminates, planes of weakness, rather than the initial flaw geometry, determine the direction of crack propagation.

A slit notch and an interlaminar delamination in a composite laminate have been identified as two typical flaws of interest. A static failure model for a laminate with a slit notch has already been developed at Materials Sciences Corporation (refs. 1 to 5). The model for a delaminated composite beam was developed under the present program. These two static failure models are discussed below:

STATIC FAILURE MODEL FOR A LAMINATE WITH A SLIT NOTCH

A brief summary of the salient features of the existent static failure model for a notched composite laminate is presented in this section. The behavior of notched laminates exhibits some features which have not been observed in metals. They are:

(i) The direction of crack growth is not always collinear with the initial crack and, for many laminates, it is a function of notch size, environment, and stacking sequence.

(ii) The measured strength reduction resulting from the introduction of a circular hole in a laminate does not correlate with that obtained from the stress concentration factor determined from anisotropic plate theory. Also, the reduction in strength increases with hole radius; that is, stress concentration factor increases with increase in hole size in an infinite plate. This, too, is contrary to the results obtained for a homogeneous anisotropic material.

(iii) In contrast to conventional metals where notch sensitivity increases as the unnotched strength increases, certain fiber composites exhibit increased notch toughness with increasing unnotched strength.

(iv) Some notched laminates show a lack of sensitivity to the size and shape of notches.

(v)   The residual static strength of some notched
      laminates subjected to fatigue loading is equal
      to or greater than their static strength. This
      is again in contrast to the high-strength metal
      alloys wherein a fatigue loading increases the
      growth of cracks, leading to unstable fracture.

The basic static failure model for axial and transverse
failure of notched composites was developed in references 1, 2,
3, and 4. The model for the static failure of a notched com-
posite laminate (ref. 1) is illustrated in figure 1. The
laminate is assumed to be under a tensile stress in the x
direction. A notch of width "a" is centered in the specimen
at x = 0. The central core region tends to "pull out" from
the notch area due to the applied tensile loading. The "pull
out," however, is restrained by shear stresses between the
core region and the adjacent intact material. These shear
stresses generally result in a region of high shear strain
parallel to the loading direction. Immediately adjacent to
the notch core, an overstressed region of average stress con-
centration of width "a_0" is assumed to exist. Everywhere out-
side the core and overstressed regions, the laminate is uni-
formly strained. Shear strain due to core pullout is assumed
to extend in the "y" direction over a region three times the
size of the overstressed fiber region "a_0". This assumption
is based on the premise that steep shear stress gradients in
the core and the average material adjacent to the overstressed
region would exist over a characteristic dimension equal to
"a_0". The laminate axial shear stress - shear strain curve is
assumed to be linear elastic - perfectly plastic.

The static failure analysis has the capability of com-
puting the axial inelastic length, the axial crack length,
and the maximum overstress in the material adjacent to the
notch for a given applied laminate tensile stress. It also
monitors the transverse crack propagation mode. The analysis
can also predict off-axis cracking in an approximate fashion

(see ref. 4). In addition to axial, transverse, and off-axis cracking, interlaminar delamination may also originate around the notch precipitating laminate failure. Modifications to the failure model to include interlaminar effects were incorporated in reference 5. The modified analysis can predict axial damage at the lamina level.

Given the laminate mechanical properties and failure stresses and strains, the unknown parameter in the analysis is "a_0" which defines the extent of the average stress concentration region. Other investigators have also recognized the need to define the dimension of this region. Examples are the "intense energy region" (ref. 6) and the distances associated with the "point stress" and "average stress" criteria (ref. 7). Accurate determination of "a_0" is an important aspect of the predictive capability of the static fatigue failure model. An empirical form (based on existing experimental data) for predicting "a_0" as a function of the notch size and laminate construction has been postulated (ref. 8). The extent of the transverse damage region "a_0" is postulated, based on some physical considerations, while the lamina axial damage regions are determined from the analysis (ref. 5).

The existent static failure analysis for notched composite laminates, described above, will be used to predict the failure modes and strengths of the notched laminates tested experimentally under this program.

STATIC FAILURE MODEL FOR A LAMINATED BEAM WITH AN INTER-LAMINAR DELAMINATION

Classical fracture mechanics is employed to develop a static failure model for a tip-loaded debonded cantilever beam. The methodology deployed herein has been used by others in solving similar problems (refs. 9 to 15). A few assumptions are made to reduce the problem to a tractable form and to gain an initial knowledge of the behavior of delaminated beams. The most important among these is the

assumption that the debond propagates along the interface
in a collinear (mode II) fashion. This assumption is justi-
fied by testing a tip-loaded cantilever beam with an implanted
delamination.

The static failure model analyzes the debonded beam as
four separate beam elements joined together at the crack tips
with the proper boundary and matching conditions (fig. 2).
Each beam element is treated as a Timoshenko beam to incor-
porate shear deformation effects. The corresponding equa-
tions, boundary conditions, and the displacement solutions
for the four elements are presented in Appendix A. The total
strain energy in the tip-loaded, cantilevered, debonded beam
is obtained using Clapeyron's theorem. The strain energy is
dependent on the location and the length of the delamination,
the magnitude of the applied load, and the material and
geometric properties of the laminated beam (Appendix A).

The criticality of the delamination is determined through
Griffith's energy balance criterion (ref. 16). This classical
fracture mechanics approach states that the loss in the total
strain energy due to an incremental change in the crack
length is equal to the surface fracture energy that is neces-
sary to create the corresponding surface area. Inherent in
the application of this criterion is the knowledge of the
measure of γ_a, the specific adhesive surface fracture energy
required to create unit surface area through the propagation
of the delamination. The change in strain energy is computed
by evaluating the energy for two different crack lengths
using the above model.

The application of Griffith's energy balance criterion
leads to a closed-form solution for $P_{cr}/\sqrt{\gamma_a}$ as a function of
the beam properties (Appendix A). The solutions for two loca-
tions of the debond in a beam having the laminate configura-
tion used in the tests are presented in figure 3. P_{cr} is the
magnitude of the tip load at which propagation of the delamina-
tion of size a/L is imminent. An experimental data point,

-11-

used with this solution, will suffice to estimate the magnitude of γ_a.

It is shown in Appendix A that the critical value of the tip load is a function of the location and length of delamination, the material and geometric properties of the beam, and the specific adhesive surface fracture energy for the given adherend-adhesive combination. The propagation of the delamination, along the interface, may take place in any of the following directions depending on the material and geometric data:

(i)   propagation of the delamination into element 1;

(ii)   propagation of the delamination into element 2;

(iii)   propagation of the delamination into elements
        1 and 2 simultaneously.

The critical load for each case is obtained and the direction in which the delamination propagates is governed by the least of the three P_{cr} values.

Finite Element Analysis of a Delaminated Beam

The design of beam specimens to study the growth of delaminations under transverse shear conditions introduces a few problems that cannot be handled by beam theory. One is the shear stress concentration directly under the load and the resultant change in the shear stress distribution from that predicted by Euler Bernoulli beam theory (fig. 4). This localized stress redistribution would lead to a lower shear stress at the crack tip if the debond is located at the midplane or in the lower half of the beam. Consequently, a larger load would have to be applied to exceed the shear strength of the debonded beam and make the delamination propagate. This could cause premature failure in the flexural mode in specimens designed to measure criticality of delaminations.

Static tests on $[0_4/\pm45_2]_{2s}$ beam specimens were conducted under this program to measure the static failure loads,

-12-

with and without interlaminar delaminations, and to obtain
a quantitative measure of the specific adhesive surface frac-
ture energy. The results are listed in table 2. It can be
seen that the debond propagated (in an unstable manner) only
in one of the tests. All the other specimens failed in
flexure, perhaps due to the effect shown in figure 4. This
prompted the use of a finite element analysis to design a
delaminated beam such that debond propagation precedes flex-
ural failure. The ANSYS code was used for this purpose.

A plane strain finite element analysis of a debonded
beam was carried out to ensure that the specimen's shear
strength is exceeded at a load level where the flexural
strength is not. The delaminated beam was modeled as shown
in figure 5 and 6. Input and output characteristics for
the constant strain elements are shown in figures 7 and 8.
The material properties of the elements in the different
layers are shown in table 3. The thickness of the beam was
scaled up by a factor of four to avoid numerical problems
due to small element aspect ratios.

Figure 9 shows the transverse shear stress variation
along the interface (midplane) containing a debond. Figure
10 shows the shear stress variation, through the thickness,
at the crack tips. For the debonded beam model in figure 5,
it is assumed that the maximum bending stress (200 ksi to
break the fibers in the 0° layer at the top) is twenty times
larger than the magnitude of the shearing stress that causes
delamination (about 10 ksi). Beam theory and results from
figures 9 and 10 show that the tip load that causes delamina-
tion is about one-fifth of the value that causes bending
failure. Hence delamination precedes, and possibly precludes,
bending failure. It is seen from both the figures that the
shear stress at the crack tip nearer the applied load and
farther from the support ($x = \ell_1 + a$) is a maximum. The
debond should, therefore, tend to propagate toward the free
end of the tip-loaded, cantilevered beam. A second set of
experiments were conducted on $[(0_4/\pm 45_2/\mp 45_2/0_4)_s]_s$ beam

-13-

specimens with a reduced test section length in order to
guarantee propagation of the debond at load levels well
below laminate flexural strength.

FATIGUE ANALYSIS

The most direct way to determine laminate tensile and
shear behavior under cyclic loads is to perform fatigue
tests on unnotched specimens. This method, though straight-
forward, would require a large number of tests for each
laminate and the results would be applicable only for the
specific laminate that was tested. Each new laminate would
require additional tests. Therefore, a method of generating
laminate fatigue behavior from lamina fatigue properties is
used.

General Philosophy

On fatigue loading of a notched or debonded laminate,
high axial and shear stresses near the crack tip cause the
material in the vicinity of the crack to be degraded much
more rapidly than the rest of the laminate. This spatial
variation of the property degradation in the laminate is a
result of the different stress states in the individual
laminae, and the large stress concentration at the crack tips
in the neighboring laminae. An analytical prediction of
the three-dimensional stress state in a flawed laminate is
a formidable task, and thus a simplified numerical solution
is used as the alternative.

The parameters that influence the three-dimensional
stress state in a flawed laminate, and hence, the property
degradations, are: the number of cycles of loading, N;
the ratio, S, of the maximum fatigue load to the static
failure load of the virgin (unnotched and without delamina-
tions) laminated beam; the stress ratio, R, that is the ratio
of the minimum to the maximum fatigue load; the frequency of
cyclic loading, ω; and the ratio, η, of the static failure
load of a flawed beam of known flaw size to the static
-14-

failure load of the virgin, unflawed laminated beam. For a debonded beam, η is a function of the initial debond size, a/L, and can be obtained from the static failure analysis (fig. 3).

The general fatigue philosophy is based on using unflawed lamina fatigue data to predict the local property changes in flawed laminates (refs. 1, 4, 5, and 8). Fatigue tests are to be conducted on unflawed coupons to span a wide range of stress states and the desired property degradations measured. These results constitute the data bank for the fatigue philosophy. A knowledge of the complex in situ stress state in each lamina can then be used in conjunction with the experimental data to predict the spatial property degradation in each ply of the flawed laminate. NDT can be employed to measure the local property degradation for correlation studies.

The static failure analysis for a flawed laminate under a given set of loading conditions requires the stiffness and strength properties as input data. Fatigue failure analysis is carried out by considering a finite number of load cycle intervals, and using the degraded properties for each interval in the static failure analysis.

The fatigue philosophy outlined above, though sound in principle, is difficult to implement. The formidable stress analysis and the need for an extensive experimental program to collect the required data deem a more approximate theory necessary. An empirical approach, used in the present program, is discussed below.

Empirical Approach Used in the Present Program

A simplified fatigue philosophy (refs. 1, 4, 5, and 8) is used in the present program to mathematically model the property degradation in an empirical manner. The spatial stress variation in each lamina is approximated by an average stress state throughout the lamina. This approximates the

spatial variation in the lamina S value (the ratio of the maximum fatigue stress to the static strength of the unflawed lamina) by an average S value for each lamina in the flawed laminate. The spatial variation of the property degradations in each ply is thus approximated by average degraded ply properties to simplify the analysis. The fatigue degradation in each ply in a flawed beam can then be assumed to be a function of N and the laminate S/η value which is the ratio of the maximum applied fatigue load to the static failure load of the flawed beam of known initial flaw size.

The fatigue analysis is carried out by computing the laminate property degradations from the lamina fatigue data using laminated plate theory. This is done for the four beam elements in the present analysis. The lamina fatigue data are obtained from experiments on unnotched, perfectly bonded uni-directional specimens. These tests are carried out at different S levels. When the lamina fatigue data are used in the fatigue failure analysis of a flawed beam, the η value corresponding to the measured flaw size is computed from the static failure analysis and the lamina fatigue data corresponding to the laminate S/η value are used in the laminate analysis to obtain average degradations in the four beam elements. Hence, for different initial flaw sizes, different levels of degradations result depending on the ratio of the maximum fatigue load to the static failure load of the flawed beam. As a further simplification in this example, the rates of property degradation in this beam are assumed to be constant in all plies. Thus the effect of the differences in property degradation resulting from different stress levels in the various plies is disregarded to simplify the example. Different rates of degradation are used, however, for the different moduli of the plies (i.e. E_1, E_2, G_{12}). These rates are the rates of degradation corresponding to the initial laminate S/η value. The effect of the change in laminate S/η on the degradation rates is ignored.

Figure 11 shows the variation in the critical load with the number of cycles and the debond size for a $[0_4/\pm45_2]_{4s}$ beam under cyclic loading. The debond is located at ℓ_1/L = 1/3 and it is at the laminate middle surface. This analysis does not have the capability to treat stable growth of the debond. The effects of crack growth will be discussed subsequently. The assumed property degradation rates are stated on the figure. These rates correspond to a laminate S/η value of two-thirds for an initial debond size of a/L = 0.2. If the initial debond size is different, different curves (for the new laminate S/η value) result for $N = 10^6$ cycles and $N = 10^7$ cycles in figure 11.

VIBRATION ANALYSIS OF A DELAMINATED BEAM

The degradation in the material properties of a flawed specimen under cyclic loading can be estimated by acoustic monitoring or ultrasonic measurements. Ultrasonic C-scans were used extensively in the present study to detect and measure flaws. Vibrational monitoring was explored as a possible NDT for future use, and for correlation studies. Frequency is used as a parameter to study the criticality of a flaw (ref. 17), because the reduction in the stiffness as well as the growth of the flaw affect the natural frequencies of vibration of the specimen. An analytical methodology to evaluate the reductions in the frequencies due to each cause is presented in Appendix B for a delaminated beam. The model is similar to the static/fatigue model that determines the criticality of interlaminar delaminations (Appendix A). The free vibration analysis (see fig. 12) assumes the beam elements to be Timoshenko beams that include shear deformation and rotary inertia effects.

The free vibration frequencies for the debonded beam are obtained by computing the determinant of a 16x16 matrix for many assumed values of frequencies, and numerically interpolating to find the frequencies corresponding to a null

determinant (Appendix B). Normalizing these frequencies
with respect to the corresponding frequencies of vibration
of the beam without any delamination, the decrease in the
frequencies with the growth of debond can be estimated. Like-
wise, for any size of the debond, the reduction in the
frequencies with cyclic degradation in the element stiffnesses
can also be evaluated.

Debonds of known sizes are implanted in specimens in the
laboratory and experimental measurements of the frequenices
made after known numbers of cycles. Periodic C-scans of these
specimens reveal the damage growth (stable) with cyclic load-
ing, making feasible a frequency-damage size relationship.
The experimentally measured frequencies for different debond
sizes could then be correlated with the analytical predic-
tions. If the debond grows in a stable manner till the onset
of catastrophic propagation, the critical state could be
acoustically monitored. Acoustic measurements could then be
used as a viable tool to predict the criticality of a flaw
(a slit notch, delamination, etc.) in laminated structures.

All the vibration tests were conducted on $[(0_4/\pm45_2)_s]_s$
beam specimens. The first four natural vibration frequencies
for these beams were obtained with no interlaminar defect
(table 4). The same frequencies were also measured for beam
specimens with 1.27 cm and 2.54 cm delaminations implanted
in them (tables 5 and 6). These results are compared with
those predicted by the vibration analysis in table 7. While
the results for an unflawed beam demonstrate good correlation,
those for a debonded beam with an a/L of 0.2 are not encour-
aging and show reasonable agreement only for the fourth fun-
damental frequency. This fact calls for further investiga-
tion to assess whether the vibration tests, when understood
well, will serve as a useful tool for NDE of damage growth
in flawed beams.

NDE METHODOLOGY TO PREDICT FLAW CRITICALITY

In evaluating the integrity of structural elements, non-destructive inspection focuses upon detection of flaws and the determination of their sizes, while non-destructive evaluation techniques translate these into a measure of the criticality of the flaws. Allowable limits for flaw size and damage growth rates must be determined to establish inspection intervals for in-service flawed structural elements, and to determine flaw characteristics that make repair mandatory. To this end, an NDE methodology is developed herein. It is built around: (i) a static/fatigue failure analysis; (ii) experimental results on flawed specimen response; and (iii) an NDE methodology to assess the criticality of a flaw using NDT.

The analytical results predicted by the static/fatigue failure model (figs. 3, 11) form the basis of the NDE methodology. For a defect of a known initial size and location, a family of curves describes the variation of the critical load with the defect size for different values of N (fig. 11). As the number of cycles (N) of known loading conditions increases, the spatial degradation of the material properties causes a lowering of the critical load at which the propagation of a delamination of known size is imminent (fig. 11). The crack growth is stable if additional load is required to increase the crack size, and unstable if an increase in a/L results in a reduction of the critical load. The present model for an interlaminar defect in a beam yields values of critical load at which the imminent propagation of the debond is unstable by nature. Unstable crack growth is represented in figures 3 and 11, where the critical load decreases with a growth in the delamination. If an applied load reaches the critical value for the existent length of debond, the debond tends to grow indefinitely. Hence, the above-mentioned family of curves describes the catastrophic debond growth for each value of N. This is of major importance to the NDE analyst.

-19-

For a known size and location of a debond in a delaminated beam, curves of "$P_{cr}/\sqrt{\gamma_a}$ versus a/L" can be drawn for various values of N as shown in figure 11. As discussed earlier, these curves are all calculated based upon the assumption that property degradation occurs throughout the laminate at constant rates (as shown in figure 11). In actuality, the degradation rates depend upon the crack size and the stress ratio S/η. For these calculations, the degradation rates used were those for a/L = 0.2 and S/η = 2/3. From curves of this type, the static failure load, P_{static}, for any initial debond size can be obtained from the N = 1 curve. For illustrative purposes, $P_{static}/\sqrt{\gamma_a}$ for an a/L value of 0.2 is selected in figure 11. If the laminate S level for fatigue loading is chosen, the maximum cyclic load, $P_{fatigue}$, can be determined as $SxP_{static}^{unflawed}$. $P_{fatigue}$ for the chosen laminate S value corresponds to a particular laminate S/η value for the known debond size. $P_{fatigue}$ for S/η = 2/3 is shown in figure 11. The line $P_{cr}/\sqrt{\gamma_a} = P_{fatigue}/\sqrt{\gamma_a}$ intersects the family of failure curves at various points. The points of intersection of $P_{fatigue}$ with the family of curves can be plotted as an "a/L versus log N" curve (fig. 13). The lower solid curve in figure 13 defines the lifetime to catastrophic propagation of an initial debond of the specified size. The upper solid curve differs from this only in the assumption that the surface energy remains constant while the stiffnesses degrade.

All of these calculations result in unstable crack propagation. Experimentally, however, a stable crack propagation is observed. Treatment of this phenomenon would greatly complicate the analysis, since, strictly speaking, once the debond grows, the η value (and hence the laminate S/η) changes. Thus, different fatigue data are required and a new family of "$P_{cr}/\sqrt{\gamma_a}$ versus a/L for various N" curves should be used. This is not done in figure 13 for reasons explained in the section "Empirical Approach used in the Present Program." The initial debond size of a/L = 0.2 is the lower

bound on the a/L value. N_f (see fig. 11) is the number of cycles after which an initial debond of size a/L = 0.2 will propagate catastrophically without any intermediate growth. N_f is a hypothetical upper bound on N, since in reality, the damage may grow with N, thus shortening lifetime. Point B corresponds to that debond size at which a static load of magnitude equal to $P_{fatigue}$ precipitates a catastrophic failure (N = 1). On fatigue loading, the debond in a laminated beam appears to grow in a stable manner, as shown by curve AED in figure 13, until the (a/L, N) combination corresponds to a catastrophic situation. The use of the curves of figure 11 is rigorously correct only if the property degradation rate is insensitive to debond size. Point D in figure 13 then represents a typical (a/L, N) combination at which catastrophic debond growth precipitates after stable crack growth.

Knowing the location and initial size of the debond, and the chosen cyclic maximum load, the boundary for catastrophic propagation of the delamination is obtained. This boundary is drawn on an "a/L versus N" plot for every value of initial debond size. The procedure for this follows the steps outlined below:

1. Determine the initial debond size (a/L and its location.

2. From the static failure analysis, obtain a "$P_{cr}/\sqrt{\gamma_a}$ versus a/L" curve for the debonded beam.

3. Given the maximum applied cyclic load and the static failure load of the unflawed, virgin beam, determine the laminate S/n value for the initial debond size from the static failure analysis results.

4. Using lamina degradation data corresponding to the initial laminate S/n value, obtain a family of curves defining catastrophic growth of defect for different values of N.

5. Corresponding to the maximum cyclic load, obtain the
   critical values of a/L (greater than or equal to the
   initial value) for different values of N.

6. Plot these points on an "a/L versus N" plot, and
   draw a curve through them to define the catastrophic
   debond growth boundary.

Figure 13 presents the instability boundary for a
$[(0_4/\pm 45_2/\mp 45_2/0_4)_s]_s$ laminated beam with a debond in the mid-
plane. BFLGC is the curve that defines unstable debond growth
or failure. While the outer curve assumes no degradation in
the specific adhesive surface energy, the inner one assumes
a degradation in γ_a that is of the same order as the shear
modulus degradation, based on the reasoning that the surface
energy is affected directly by a deterioration in the shear
resistance at the adherend-adhesive interface. The initial
defect size (a/L = 0.2) is labeled A, and the critical defect
size for static failure at the maximum cyclic load is labeled
B. Point C denotes the hypothetical number of cycles the
beam can go through until failure without any growth of the
defect. This is not a physically realizable state since the
damage generally grows when the flawed specimen is subject
to cyclic loading.

The actual growth of the damage, which can be monitored
ultrasonically, may follow a path similar to that shown by
the discontinuous line AED. From an NDE point of view, if
the specimen is inspected after a few cycles and the defect
has grown to the extent shown by E, the residual strength and
lifetime of the specimen have to be determined to decide on
the need for mandatory repair. If the initial debond (a/L =
0.2) has grown to state E after about 5.75×10^6 cycles, FDG
becomes the new envelope that bounds stable crack growth.
At E, if the fatigued beam specimen were tested statically,
from the measure of EF and the static failure analysis (fig.
3), the residual strength in the beam may be computed. Also,
an overestimation of the residual lifetime of the beam may

be obtained from the measure of EG. EG is an overestimation
of the residual lifetime since it assumes the debond size at
E to remain constant when cyclic loading on the delaminated
beam is assumed to be applied for an additional number of
cycles (given by EG). Hence, from figure 13, it is seen that
EF is a measure of the residual strength in the specimen and
EG is an overestimation of its residual lifetime. These could
then be compared with a quantified criterion for mandatory
repair and serve as an assessment of the criticality of the
flaw.

EXPERIMENTAL PROGRAM

The primary objectives of the experimental program are:
(i) to develop material property data required to support
the analysis; (ii) to produce realistic birth and service
defects in the composite material laminates for subsequent
periodic nondestructive evaluation; and (iii) to conduct
experiments required to evaluate the accuracy and limitations
of the developed analytical models in assessing flaw criti-
cality in composite material systems. The two generic de-
fects to be examined are the slit notch (through the thick-
ness) and the interlaminar debond or delamination.

The above-mentioned objectives are met through the fol-
lowing experimental tasks:

(i) Fabrication of AS/3501 Gr/epoxy (flawed and un-
flawed) laminates and conduct ultrasonic ND
testing of laminates after fabrication.

(ii) Determination of static (longitudinal and trans-
verse tension, inplane and interlaminar shear)
and fatigue (S-N and residual strength/stiffness-N
for longitudinal tension and inplane shear) proper-
ties for the AS/3501 material system. These data
are utilized in the analysis presented earlier.

(iii) Performance of unnotched and notched (slit notch)
laminate static and fatigue tests to determine
damage growth, residual strength, and lifetime.

(iv) Performance of unflawed and flawed laminated
beam static/fatigue tests to determine load-
deflection characteristics and growth of debond.
The ND tests for damage detection and damage
growth determination are performed.

(v) ND vibration tests on the laminated beam to assess
the effect of debond growth on the first four fun-
damental frequencies of vibrations.

SPECIMEN FABRICATION

All test specimens were fabricated from a single graphite-epoxy prepreg system (Hercules AS/3501) purchased in accordance with the acceptance standards of the McDonnell-Douglas Corporation. All graphite-epoxy laminates were fabricated in a controlled environment using hand layup procedures and processed in the University of Delaware autoclave system, using conditions which yield properties typical of the given composite system (AS/3501). Sufficient acceptance testing was performed to assure the quality of composite laminates fabricated. After fabrication, samples of all laminates were supplied to the NADC technical monitor for inspection (see figs. 14, 15).

MECHANICAL CHARACTERIZATION

This section describes the mechanical characterization test program required to characterize the Hercules AS/3501 composite material system.

Fiber Direction Tension Properties

The axial tension tests were conducted on specimens of geometry shown in figure 15. The test specimen geometry was 22.86 cm (9.0 inches) in length and 1.27 cm (0.5 inch) in width with a test section of 15.24 cm (6.0 inches). The failed eight-ply specimens are shown in figure 16 where considerable axial splitting is apparent. The average mechanical properties determined from the tests (fig. 17 and table 8) are as follows: ultimate tensile strength of 1703 MPa (247 ksi); Young's modulus (E_1) of 125 GPa (18.2×10^6 psi); and Poisson's ratio (v_{12}) of 0.28.

Transverse Tension Properties

Test specimen geometry for the transverse tension test is also shown in figure 15. The specimen is 22.86 cm (9.0 inches) in length and 2.54 cm (1.0 inch) in width. The failed eight-ply specimens are shown in figure 18. Mechanical properties determined from the transverse tension tests (fig. 19 and table 8) are: a Young's modulus (E_2) of 9.93 GPa (1.44×10^6 psi) and an ultimate transverse tensile strength of 58.8 MPa (8.53 ksi).

Inplane Shear Properties

The inplane shear properties for the graphite-epoxy composite were determined with the $[\pm 45]_s$ tensile coupon test specimens shown in figure 15. Test specimen dimensions were identical to those of the transverse tension test specimens described in the previous paragraph. Inplane shear properties determined (fig. 20 and table 8) include an ultimate shear strength of 88.2 MPa (12.7 ksi) and a shear modulus of 5.45 GPa (0.79×10^6 psi). The failed eight-ply $[\pm 45]_s$ laminate test specimens are shown in figure 21.

Interlaminar Shear Properties

The interlaminar shear properties were determined (fig. 22 and table 9) through the thick laminate, short beam, shear tests. The test specimens were beams of aspect ratio 4/1 carrying a concentrated load at midspan. Shear strain was monitored by means of a strain rosette at the beam quarter-span. Specimen geometry was 1.27 cm (0.5 inch) in thickness, 7.62 cm (3.0 inches) in length, and 0.76 cm (0.3 inch) in width. The short beam shear specimens are shown in figure 23. The test apparatus, with the beam mounted in place, is shown in figure 24.

STATIC LAMINATE TESTS

Laminates with and without defects have been studied experimentally.

Unnotched Laminate Properties

The response of the unnotched $[45/0/-45/0]_s$ laminate was determined for tensile loadings of the laminate specimen shown in figure 15. The specimen geometry was 30.4 cm (12.0 inches) in length and 3.81 cm (1.5 inches) in width, with a t st section of 22.9 cm (9.0 inches). The measured laminate properties (fig. 25 and table 8) included an ultimate tensile strength of 866.0 MPa (125.7 ksi), Young's modulus of 72.6 GPa (10.5×10^6 psi), and Poisson's ratio of 0.70. The failed laminate specimens are shown in figure 26.

Notched Laminate Properties

The response of the $[45/0/-45/0]_s$ laminate containing a slit notch defect was investigated next. The slit notch was ultrasonically machined into the specimen (fig. 27). The slit notch was 0.952 cm (0.375 inch) in length with a notch tip radius of 1.9×10^{-2} cm (7.5×10^{-3} inches). The static test results are shown in figure 28. The average ultimate strength was determined (table 8) to be 292.4 MPa (42.4 ksi) and the measured Young's modulus was 72.4 GPa (10.5×10^6 psi). The failed notched laminates are shown in figure 29.

Laminate Flexural Behavior

In order to assess the influence of an interlaminar defect upon the flexural strength of a composite laminate, defects were induced by a tubular film embedded between plies 32 and 33 in a 64-ply $[0_4/\pm45_2]_{4s}$ laminate. Defect lengths of 2.54 cm and 1.27 cm (1.0 inch and 0.5 inch) were considered. The beam was 2.54 cm (1.0 inch) wide with a span

of 7.62 cm (3.0 inches). A typical interlaminar defect is
shown at 400X magnification in figure 30. Failure resulted
through the unstable propagation of the interlaminar defect
to complete failure. Typical failure specimens are shown in
figure 31. Average failure load (table 10) for the 2.54 cm
defect was 2870 (292 kg) and 4652 (466 kg) for the 1.27 cm
defect. Load-deflection curves for an unflawed specimen and
one with an implanted debond are presented in figures 32 and
33. These can be used to measure the bending stiffness of
the beam specimens for correlation studies.

Birth Defect Detection

The ultrasonic "C" scan technique was employed to examine
each laminate after fabrication to locate birth defects intro-
duced during the fabrication process. Figure 34 shows a typ-
ical "C" scan of a $[45/0/-45/0]_s$ laminated panel. Note that
fiber orientations and regions of thickness variation are
readily observed. Specimens were machined out of this panel
to be used in the various tests. To account for damages due
to the machining process, the ultrasonic technique was again
deployed, after each specimen was fabricated and prior to
installation of instrumentation. This was to assess total
specimen fabrication damage and to provide a reference stand-
ard. Figure 35 shows results for several unnotched laminate
specimens.

FATIGUE AND VIBRATION TESTS

Fatigue tests were performed both on unidirectional ma-
terial coupons and on laminates. Vibration tests were con-
ducted on beams containing interlaminar disbonds.

Fiber Direction Tension Fatigue Behavior

Axial tension specimens were subjected to fatigue load-
ings of R = 0.1 at 30 Hertz, and at stress levels of S = 0.67

and 0.80 (ratios of cyclic maximum to static failure stress).
All specimens subjected to 80 percent loadings exhibited
fatigue failures (table 11). The specimens subjected to 67
percent loadings and cycled to 500,000 and 1,000,000 cycles
exhibited no reduction in strength. In addition, no damage
was detected by ultrasonic inspection.

Inplane Shear Fatigue Behavior

The inplane shear fatigue damage was examined by subjec-
ting $[\pm 45]_s$ coupons to tension-tension fatigue loadings for
$S = 0.45$ and 0.55 at 30 Hertz, and $R = 0.1$. Figure 36 shows
the difference between ultrasonic traces for samples before
and after a fatigue loading of $S = 0.45$ and $N = 10,000$ cycles.
The figure shows the free edge damage in the specimen due to
fatigue loading. The corresponding results are presented in
table 12.

Laminate Tension-Tension Fatigue Behavior

The unnotched $[45/0/-45/0]_s$ laminate was subjected to
fatigue loadings of $S = 0.67$ and 0.80 at 30 Hertz, and $R = 0.1$.
The results are presented in tables 13 and 14. The accumula-
tion of edge damage after 500,000 and 1,000,000 cycles at
$S = 0.67$ is shown in figure 37. The figure shows that signif-
icant edge damage results from tensile fatigue loading of the
specimen and that ultrasonic techniques are sufficient for its
detection. The variation in the experimentally measured
residual strength and the residual modulus of the unnotched
$[45/0/-45/0]_s$ laminate with the number of cycles of fatigue
loading is shown in figure 38.

Ultrasonic inspection results for pristine notched lam-
inate specimens are shown in figure 39. After these specimens
were subjected to 10^5, 5×10^5, and 10^6 cycles (table 15),
ultrasonic inspection was carried out to examine the damage
in the vicinity of the notch. These results are shown in fig-
ures 40 and 41, where the ultrasonic frequencies are 4.2 MHz and

7.2 MHz, respectively. Subsurface damage at the tip of the
slit notch for each specimen is particularly noticeable in
figure 41. In addition, the damage area is seen to increase
with an increase in the number of cycles. A magnified view
of a fatigued specimen (X212B) in figure 40 is shown in
figure 42 for a better picture of the damage. The results
in table 15 are plotted in figures 43 and 44 to show the varia-
tion in the residual strength and the residual modulus at two
S values for a notched $[45/0/-45/0]_s$ laminate.

Laminate Flexural Fatigue Behavior

Graphite/epoxy laminates containing implanted interlaminar
defects were subjected to flexural fatigue loadings to examine
cyclic propagation of interlaminar defects. The flexural ap-
paratus is shown in figure 45, where it is seen that the load
is introduced at midspan and resisted by simple supports.
The implanted defect is at quarter-span. The complete fatigue
set-up is shown in figure 46. Typical results, presented in
figure 47, show that the interlaminar defect propagates from
the point of intersection of the loading edge of the defect
and the free edge of the specimen. In addition, these results
show that the defect propagates parallel to the 45° fibers in
the laminate although the defect is positioned between two 0°
layers in the laminate. At an S level of 0.5, the damage is
shown to grow exponentially, and catastrophic failure occurs
at $N = 90,000$ cycles. Again, the ultrasonic technique is
shown to be adequate for detection of the damage and its sub-
sequent propagation. The damage growth measured ultrasonically
is plotted in figures 48 and 49.

Laminate Flexural Vibration Characteristics

The $[0_4/\pm 45_2]_{2s}$ laminated beam specimens were subjected
to vibration tests after known cycles of fatigue loadings to
assess the influence of interlaminar damage upon the material

frequencies. The vibration apparatus, with the specimen exhibiting the third and fourth mode shapes, is shown in figures 50 and 51, respectively. Relatively insignificant dependence of natural frequency on interlaminar damage was observed in the experiments (tables 4, 5 and 6).

DISCUSSION OF RESULTS

SLIT NOTCH STUDY

A slit notch, through the thickness of the laminate, was chosen to be one of the two flaws to be studied under the present program because of the importance of through holes and of the availability of an existing analysis to study the effect of a slit notch under tensile fatigue loading. Notched $[45/0/-45/0]_s$ AS/3501 laminates were chosen and the virgin specimens C-scanned (fig. 39). Some of these specimens were used to characterize the notched laminate properties (figs. 28, 29 and table 8). The others were used to study the fatigue behavior of the notched specimens (figs. 40, 41, 42 and table 15).

The ratio of the average residual Young's modulus after a known number of cycles to the static (notched) modulus and the ratio of the average residual strength to the static notched strength are plotted (figs. 43, 44) for two S values. Allowing for a reasonable scatter in the experimental results, the Young's modulus seems to remain almost constant. The residual strength increases with N for an S value of 0.67 (fig. 43). But for S = 0.8, the residual strength increases until $N = 5 \times 10^5$ cycles, and then decreases.

The existing static failure analysis (ref. 5) was used to predict the damage growth in the notched $[45/0/-45/0]_s$ AS/3501 specimen under a static tensile load. The analysis yields a curve relating the length of the axial damage (including both the inelastic zone and the axial crack) to the applied load. The results, shown in figure 52, assume the yield values for the shear stresses for the 0° and ±45° layers to be 10 ksi and 65 ksi, respectively. The other properties are taken from table 8. The basic curve (Curve II) turns out to be a point (fig. 52). This shows that this notched laminate will fail in the transverse mode (the crack running normal to the load direction) prior to any axial damage.

This is based upon the measured value (table 8) of the transverse failure stress σ^T (42.4 ksi). No other damage is predicted to occur before failure if this is the material strength. However, this prediction is based on assumed shear yield stress values.

On changing σ^T to a higher value, Curve I results. It is seen that the 0° layers become inelastic first; the ±45° layers go plastic at a higher load value; and the laminate fails in the transverse mode eventually. This behavior can also be expected if the shear yield stress values are lower than the assumed values and σ^T is the measured value, which may be the case for fatigue.

One of the earlier objectives in this study was to ultrasonically measure the degraded properties of the notched laminate after subjecting it to known fatigue loading conditions. This could not be achieved, and as a result, analytical predictions of the fatigue behavior of notched laminates (that requires degraded properties as input data) were hampered. The fatigue damage growth, though, can be extracted from the ultrasonic C-scans (figs. 40 to 42). It is seen that the extent of such damage is small.

The limited success with notched laminates restricted the further application of the NDE methodology to the delamination flaw in composite structures.

DELAMINATED BEAM STUDY

The closed-form solution for the static failure analysis of a debonded beam (Appendix A) is plotted in figure 3 for two locations of the delamination through the thickness of the midplane-symmetric beam. It is seen that the critical load at which the debond tends to propagate increases when the debond is located away from the midplane. The same effect was observed in the study on the criticality of a delamination in a laminated cylinder (ref. 15). On comparing the results for the beam (fig. 3) with those for the debonded cylinder

(ref. 15), an interesting contrast is noticed. The debond in
the cylinder generally tends to grow in an unstable fashion
for small crack lengths, followed by a stable growth and,
subsequently, a region of debond growth at a constant load
(ref. 15). This behavior was observed in an infinitely long
cylinder for two types of loading: (i) a pressure on the
debond surface and (ii) a constant loading on the inner sur-
face of the cylinder. In contrast, the beam analysis of the
present program (Appendix A) predicts an unstable crack
growth in every case (fig. 3). The curve in figure 3, there-
fore, represents the catastrophic crack growth boundary for
the delaminated beam.

The results from the static tests on $[(0_4/\pm45_2/\mp45_2/0_4)_s]_s$
AS/3501 beam specimens are shown in table 10. In this case,
unstable propagation of delamination, in the direction predic-
ted by the finite element analysis, was observed. The results
(P_{cr}) from table 10 and the corresponding solutions (P_{cr}/γ_a)
from the static analysis (fig. 3) yield a measure of the
specific adhesive surface fracture energy (table 16). Taking
into consideration the fact that a simplified beam analysis was
used, estimated surface energy values for two debond sizes are
in fair agreement. The quantitative discrepancy can be explained
with the help of the elasticity solutions presented in figure
53. When the debond size is large, the crack tip nearer the
applied loading is affected by the elasticity effect shown in
figure 53. Since the debond tends to propagate into this direc-
tion, the additional load needed to overcome the compressive
stresses at the crack tip results in an increase in the magni-
tude of the critical load. Hence the larger value of γ_a for
the 2.54 cm debond in comparison to that for the 1.27 cm debond
in table 16.

Figure 11 shows the effect of fatigue on the debond
growth. A simplified fatigue philosophy is used to account
for the spatial degradation of the stiffnesses due to cyclic
loading, and typical degradations, from earlier experimental

observations, are incorporated into the static/fatigue failure model. As expected, figure 11 shows a decrease in the critical load (P_{cr}) with an increase in the number of fatigue load cycles (N). The degradation is relatively insignificant for almost a million cycles.

Figures 48 and 49 show the growth of the damage area with fatigue loading for two initial debond sizes in a $[(0_4/\pm45_2)_s]_s$ laminated beam. The damage areas in the figures are measured off the ultrasonic "C" scans at the failure site. The correspondence between the damaged area measured off the "C" scan and the damage area addressed in the analysis needs further investigation. If this relationship can be established, figures 48 and 49 define the path labeled AED in figure 13.

As explained in the section entitled "Analytical Methodology," figure 13 presents the instability curves for a $[0_4/\pm45_2]_{4s}$ laminated beam with a debond in its midplane. One boundary assumes that there is no degradation in the specific adhesive surface energy due to cyclic loading. The other solid curve represents the instability boundary when the surface energy degenerates at the same rate as the shear modulus. In the latter case, a degradation in the surface energy leads to catastrophic failure earlier. This can be seen by following the actual, stable damage path AED in the figure. Surface energy degradation also causes a reduction in the residual strength and lifetime of the fatigued structural element. Changes in EF and EG in figure 13 give a measure of these reductions.

EXPLORATORY STUDIES

Vibrational monitoring was explored as a candidate NDT to measure flaw size and to detect flaw growth. Correlation between analytical predictions and experimental measurements was fair (table 7). But further improvement is necessary before vibrational monitoring can be employed as an NDT. A higher order analysis may be required to achieve this objective.

Figures 32 and 33 trace the load-deflection curves for
a $[(0_4/\pm45_2/\mp45_2/0_4)_s]_s$ laminated beam with and without an
interlaminar debond. These results, while they do not form an
integral part of the NDE logic, serve as a potential NDT to
estimate stiffness degradation due to fatigue loading. While
the unflawed beam failed in flexure, the delaminated beam
failed in shear, manifested by a catastrophic growth of the
debond. The slope of the load-deflection curve gives a measure
of the beam stiffness. A comparison of the slopes of figures
32 and 33 shows a fifty percent reduction in the beam stiffness
for an a/L of 1/3. Similar curves, if obtained for fatigued
specimens, provide an alternative method to estimate the
stiffness degradation due to fatigue loading.

CONCLUSIONS

A logic for an NDE methodology to evaluate the integrity of structural elements was explored under the premise that the goal is quantitative measurement of residual strength and lifetime of flawed components. The methodology was based on: a static failure analysis to predict flaw criticality; a simplified fatigue philosophy to predict flaw growth; an experimental program to support and verify the analysis; and an NDE technique to use NDI measurements in conjunction with the analysis to determine flaw criticality.

A slit notch through the thickness of a laminate and an interlaminar debond in a layered beam were identified as critical flaws of interest. An existent static/fatigue failure model for the slit notch study was used and related experiments carried out. Correlation between analysis and experiments was hampered by many factors. Most of the observed damages were due to free edge effects that are not accounted for in the analysis, and degraded properties of the fatigued specimens could not be obtained in enough detail.

A static failure analysis was developed to predict the critical loads for the growth of debonds in layered beams within the limitations of a Timoshenko beam analysis. A simplified fatigue philosophy was adapted to yield a static/ fatigue failure model for debonded beams to establish instability boundaries. The varying levels of degradation in the material properties with a growth in the debond size were approximated by those corresponding to the initial debond size. The restrictions involved in obtaining these bounds should be relaxed in future investigations.

An experimental program was conducted to support the analysis and to measure the specific adhesive surface fracture energy quantitatively. The discrepancy in the measured γ_a values for two different debond sizes suggests the need for a more refined analysis to account for the factors that cause it, or a change in the experimental method of obtaining P_{cr} to eliminate unwanted effects.

Vibrational monitoring of the specimens to detect damage growth and a vibration analysis were carried out for correlation studies and to explore the possibility of establishing a reliable NDT. Initial success in the experimental-analytical correlation study suggests an improvement in the analysis for better agreement in the results.

Ultrasonic "C" scans were used to ensure quality control and to determine damage growth rates. The correspondence between the damage area in the "C" scans and the damage area addressed in the analysis is not obvious and calls for further study.

The study carried out in this report defines the potential of a methodology for quantitatively assessing residual properties and lifetime of flawed composite structural elements. The translation of this approach into a quantified criterion for damage tolerance is the goal, and this would establish flaw criticality and hence the need, or lack of it, for mandatory repair. The results identify areas where further investigation is mandatory. Limited success with the slit notch study suggests that effort should focus on an improved delamination study to establish the proposed NDE methodology as a workable design tool. A higher order analysis for this interlaminar defect study and improved experimental methods for defining damage growth are required. Also, the validity of this methodology and the definition of a procedure for its application to real structures have to be established.

REFERENCES

1. Kulkarni, S. V. and Rosen, B. W., "Design Data for Composite Structure Safelife Prediction: Analysis Evaluation," TFR/2221, Materials Sciences Corporation, August 1973.

2. Zweben, C. H., "Analysis of the Test Methods for High Modulus Fibers and Composites," ASTM STP 521, 1973, pp. 65-97; also, Materials Sciences Corporation Report, 1972.

3. Rosen, B. W. and Zweben, C. H., "Tensile Failure Criteria for Fiber Composite Materials," NASA CR-2057, National Aeronautics and Space Administration, Langley Research Center, Hampton, VA, 1972.

4. McLaughlin, P.V., Jr., Kulkarni, S. V., Huang, S. N., and Rosen, B. W., "Fatigue of Notched Fiber Composite Laminates, Part I: Analytical Model," NASA CR-132747, National Aeronautics and Space Administration, Langley Research Center, Hampton, VA, March 1975.

5. Ramkumar, R. L., Kulkarni, S. V., and Pipes, R. B., "Evaluation and Expansion of an Analytical Model for Fatigue of Notched Composite Laminates," Final Report, NAS1-13937, NASA, Langley Research Center, November 1977.

6. Waddoups, M. E., Eisenmann, J. R., and Kaminski, B. E., "Macroscopic Fracture Mechanics of Advanced Composite Materials," J. Composite Materials, Vol. 5, pp. 446-454, October 1971.

7. Whitney, P. M., and Nuismer, R. J., "Stress Fracture Criteria for Laminated Composites Containing Stress Concentrations," J. Composite Materials, Vol. 8, pp. 253-265, July 1974.

8. Kulkarni, S. V., McLaughlin, P. V., Jr., and Pipes, R. B., "Fatigue of Notched Fiber Composite Laminates, Part II: Analytical and Experimental Evaluation," NASA CR-145039, National Aeronautics and Space Administration, Langley Research Center, Hampton, VA 1976.

9. Williams, M. L., "Proceedings of the 5th U.S. National Congress of Applied Mechanics, 1966.

10. Williams, M. L., Journal of Adhesion, Vol. 4, 1972.

11. Williams, M. L., Journal of Applied Polymer Science, Vol. 13, pp. 26-40, 1969.

12. Williams, M. L., Journal of Applied Polymer Science, Vol. 14, pp. 1121-1126, 1970.

13. Kulkarni, S. V., and Frederick, D., International Journal of Fracture Mechanics, Vol. 9, 1973.

14. Updike, D. P., International Journal of Fracture, Vol. 12, pp. 815-827, 1976.

15. Ramkumar, R. L., Ph.D. Dissertation, Virginia Polytechnic Institute and State University, 1976.

16. Griffith, A. A., "The Phenomena of Rupture and Flow in Solids," Philosophical Transactions," Royal Society, London, Series A, Vol. 221, pp. 163-198, 1920.

17. Kulkarni, S. V., and Frederick, D., "Frequency as a Parameter in Delamination Problems - A Preliminary Investigation," J. Composite Materials, Vol. 5, pp. 112-117, Jan. 1971.

18. Pipes, R. B., "Interlaminar Shear Fatigue Characteristics of Fiber-Reinforced Composite Materials," ASTM STP 546, pp. 419-431, 1974.

19. Fung, Y. C., Foundations of Solid Mechanics, Prentice-Hall of India: New Delhi, 1968.

20. Handbook of Engineering Mechanics, edited by Flügge, W., Mc-Graw-Hill: New York, 1962.

Table 1. Types of Flaws and Imperfections
          in Composite Structures

1. THROUGH-THE-THICKNESS FLAWS

    a. Slit Notch

    b. Openings or Cutouts (circular, elliptical,
        rectangular, arbitrary shape)

    c. Bolted Joints, Interference-Fit Fasteners

2. SURFACE FLAWS

    a. Region Of Broken Fibers

    b. Breaks Along The Length Of A Fiber

    c. Cracks Parallel To The Fibers

3. SUB-SURFACE FLAWS

    a. Interlaminar Damage

    b. Cracks Parallel To The Fibers

    c. Regions Of Broken Fibers

    d. Breaks Along The Length Of A Fiber

    e. Matrix Porosity

4. OTHER IMPERFECTIONS

    a. Variation Of Local Fiber Orientation And
                    Spacing

    b. Local Fiber Microbuckling (in the vicinity of
                    bolt bearing surface)

Table 2. Static Test Data for $[(0_4/+45_2/\overline{+45}_2/0_4)_s]_s$ AS/3501 Laminates With and Without Interlaminar Delaminations

Specimen	Width (cm)	Thickness (cm)	Test Section* Length (cm)	Debond Size** (cm)	Location	Failure Load*** (N)
1/2-1-16/17	2.510	0.460	22.86	1.27	Between	588.5
1/2-2-16/17	2.545	"	"	*	plies	1005.5
1/2-3-16/17	2.550	"	"	*	16 and 17	1398.0
					Average:	997.5
1/2-1-12/13	2.548	"	"	"	Between	1471.5
1/2-2-12/13	2.543	"	"	"	plies	1447.0
1/2-3-12/13	2.550	"	"	"	12 and 13	1363.5
					Average:	1427.5
1-1-16/17	2.543	0.445	"	2.54	Between	1682.5
1-2-16/17	2.545	"	"	"	plies	1300.0
1-3-16/17	2.553	"	"	"	16 and 17	1314.5
					Average:	1432.5
0-7L	2.532	0.460	15.24	0.0		1457.0
1/2-7L	2.535	0.455	"	1.27		1275.5
1-7L	2.530	0.457	"	2.54		1309.5****

*Total length of specimen = 25.4cm
**Debond was centered in the test section
***Failure mode was flexural
****Catastrophic propagation of debond

Table 3. Input Data for the Finite Element Model

Property	Layers 1 and 5	Layers 2 and 4	Layer 3
Lay-up	$[0]_{16}$	$[\pm 45_8/0_{16}]$	$[\pm 45_{16}]$
Thickness (mm)	2.235	4.470	4.470
E_x (GPa)	127.550	66.360	19.150
$E_y = E_z$ (GPa)	10.070	20.570	19.150
G_{xy} (GPa)	5.520	17.130	33.100
$\nu_{xy} = \nu_{yz} = \nu_{xz}$	0.310	0.201	0.736

Table 4. Vibration Results for a $[(0_4/\underline{+}45_2)_s]_s$ AS/3501 Laminate with No Interlaminar Defect (S=0.5)

Specimen*	Width (cm)	Thickness (cm)	N (cycles)	ω_1 (Hz)	ω_2 (Hz)	ω_3 (Hz)	ω_4 (Hz)
0-1L	2.56	0.462	0	345	2059	5425	10353
			5×10^5	343	2047	5390	10327
0-2L	2.55	0.460	0	342	2046	5409	10353
			5×10^5	341	2025	5435	10338
0-3L	2.56	0.452	0	340	2041	5386	10322
			5×10^5	338	2026	5314	10286
Average Frequencies:			0	342	2049	5407	10343
			5×10^5	341	2045	5380	10336

*Total length of specimen (vibration) = 25.4cm

Test section length (fatigue) = 15.24cm

Table 5. Vibration Results for a $[(0_4/\underline{+}45_2)_s]_s$ AS/3501 Laminate With a 1.27cm Delamination at $\ell_1/L = 0.25$

Specimen*	Width (cm)	Thickness (cm)	N (cycles)	S	ω_1 (Hz)	ω_2 (Hz)	ω_3 (Hz)	ω_4 (Hz)
1/2-1L	2.555	0.457	0	-	341	2030	5461	9381
1/2-2L	2.558	0.462	$0;10^5;$ $1.5 \times 10^5 ; 3 \times 10^5$	0.5	340	2030	5353	10101
1/2-3L	2.558	0.457	$0;1.5 \times 10^5$ $3 \times 10^5 ; 4.5 \times 10^5$	0.67	340	2023	5406	10136
1/2-4L	2.545	0.460	$0;10^5 ; 2 \times 10^5$	0.75	345	2023	5421	10191

*Total length of specimen (vibration) = 25.4cm

Test section length (fatigue) = 15.24cm

-45-

Table 6. Vibration Results for a $[(0_4/+45_2)_s]_s$ AS/3501 Laminate with a 2.54cm Delamination at $\ell_1/L = 0.2$

Specimen*	Width (cm)	Thickness (cm)	N (cycles)	S	ω_1 (Hz)	ω_2 (Hz)	ω_3 (Hz)	ω_4 (Hz)
1-1L	2.555	0.457	0	-	342	1973	5364	9628
			8320	0.8		Specimen failed		
1-2L	2.520	0.462	0	-	337	1948	5337	9578
			5×10^4	0.5	335	1932	5296	9257
			6×10^4	0.5	305	1849	4562	9135
1-3L	2.553	0.462	0	-	341	1966	5387	9586
			5×10^4	0.5	338	1960	5231	9398
			9×10^4	"	315	1866	5185	8935
			9×10^4**	"	314	1488	3569	7132

*Total length of specimen (vibration) = 25.4cm

Test section length (fatigue) = 15.24cm

**The delamination in this case had extended over most of the test section (fig. 47)

Table 7. Comparison of Experimental and Analytical
Frequencies of Vibration of $[(0_4/\pm45_2)_s]_s$
AS/3501 Laminates With and Without Inter-
laminar Delaminations

Frequency (Hz)	a/L = 0		a/L = 0.2*	
	Analysis	Experiment	Analysis	Experiment
ω_1	313	342	255	340
ω_2	1958	2049	1653	1961
ω_3	5483	5407	4635	5351
ω_4	10745	10343	8812	9603

*$\ell_1/L = 0.2$

$L = 12.7cm$

Table 8. Summary of Static Tension Test Data for Various AS/3501 Laminates

Specimen	Laminate Layup	Width (cm)	Thickness (cm)	Total Length (cm)	Test Section Length (cm)	Modulus (GPa)	Poisson's Ratio	Ultimate Strength (MPa)	Ultimate Strain (µm/mm)
0129	[0]	1.273	0.112	22.86	15.24	124.2	0.286	1689	12,790
0121	"	1.275	0.114	"	"	124.8	0.258	1614	12,220
0111	"	1.273	0.109	"	"	127.3	0.293	1806	13,140
					Average:	125.4	0.279	1703	12,717
9113	[90]	2.543	0.112	22.86	15.24	9.908	0.0140	58.55	6220
9112	"	"	"	"	"	9.694	0.0802	60.96	6800
9111	"	"	"	"	"	9.894	0.0298	56.83	6180
					Average:	9.832	0.0413	58.78	6400
4111	[±45]ₛ	2.54	0.109	22.86	15.24	5.618		91.36	
4121	"	"	0.114	"	"	5.362		87.30	
4131	"	"	0.114	"	"	5.377		85.87	
					Average:	5.452		88.18	
X411	[+45/0/-45/0]ₛ (Unnotched)	3.805	0.112	30.48	22.86	69.02	0.6554	897.7	12,460
X431	"	3.805	0.109	"	"	72.74	0.7011	836.2	11,240
X151	"	3.810	0.114	"	"	76.05	0.7004	865.5	11,180
					Average:	72.60	0.6856	866.5	11,627
X233	[45/0/-45/0]ₛ (Notched)	3.807	0.114	30.48	22.86	76.60	-	285.6	3860
X311	"	3.813	0.114	"	"	67.68	0.6436	291.9	4160
X263	"	3.797	0.112	"	"	72.88	0.6311	299.8	3970
					Average:	72.39	0.6374	292.4	3997

Table 9. Static Short Beam Shear Test Results for a [0] AS/3501 Laminate*

Specimen	Width (cm)	Thickness (cm)	Shear Strength (MPa)	Ultimate Shear Strain (μcm/cm)	Shear Modulus (GPa)
SB1	0.978	1.27	86.19	18,780	5.69
SB2	"	"	97.91	26,030	5.57
SB3	0.965	"	91.70	23,620	6.01
		Average:	91.93	22,810	5.76

*Total length of specimen = 8.89cm

Test section length = 7.62cm

Table 10. Static Test Results for $[(0_4/\pm45_2/\mp45_2/0_4)_s]_s$ AS/3501 Laminates With and Without Interlaminar Delaminations

Specimen*	Width (cm)	Thickness (cm)	Debond Size** (cm)		Critical Load P_{cr}*** (N)
1	2.545	0.902	1.27 and 2.54****		3139.0
2	2.543	"	"		3090.0
3	2.545	"	"		2894.0
				Average:	3041.0
1-1	2.535	0.907	2.54		3188.5
1-2	2.558	0.914	"		3384.5
1-3	2.568	0.887	"		2305.5
1-4	2.532	0.881	"		2599.5
				Average:	2869.5
1/2-1	2.545	0.907	1.27		4660.0
1/2-2	"	0.914	"		4512.5
1/2-3	2.558	"	"		4782.5
				Average:	4651.5
0-1	2.543	0.912	0.0		4856.0(FF)*****
0-2	"	0.884	"		4463.5(FF)
0-3	2.548	0.917	"		4610.5(FF)
				Average:	4643.5

*Total length = 17.78cm; Test section = 15.24cm

**Debond was centered in the test section

***Catastrophic propagation of delamination

****One size on one half of the specimen

*****FF denotes flexural failure

Table 11. Summary of Fatigue Test Data for Unnotched [0] AS/3501 Laminates*

Specimen	Width (cm)	Thickness (cm)	S	N (cycles)	Residual Strength (MPa)	Residual Strain (μcm/cm)
0118	1.273	0.114	0.67	10^6	1547	11,210
0221	1.273	0.112	"	"	1806	12,410
0231	1.265	0.114	"	"	1726	11,230
				Average:	1693	11,617
0232	1.275	0.114	0.67	5×10^5	1830	12,210
0237	1.267	0.112	"	"	2035	12,540
0228	1.278	0.109	"	"	1806	12,750
				Average:	1890	12,500
0311	1.262	0.117	0.80	71640	FF**	

*Total length of specimen = 22.86cm; Test section length = 15.24cm

**FF denotes fatigue failure

-51-

Table 12. Summary of Fatigue Test Data for [±45]$_s$ AS/3501 Laminates (R=0.1)

Specimen*	Width (cm)	Thickness (cm)	S	Frequency (Hertz)	N (cycles)	Residual Strength (MPa)	Residual Modulus (GPa)
4213	2.535	0.114	0.45	30	5x10^4	101.3	5.37
4233	2.537	0.122	"	"	"	96.5	5.16
4134	2.527	0.117	"	"	"	-	-
					Average:	98.9	5.27
4212	2.537	0.114	0.45	30	10^4	105.1	5.48
4214	2.540	0.117	"	"	"	99.4	5.07
4143	"	"	"	"	"	-	-
					Average:	102.3	5.28
4234	2.540	0.109	0.55	30	5x10^4	109.0	6.18
4221	2.535	0.112	"	"	"	104.5	5.39
4124	2.537	0.117	"	"	"	-	-
					Average:	106.8	5.79
4222	2.540	0.114	0.55	30	10^4	104.2	5.67
4224	"	0.117	"	"	"	98.9	4.95
4142	"	"	"	"	"	-	-
					Average:	101.6	5.31
4114	2.540	0.117	0.55	10**	10^4	92.33	4.66
4211	2.535	"	"	"	"	-	-
4232	2.543	0.122	"	"	"	-	-

*Total length of specimen = 22.86cm; Test section length = 15.24cm.

**The steady state temperature for 30Hz was 145° while that for 10Hz was about 90°F.

Table 13. S-N Data for Unnotched $[45/0/-45/0]_s$ AS/3501 Laminates

Specimen*	Width (cm)	Thickness (cm)	S	N to Failure (cycles)
X161	3.813	0.114	0.8	14,300
X441	3.805	0.117	"	860
X131	3.813	"	0.75	6,970
X162	3.820	"	"	1,500

*Total length = 30.48 cm

Test specimen length = 22.86 cm

Table 14. Residual Properties for Unnotched [45/0/-45/0]$_s$ AS/3501 Laminates after N cycles (30Hz)

Specimen*	Width (cm)	Thickness (cm)	S	N (cycles)	Residual Strength (MPa)	Residual Modulus (GPa)
X121	3.820	0.117	0.8	5000	855.1	73.98
X123	3.813	"	0.75	"	779.9	73.22
X122	3.823	"	0.67	5×10^5	876.4	68.49
X111	"	"	"	"	898.3	72.46
X163	"	"	"	"	788.8	69.91
				Average:	854.5	70.29
X112	3.825	"	"	10^6	859.4	73.02
X132	"	"	"	"	886.8	69.84
X133	3.818	0.114	"	"	852.2	66.79
				Average:	866.1	69.88

*Total length = 30.48cm

Test section = 22.86cm

Table 15. Summary of Fatigue Test Data for Notched $[45/0/-45/0]_s$ AS/3501 Laminates (R=0.1 at 30Hz)*

Specimen**	Width (cm)	Thickness (cm)	S	N (cycles)	Residual Strength (MPa)	Residual Modulus (GPa)
X242	3.807	0.114	0.67	10^6	314.8	72.0
X212	"	0.119	"	"	316.5	69.8
				Average:	315.7	70.9
X313	3.813	0.117	"	5×10^5	325.1	75.2
X252	3.805	0.114	"	"	299.3	71.1
				Average:	312.2	73.2
X253	3.800	"	"	10^5	288.4	74.5
X243	3.797	0.117	"	"	295.6	75.6
				Average:	292.0	75.1
X231	3.787	0.112	0.8	10^6	305.2	70.7
X232	3.805	0.114	"	"	319.5	67.3
				Average:	312.4	69.0
X211	3.807	"	"	5×10^5	332.8	72.4
X323	3.813	0.117	"	"	325.1	74.1
				Average:	329.0	73.3
X262	3.807	0.119	"	10^5	312.2	71.0
X322	3.813	0.114	"	"	334.6	70.0
				Average:	323.4	70.5

*Total length of specimen = 30.48cm; Test Section Length = 22.86cm.

**Notch size = 0.9525cm.

Table 16. Computed γ_a Values for Two Delamination Sizes

Specimen*	a/L	P_{cr} (lb)	$P_{cr}/\sqrt{\gamma_a}$ From Analysis (lb.in)$^{1/2}$	γ_a (lb/in)
1-1	1/3	716.5	456.4	2.46
1-2	"	760.5	"	2.78
1-3	"	518.0	"	1.29
1-4	"	584.0	"	1.64
			Average:	2.04
1/2-1	1/6	1047.0	912.8	1.32
1/2-2	"	1014.0	"	1.23
1/2 3	"	1075.0	"	1.39
			Average:	1.31

*Debond is in the midplane and is centered in the test
section of length = 7.62 cm.
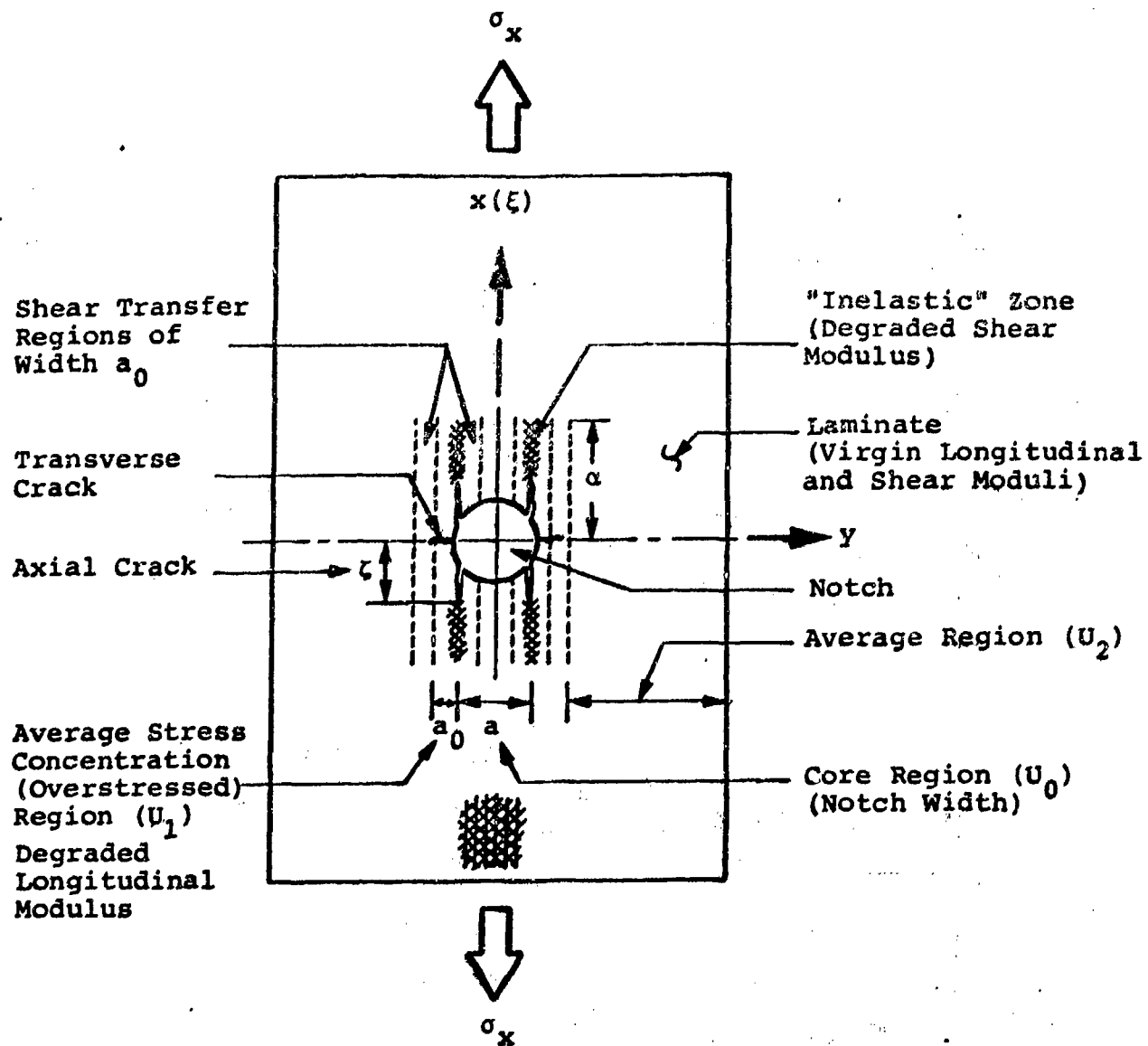
Figure 1. Minimechanics Model for a Notched Laminate
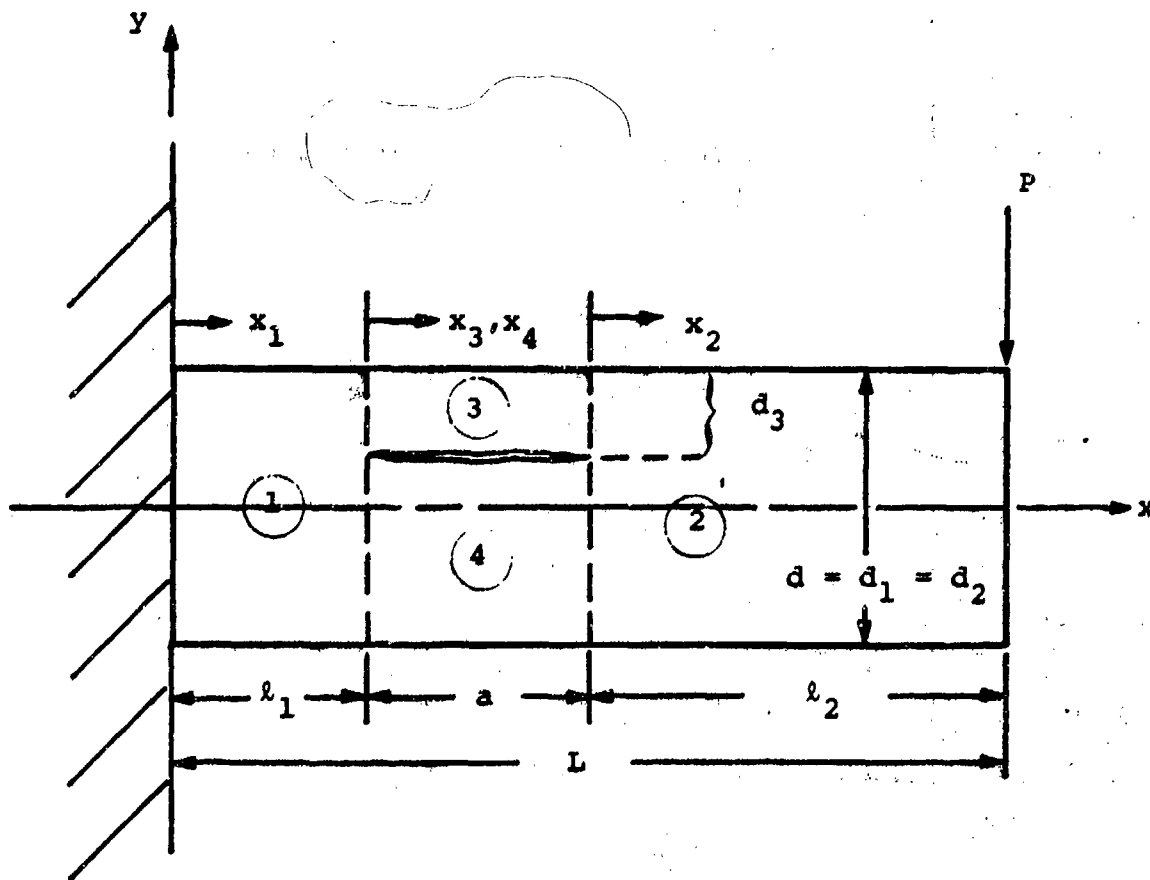
Figure 2. Tip-Loaded AS/3501 Layered, Cantilevered Beam
with an Interlaminar Delamination
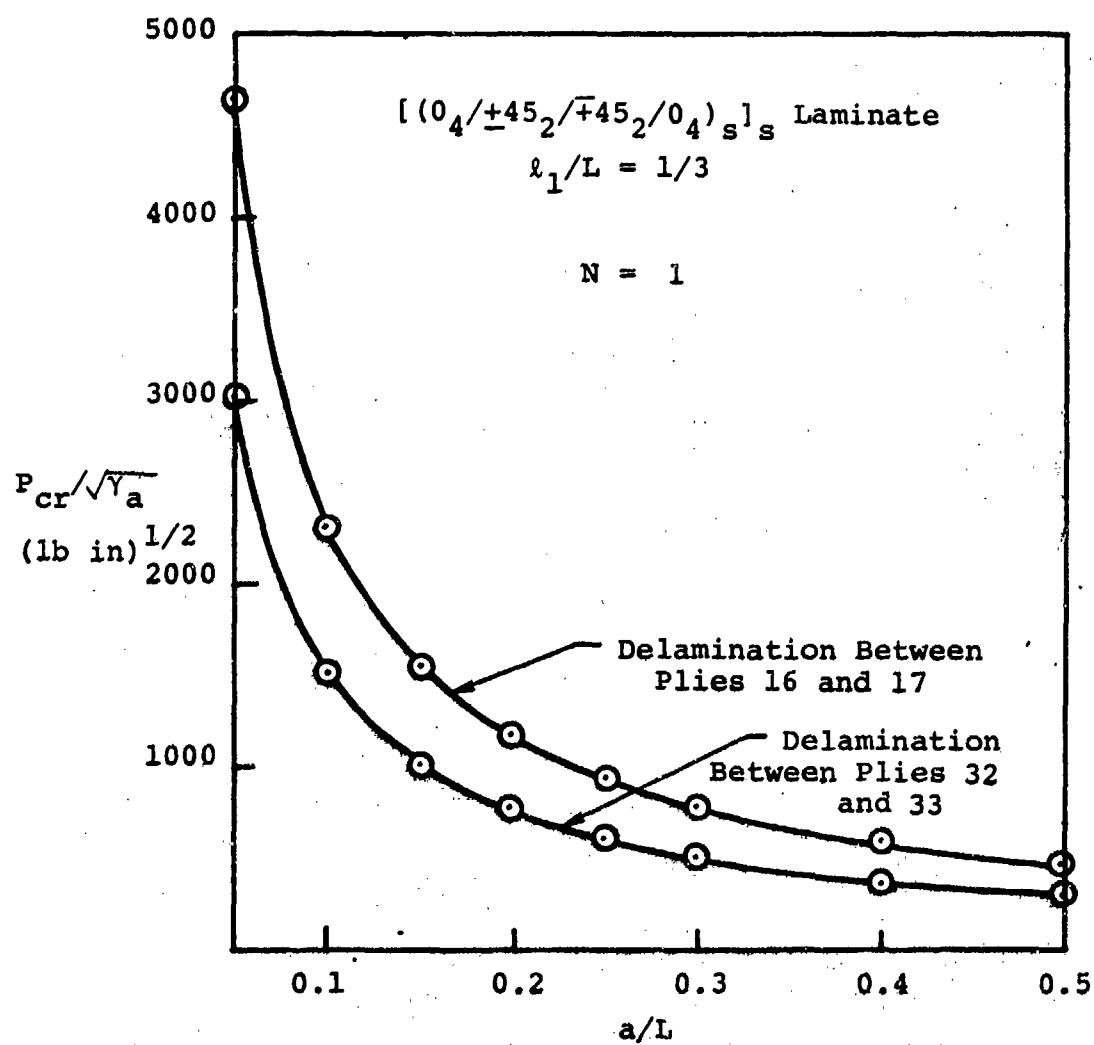
Figure 3. Effect of Crack Location on the Critical Delamination Load for a $[(0_4/\pm45_2/\mp45_2/0_4)_s]_s$ Laminate
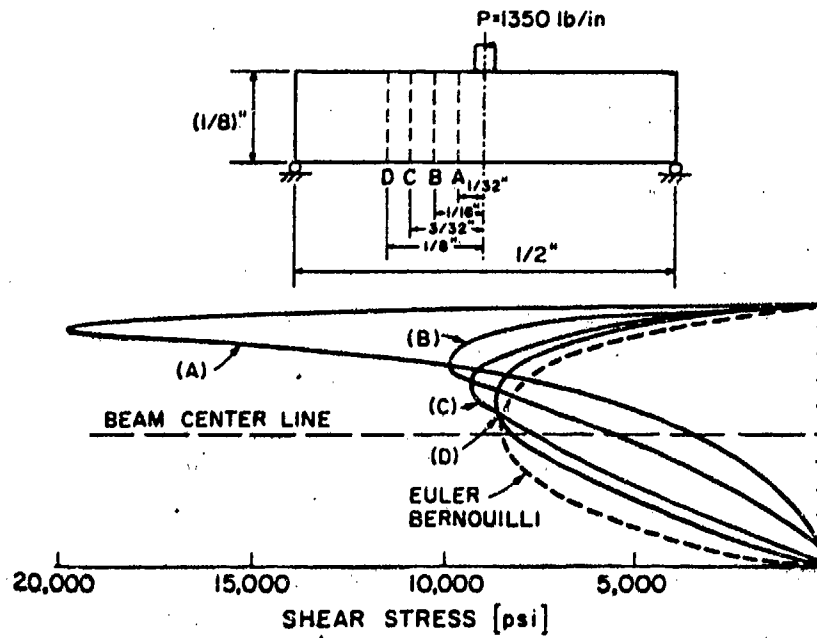
Figure 4. Shear Stress Distribution in Orthotropic Elastoplastic Short Beam Under Three-Point Bending at Four Cross Sections: A, B, C & D. (Reproduced from C. A. Berg, et al., "Analysis of Short Beam Bending of Fiber Reinforced Composites", ASTM-STP 497).
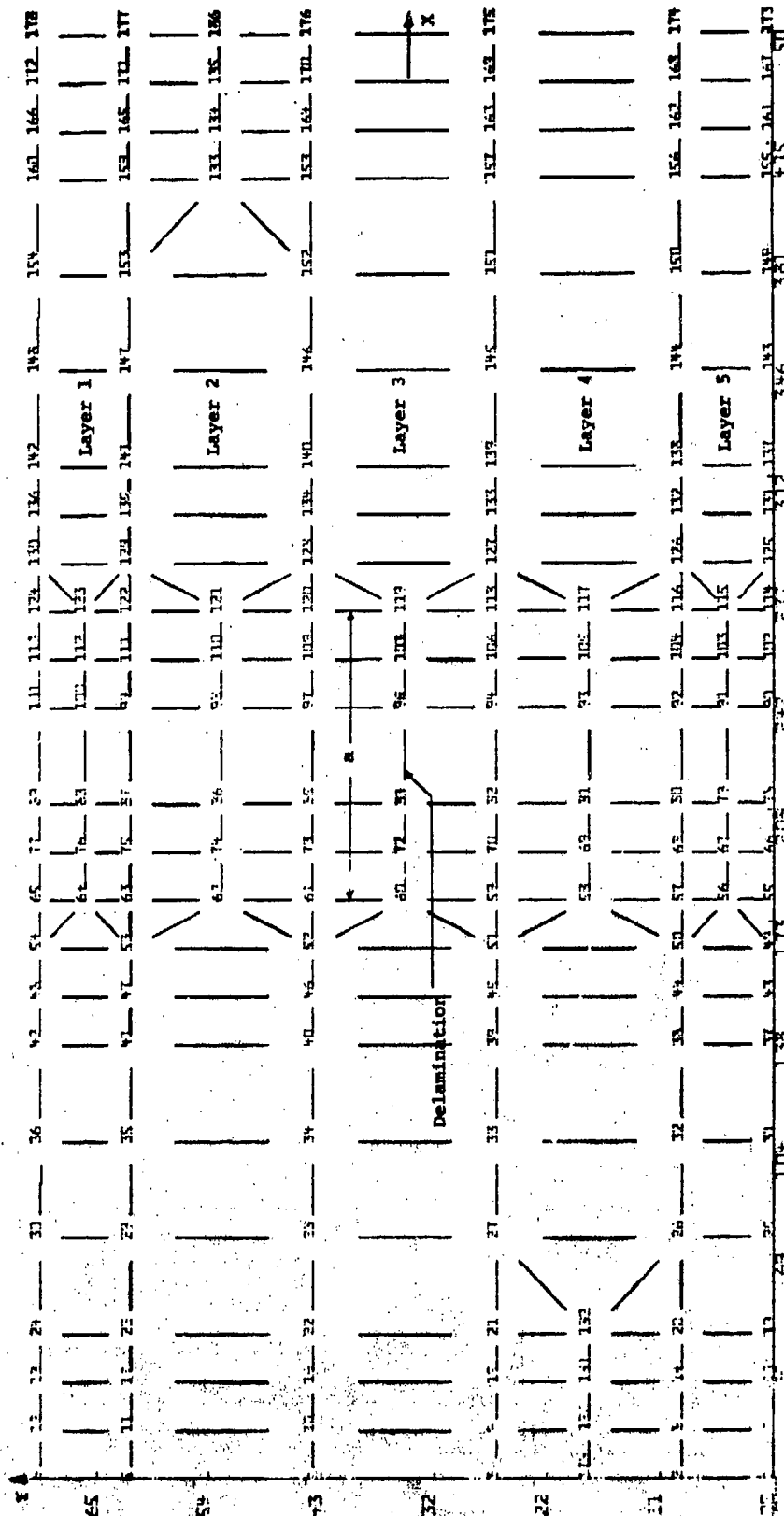
Figure 5. Mesh Geometry and Node Numbers for the Finite Element Model of a Debonded Beam
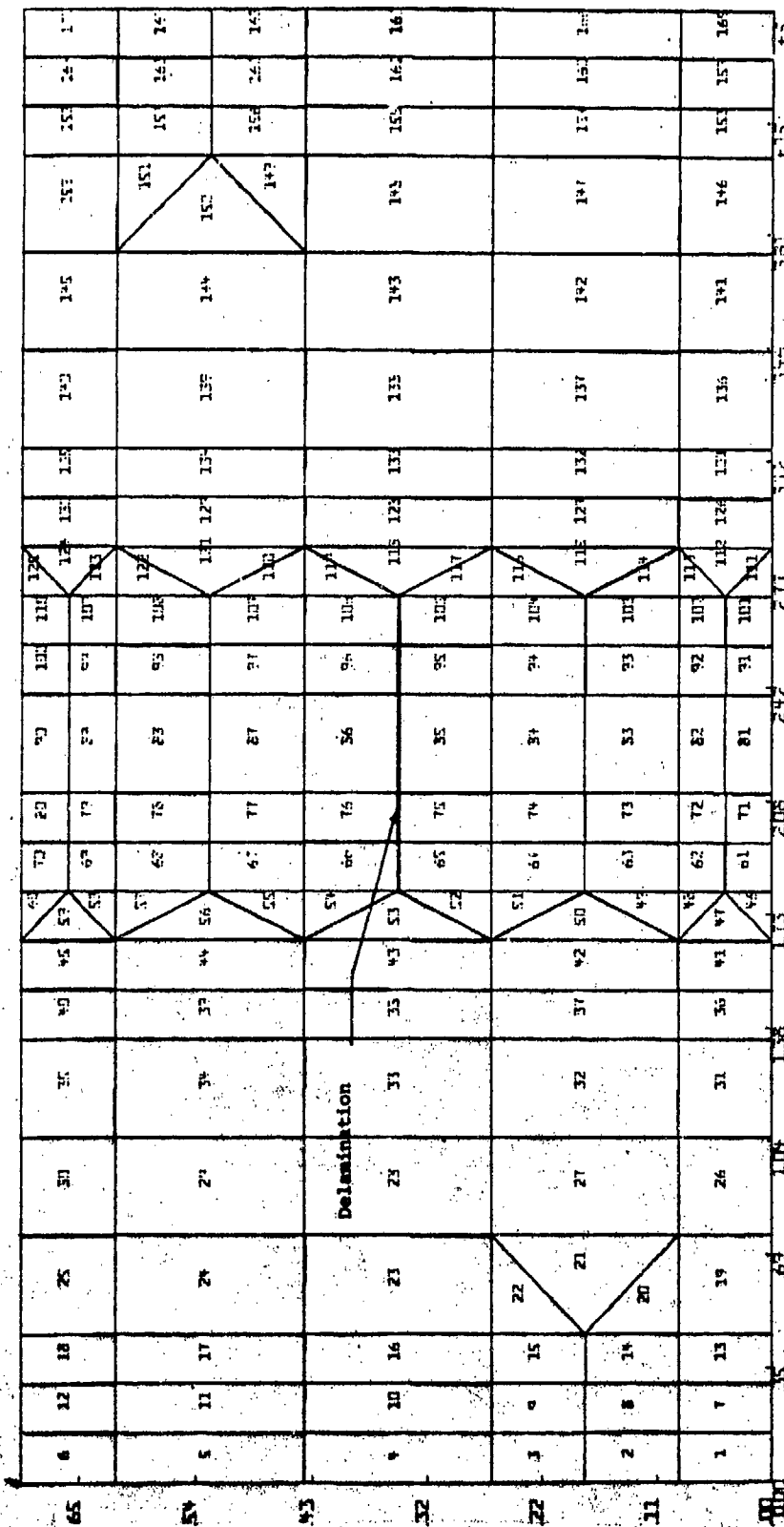
Figure 6. Element Numbering for the Finite Element Model
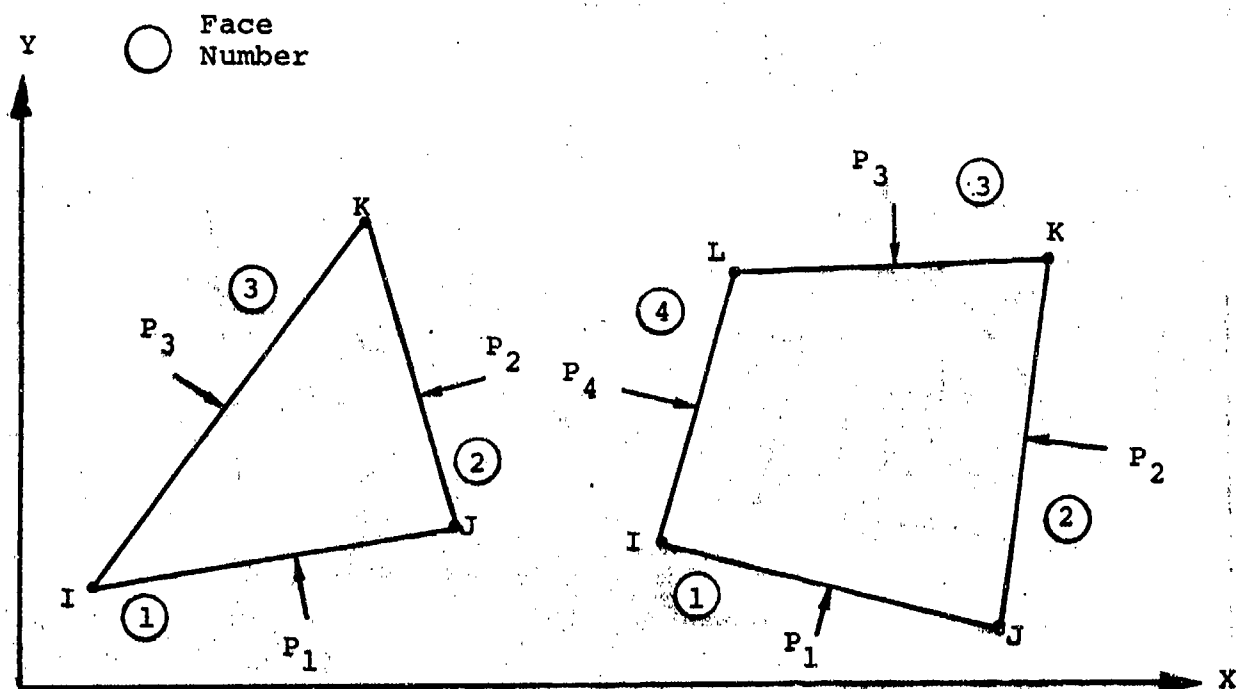
Figure 7. Triangular and Quadrilateral Constant Strain Elements
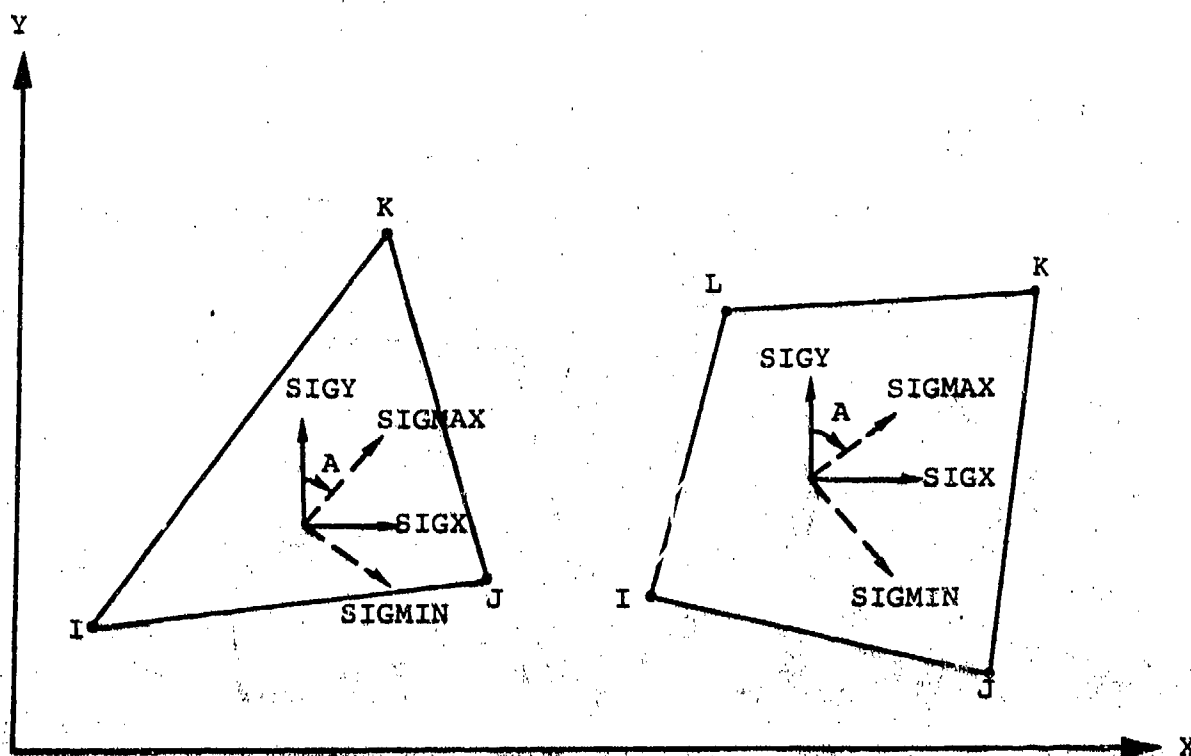
Figure 8.   Constant Strain Element Output
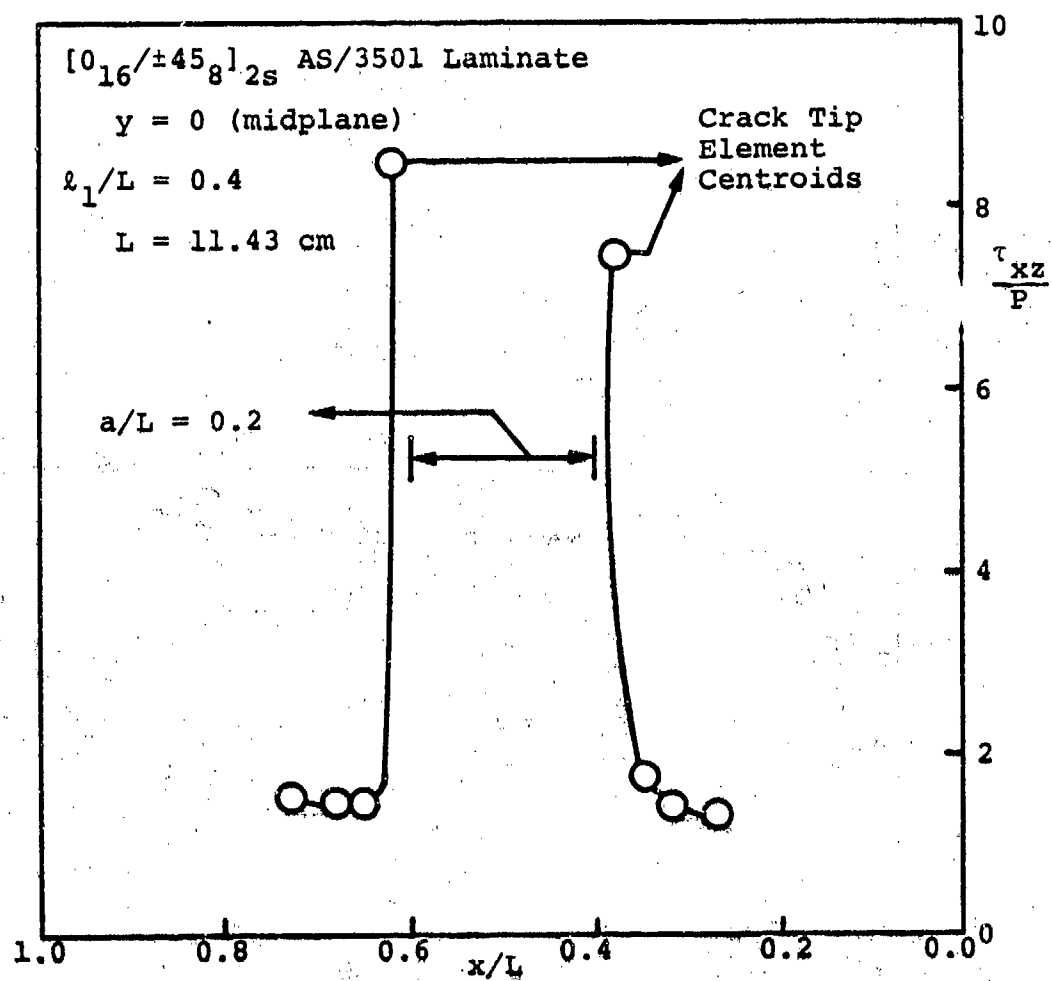
Figure 9. Centroidal Transverse Shear Stress Distribution Along the Interface Containing the Debond in a $[0_{16}/\pm45_8]_{2s}$ AS/3501 Laminated Beam from the Finite Element Analysis
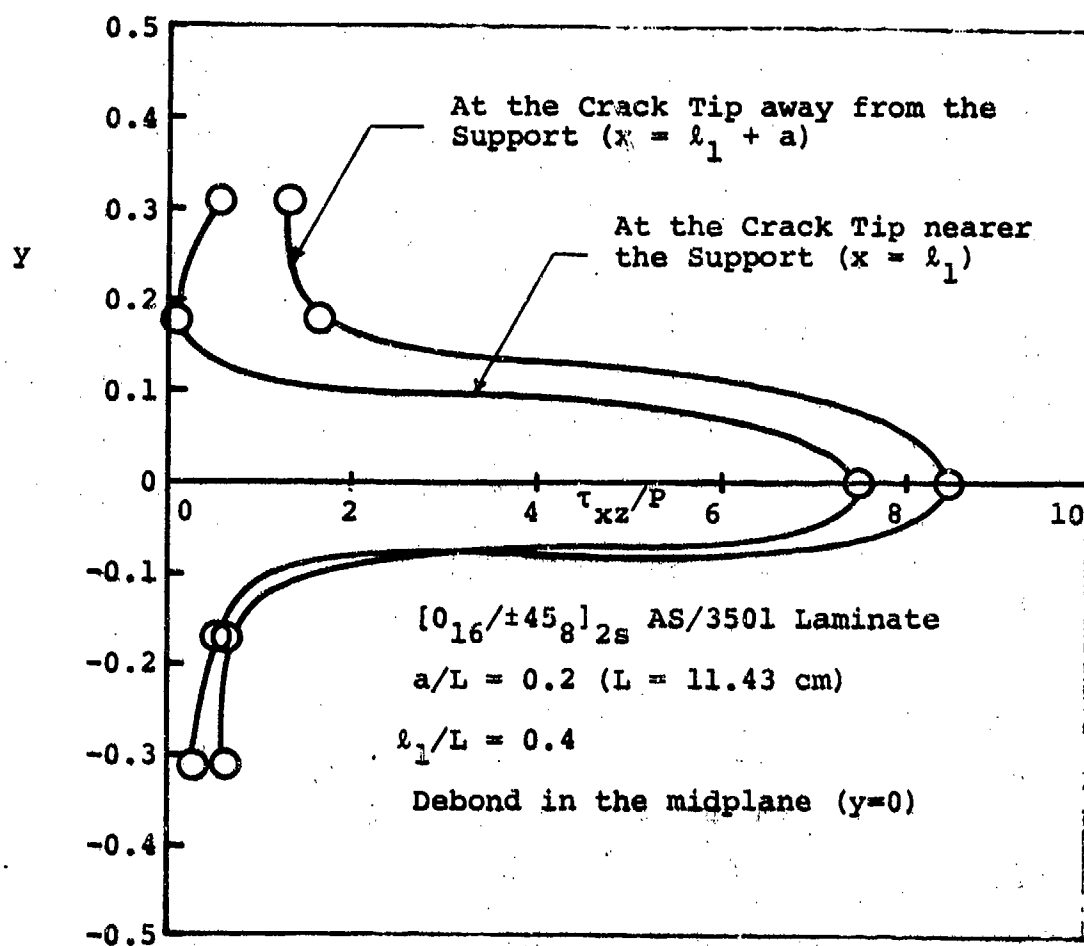
Figure 10. Centroidal Transverse Shear Stress Distributions at
the Crack Tips for a $[0_{16}/\pm45_8]_{2s}$ AS/3501 Laminated
Beam from the Finite Element Analysis
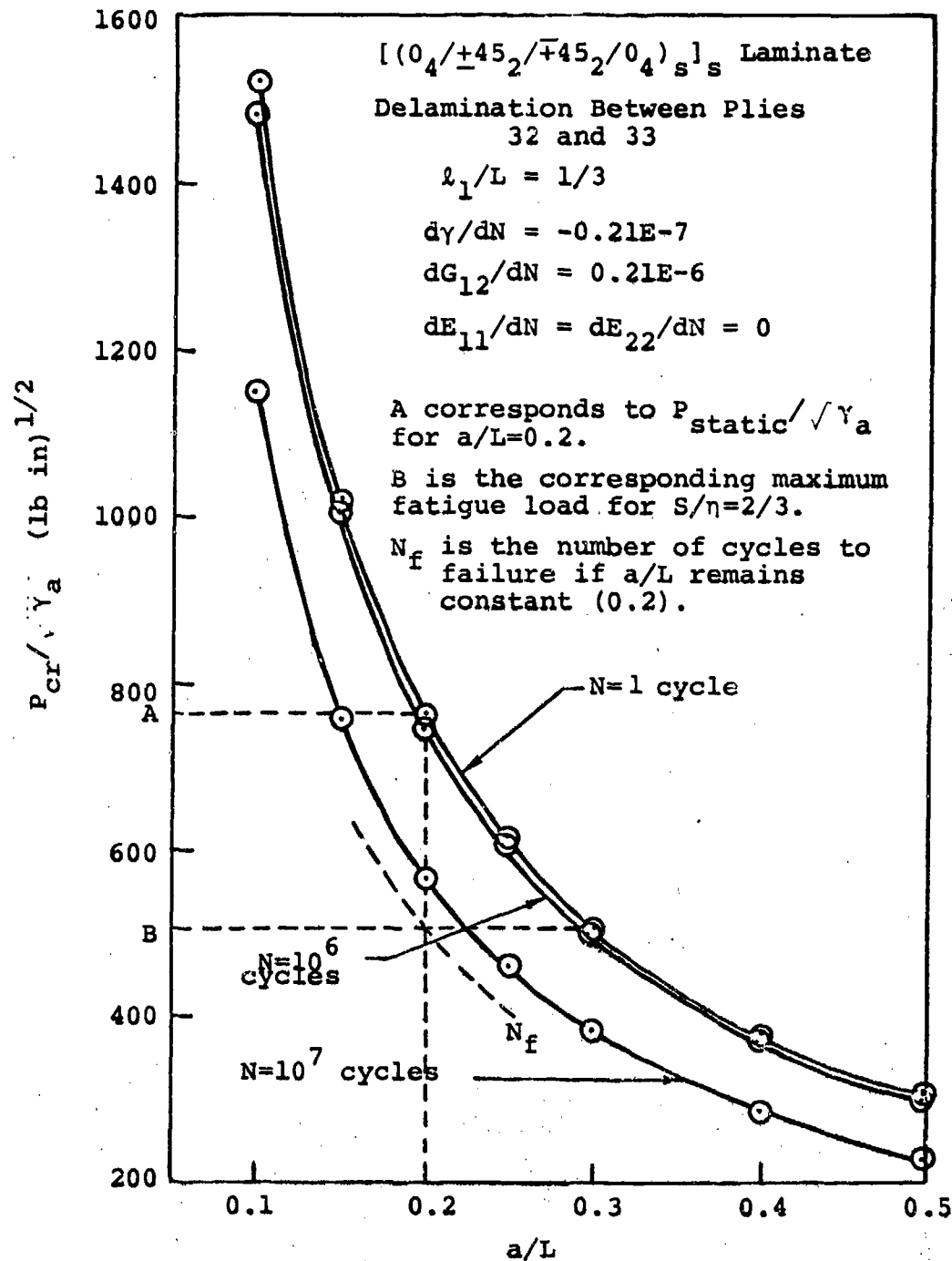
Figure 11. Effect of Fatigue Cycles on the Critical Delamination Load for a $[(0_4/\pm 45_2/\mp 45_2/0_4)_s]_s$ Laminate
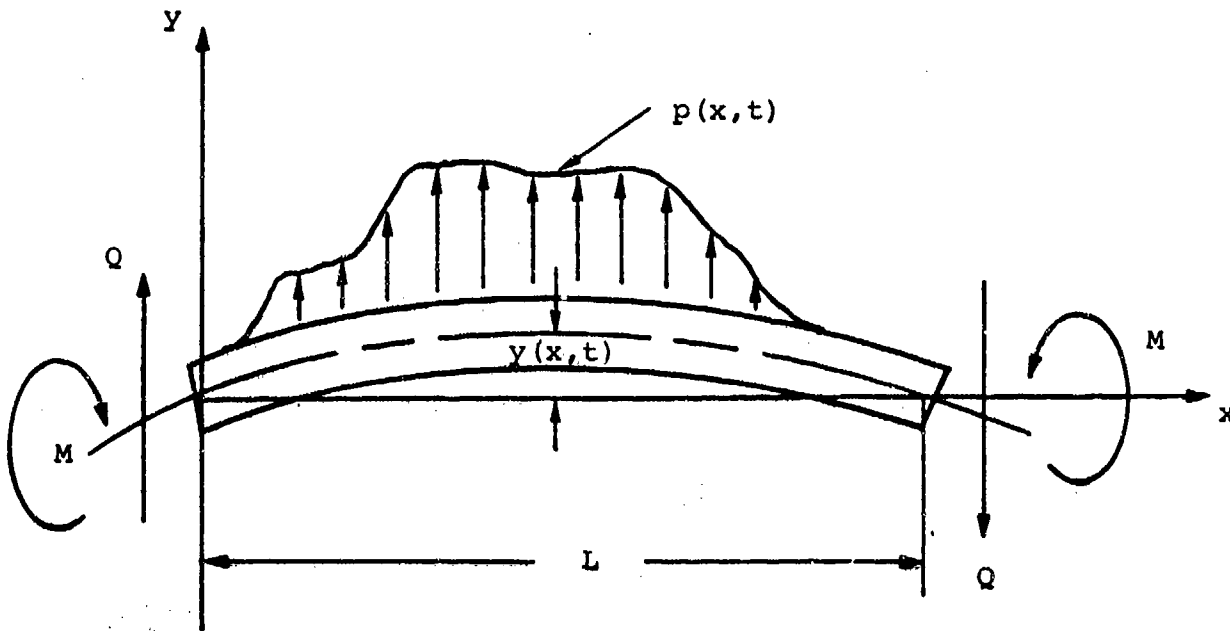
Figure 12. Beam Element and Sign Conventions Used in the Vibration Analysis
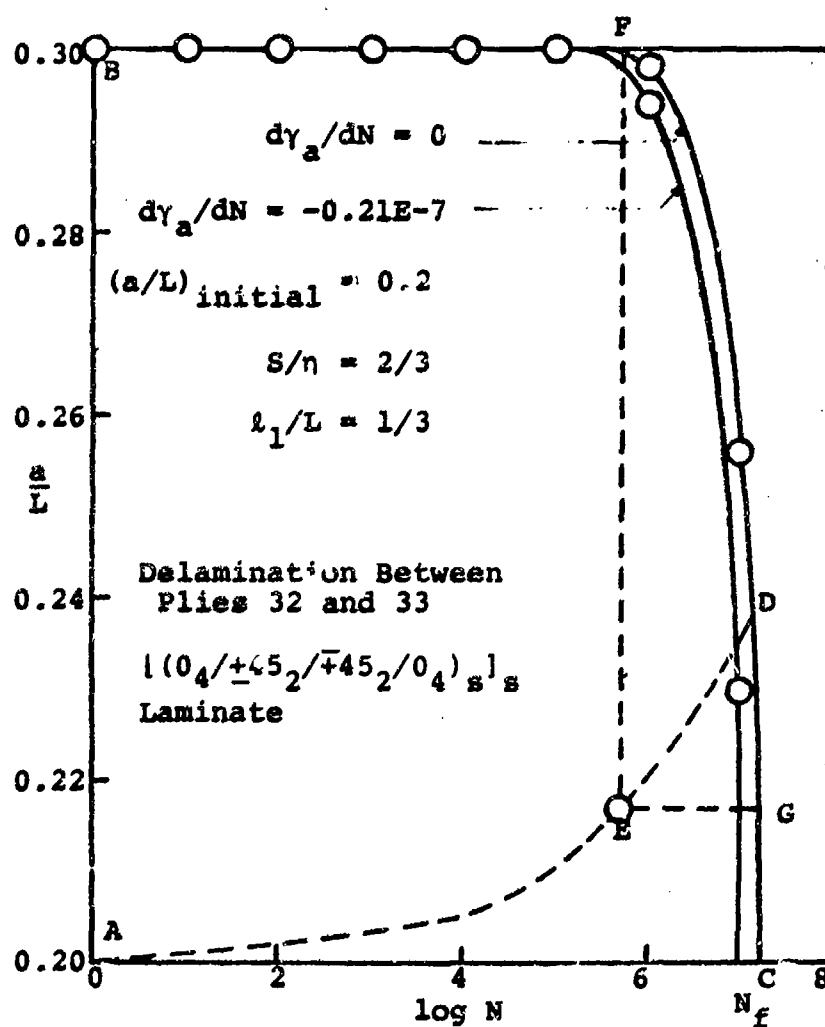
Figure 13. Catastrophic Crack Growth Boundary for an
Initial $a/L = 0.2$ and $S/\eta = 2/3$ for a
$[(0_4/\pm45_2/\mp45_2/0_4)_s]_s$ Laminate

SPECIMEN FABRICATION PROCEDURE

COMPOSITE PLATE CUT TO SIZE   END TAB APPLICATION   SPECIMEN

Figure 14.   "C" Scans of a Composite Plate after Fabrication,
            a Plate with End Tabs, and a Machined Specimen
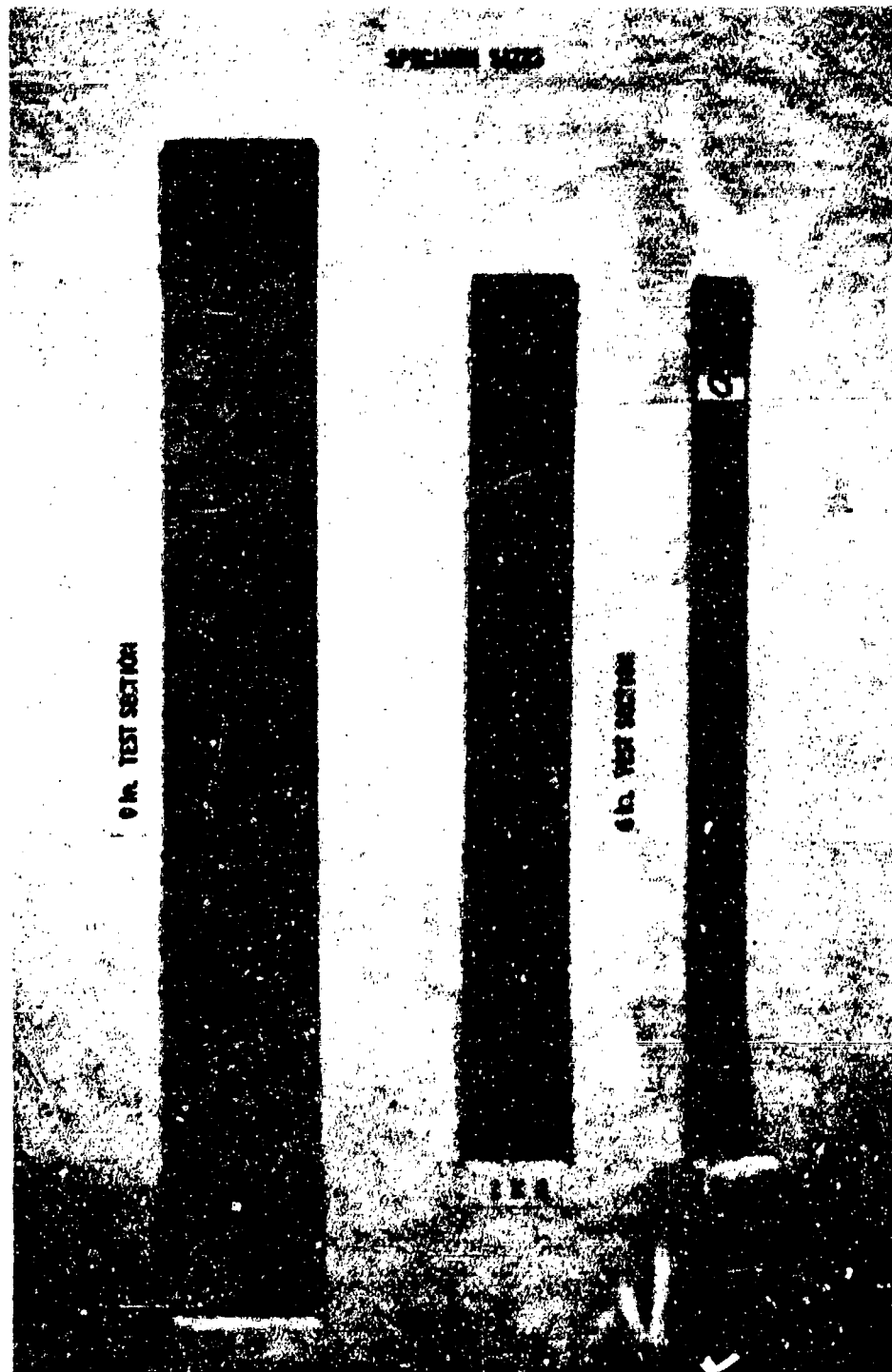
Figure 15. Geometries of AS/3501 Tension Test Specimens
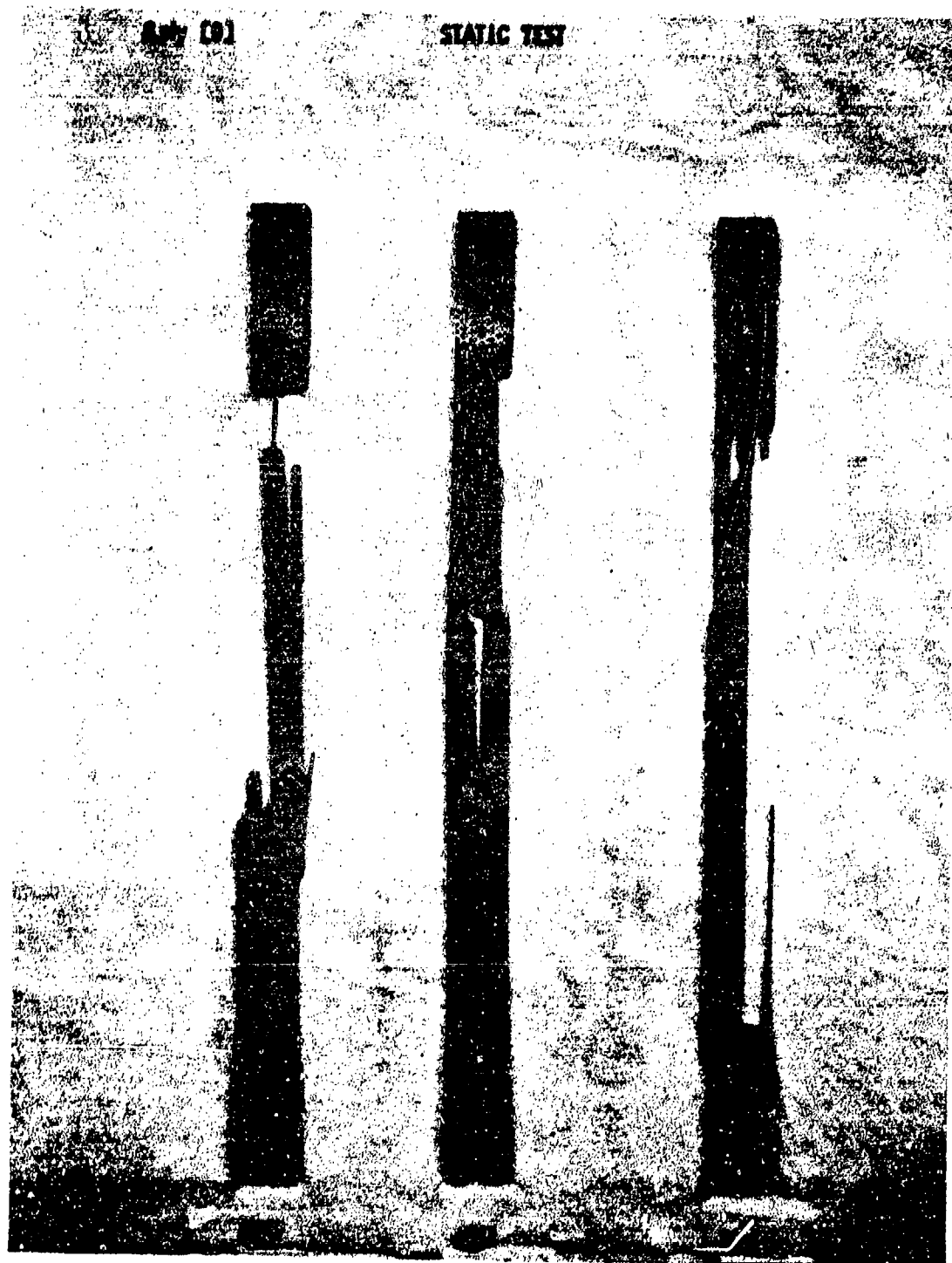
Figure 16. Failed 8-Ply [0] AS/3501 Specimens used in the Static Tensile Tests.
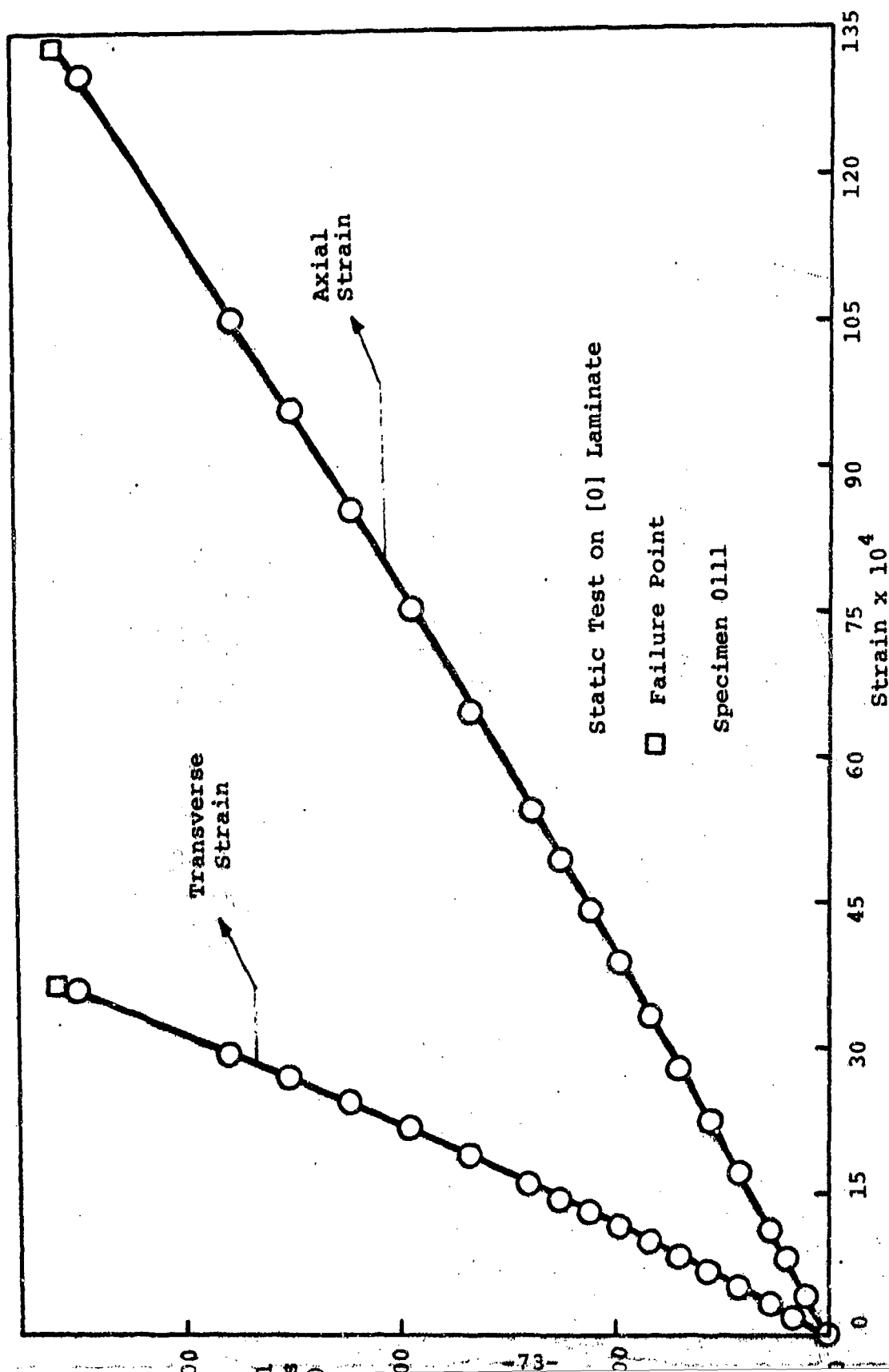
Figure 17. Typical Stress-Strain Curve for a [0] AS/3501 Laminate
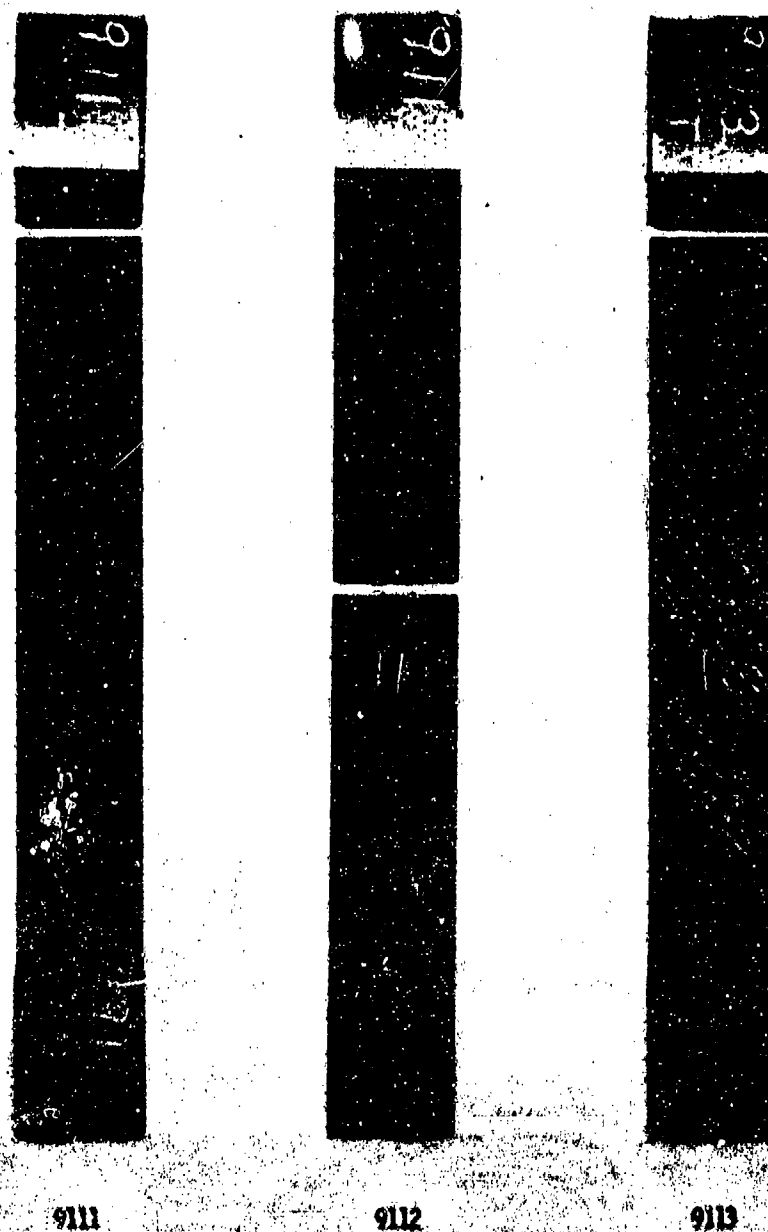
Figure 18.   Failed 8-Ply [90] AS/3501 Specimens used in the
             Static, Transverse Tension Tests
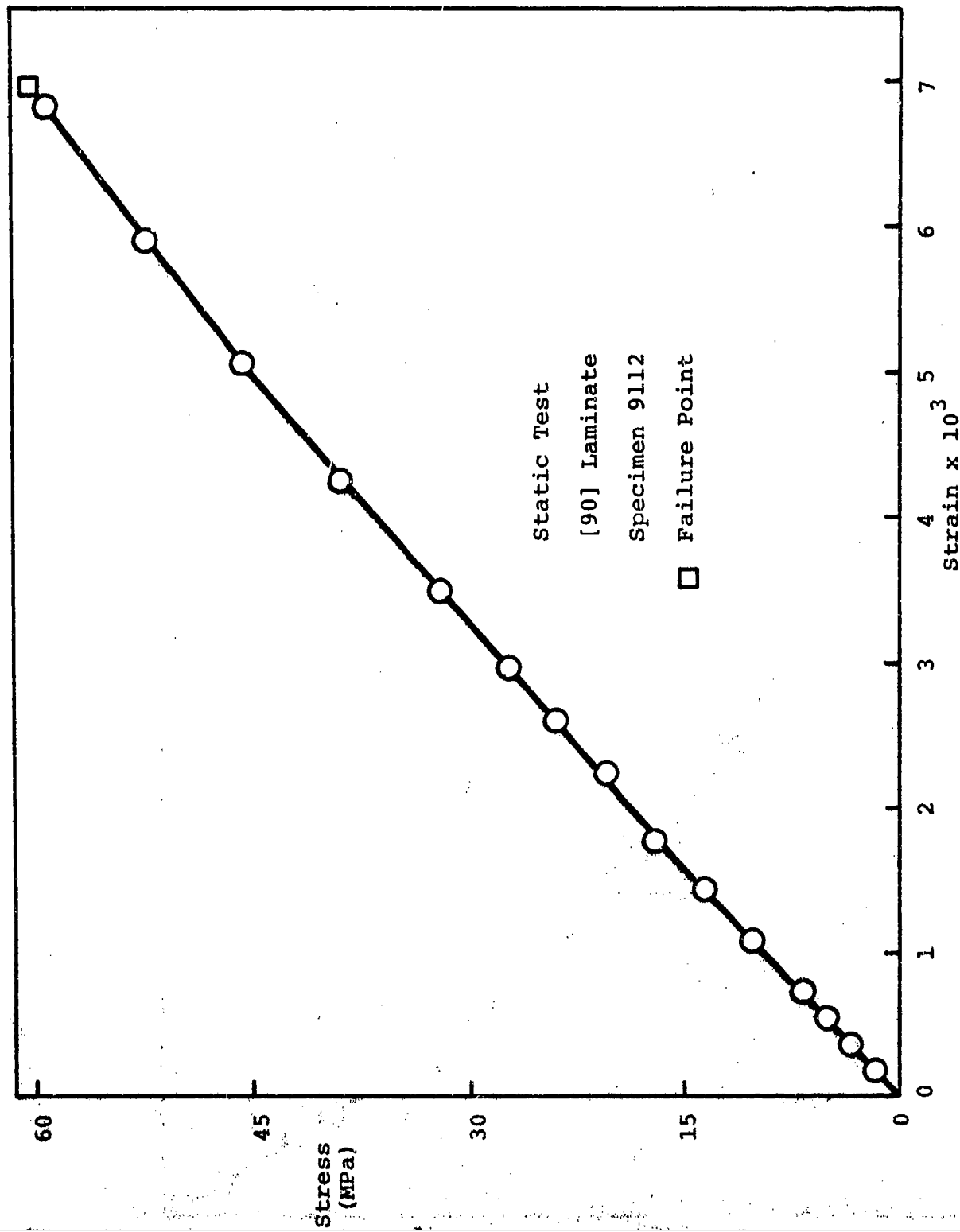
Figure 19. Typical Stress-Strain Curve for a [90] AS/3501 Laminate
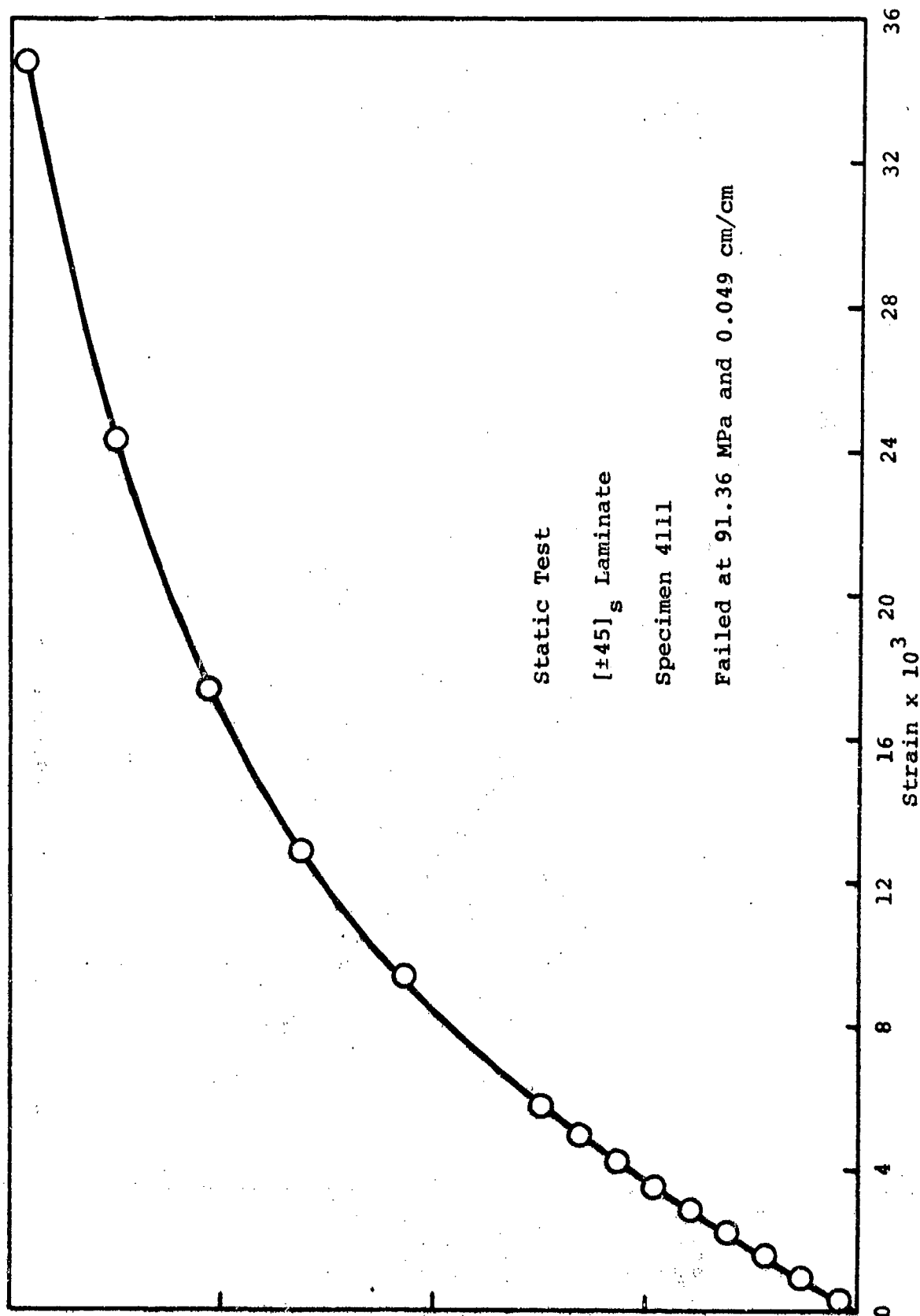
Figure 20. Typical Stress-Strain Curve for a $[\pm 45]_s$ AS/3501 Laminate.

Static Test

$[\pm 45]_s$ Laminate

Specimen 4111

Failed at 91.36 MPa and 0.049 cm/cm

Strain x 10^3
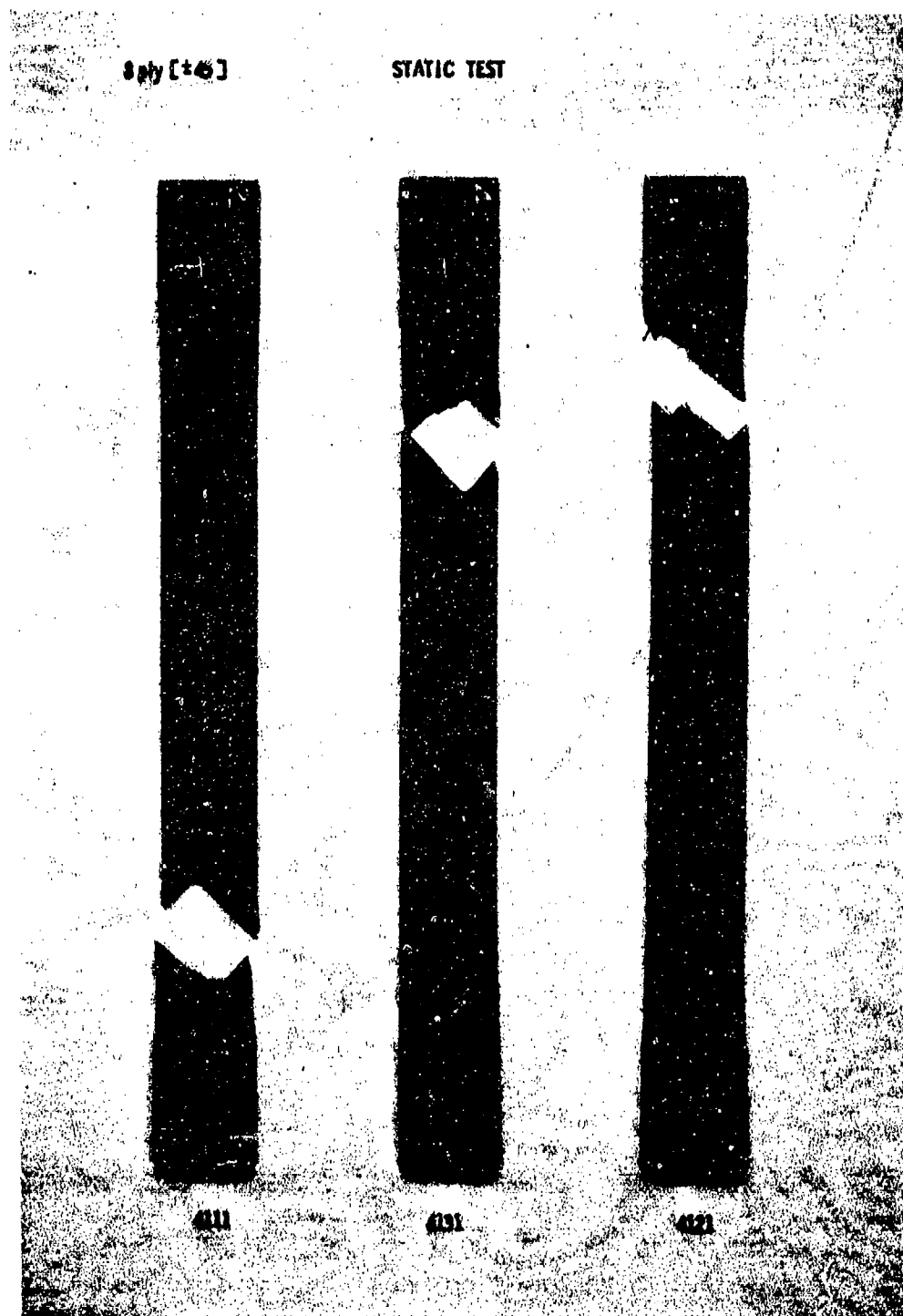
Figure 21. Failed 8-Ply [±45]$_s$ AS/3501 Specimens used in the Inplane Shear Tests
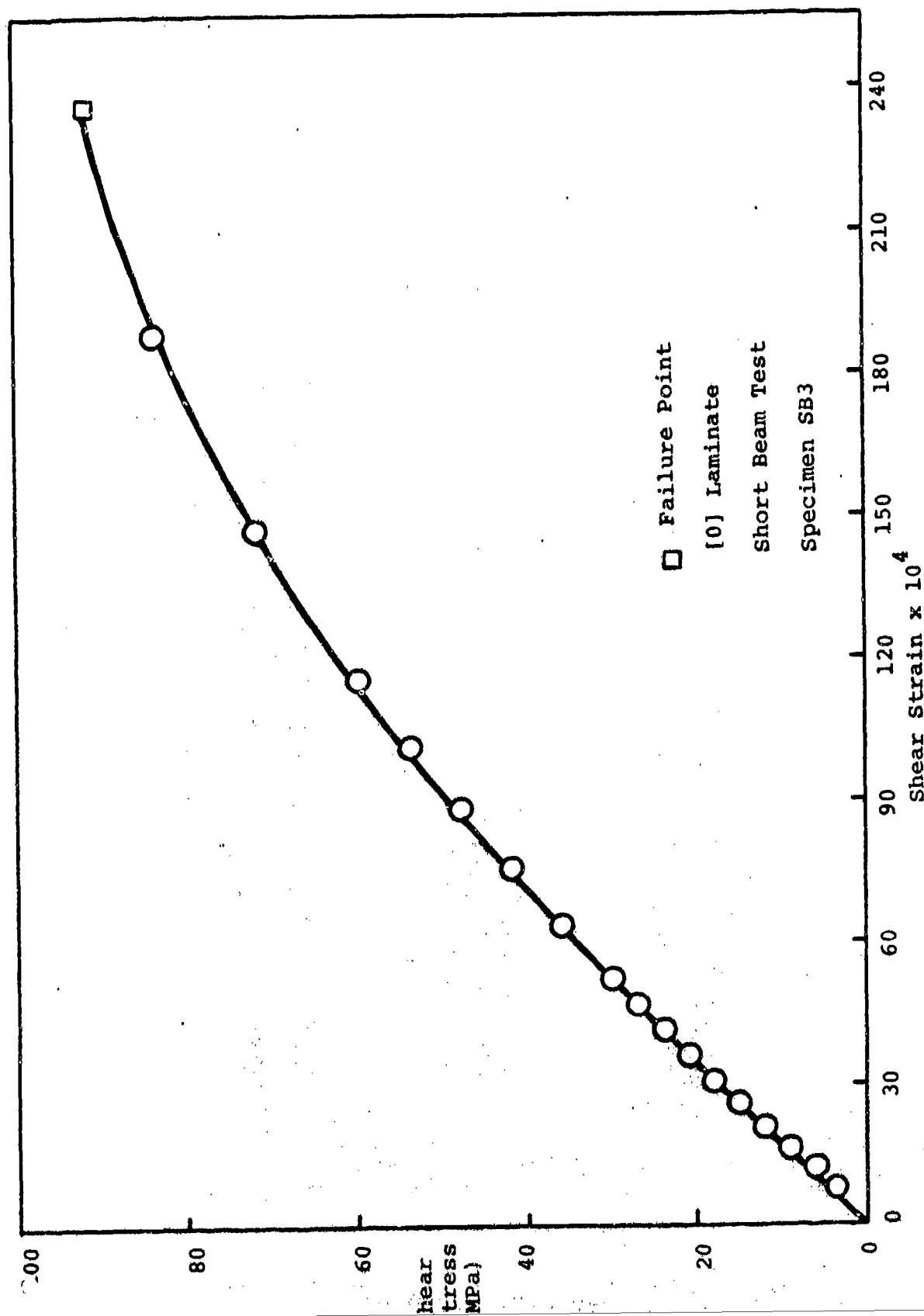
Figure 22. Transverse Shear Strength Data from a Short Beam Test on a [0] AS/3501 Laminate

SHORT BEAM SHEAR TEST

[0] ORIENTATION   ASPECT RATIO = 4
SPECIMEN HEIGHT = 0.5 in.

SPECIMEN TESTED TO INITIAL FAILURE

SPECIMENS TESTED TO COMPLETE FAILURE

Figure 23.   Thick [0] AS/3501 Specimens in the Short Beam
Shear Tests

Figure 24. Test Apparatus for the Short Beam Shear Tests, with a Mounted Specimen
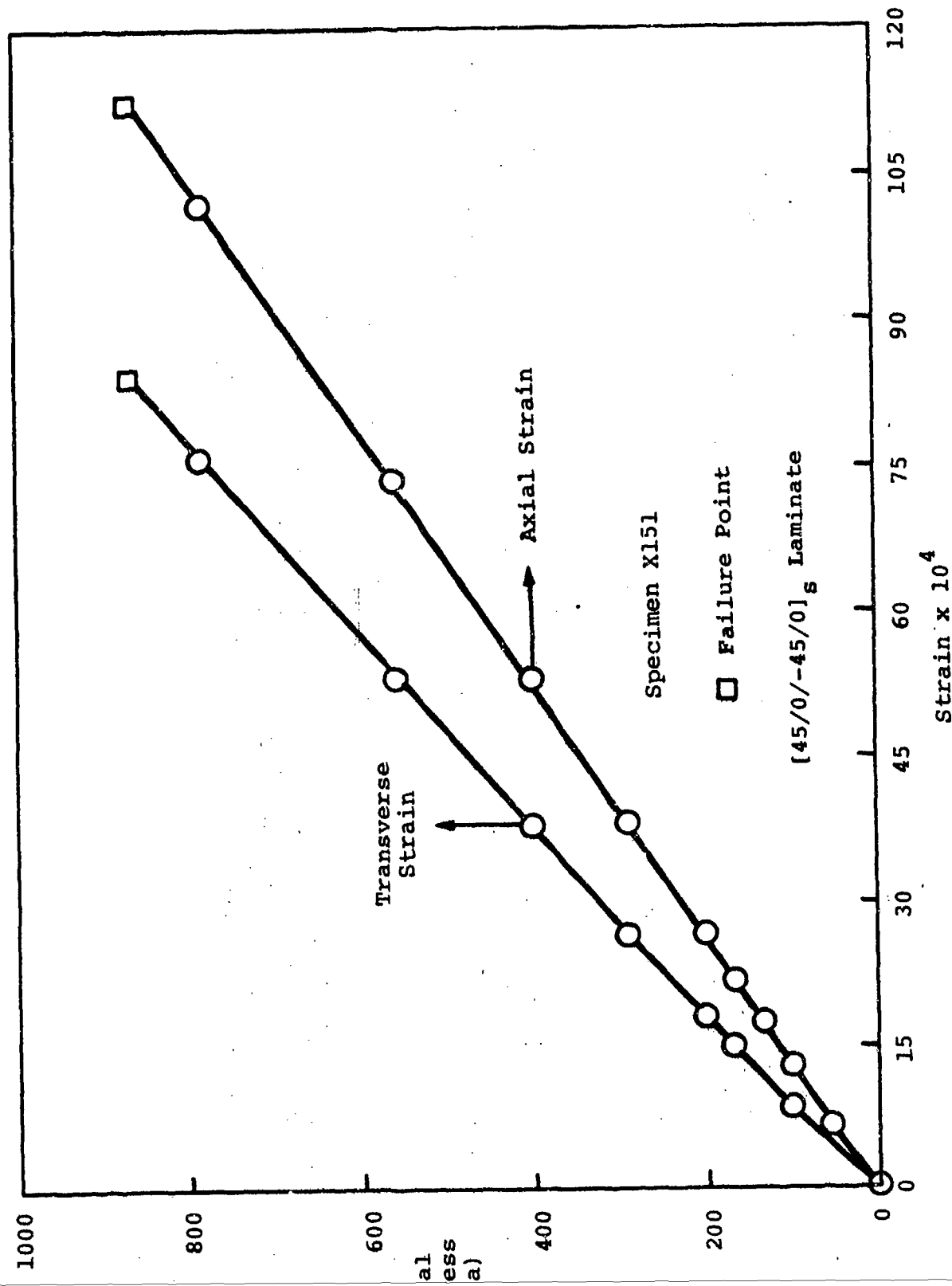
Figure 25. Typical Stress-Strain Curves for an Unnotched [45/0/-45/0]$_s$ AS/3501 Laminate

Figure 26. Unnotched $[45/0/-45/0]_s$ AS/3501 Laminate Specimens
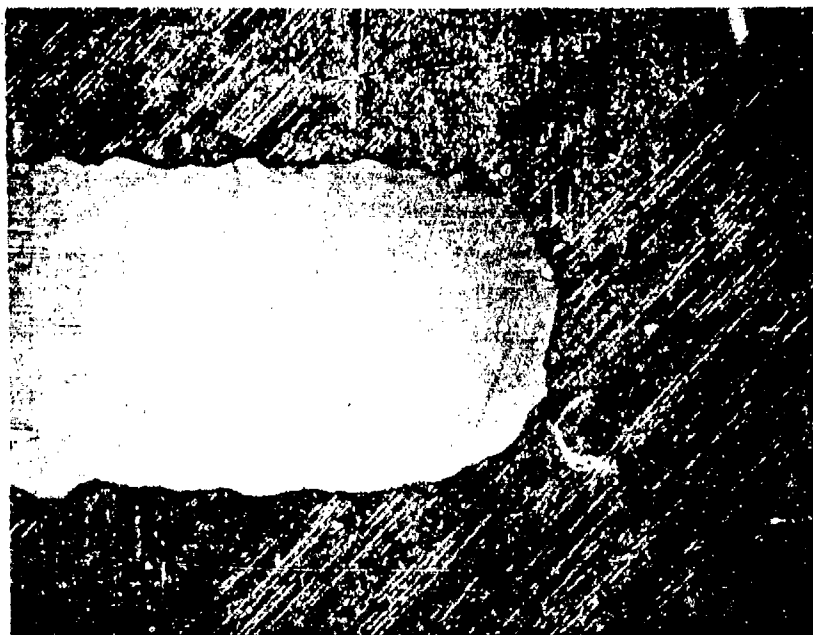
Figure 27.   A Magnified (X100) View of the Notch Tip
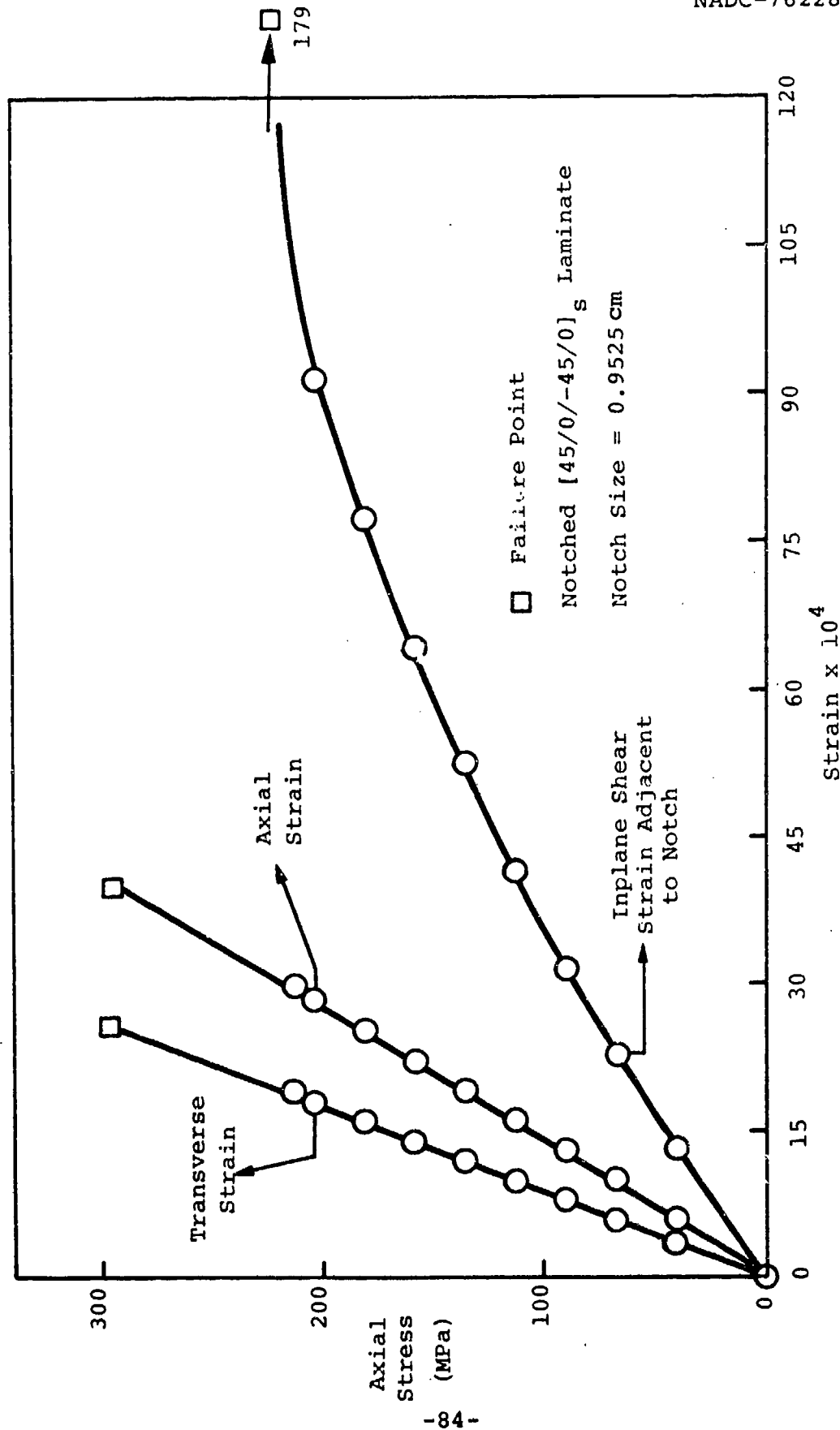
Figure 28. Typical Stress-Strain Curves for a Notched [45/0/-45/0]$_s$ AS/3501 Laminate
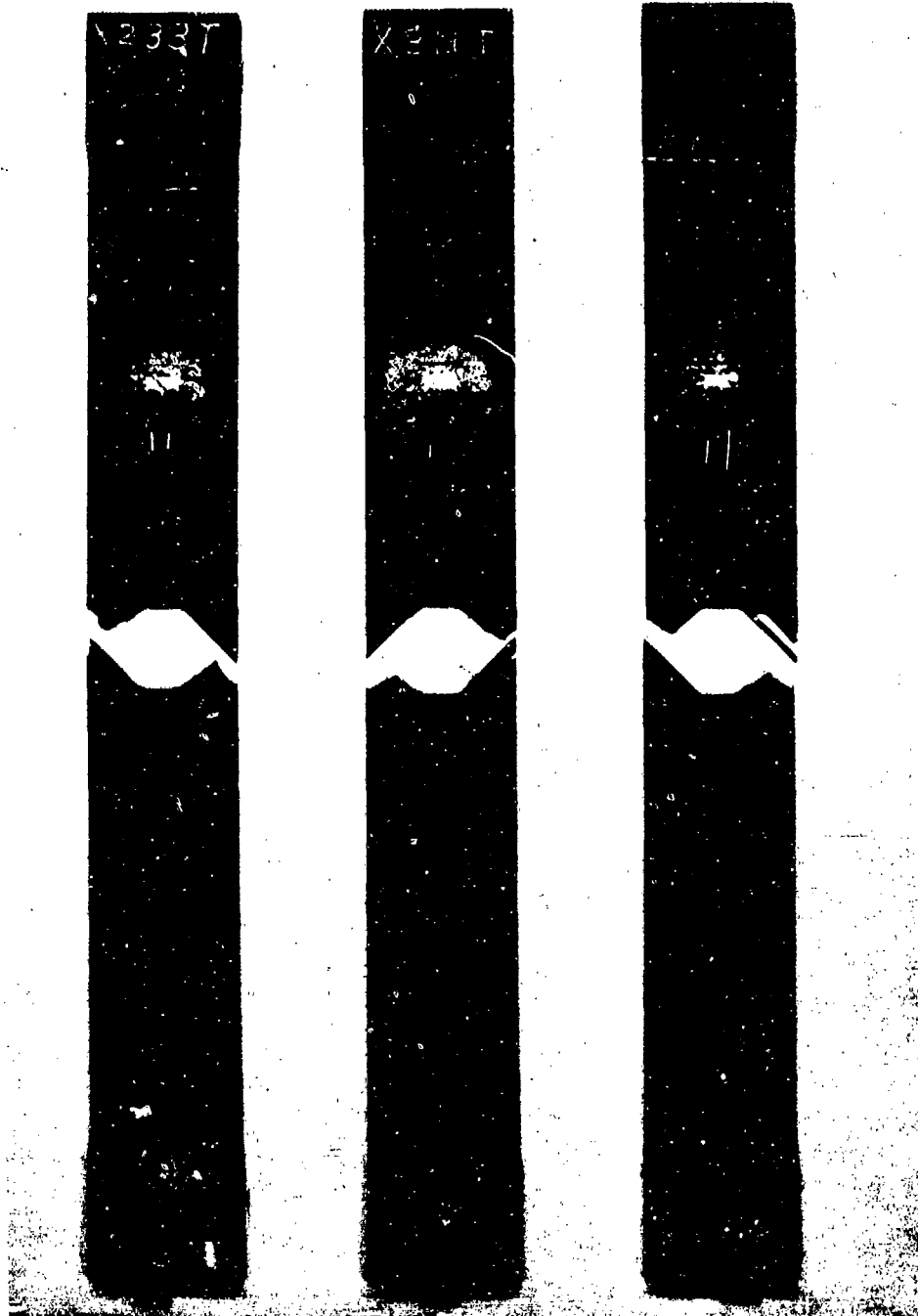
Figure 29. $[45/0/-45/0]_S$ AS/3501 Specimens used in the Slit Notch Static Tests
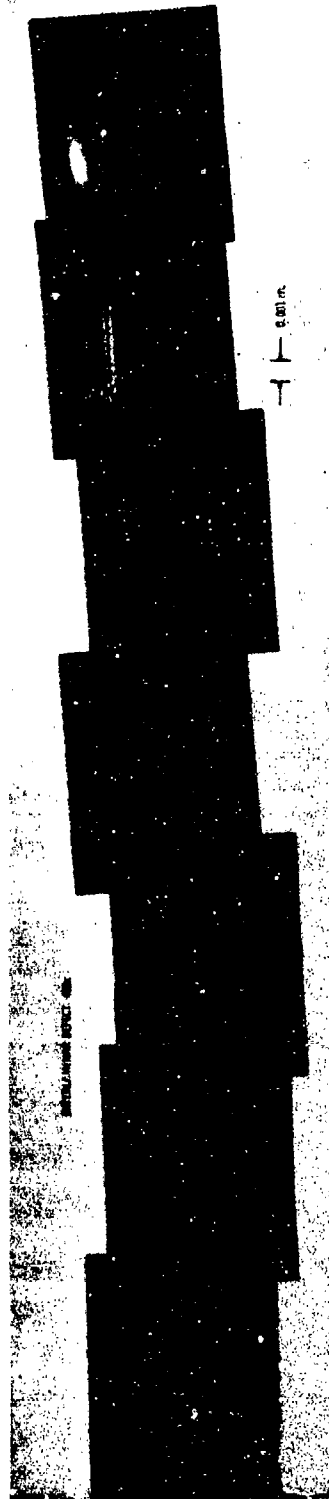
Figure 30. An Implanted Interlaminar Defect with a Magnification Factor of 400

INTERLAMINAR DEFECT STUDY
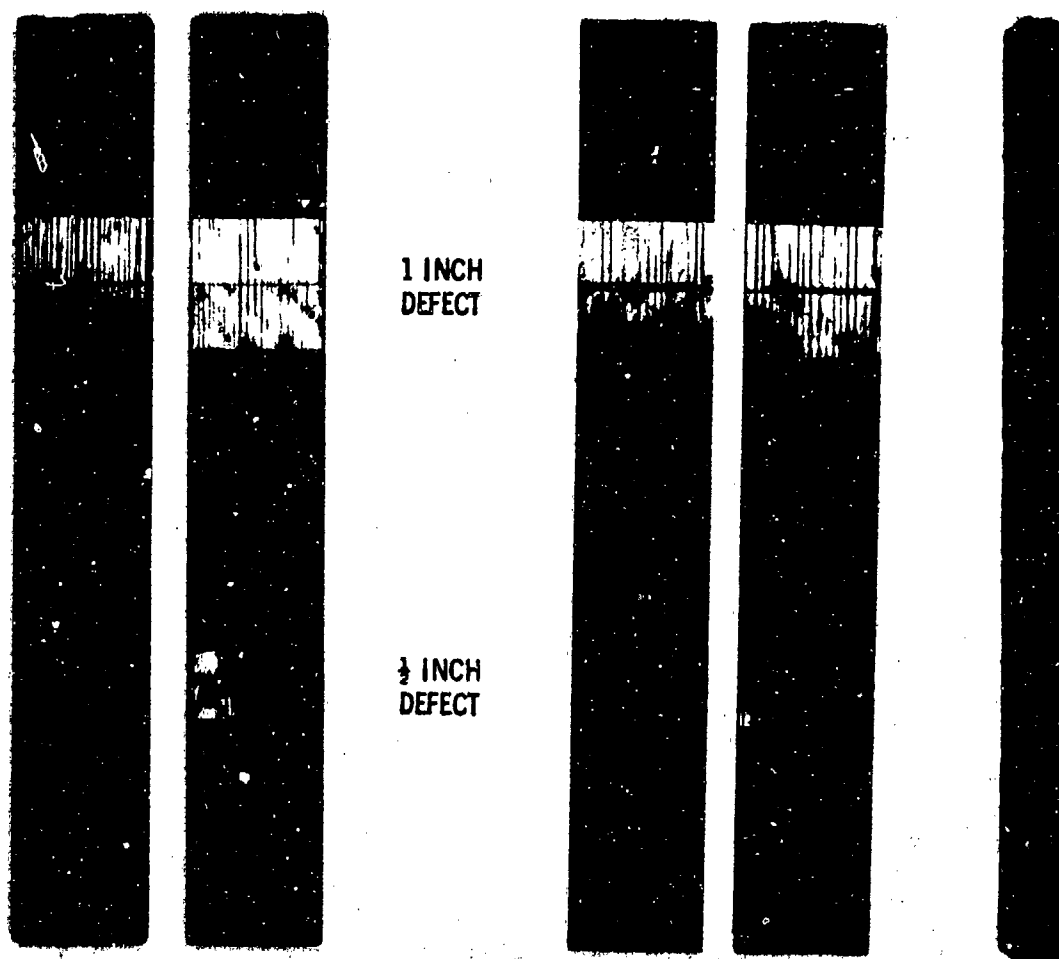
Figure 31. $[(0_4/+45_2/\overline{\mp}45_2/0_4)_s]_s$ AS/3501 Specimens, with a 2.54 cm and a 1.27 cm Debond Between Plies 32 and 33, Tested Flexurally to Cause Unstable Debond Growth to Failure
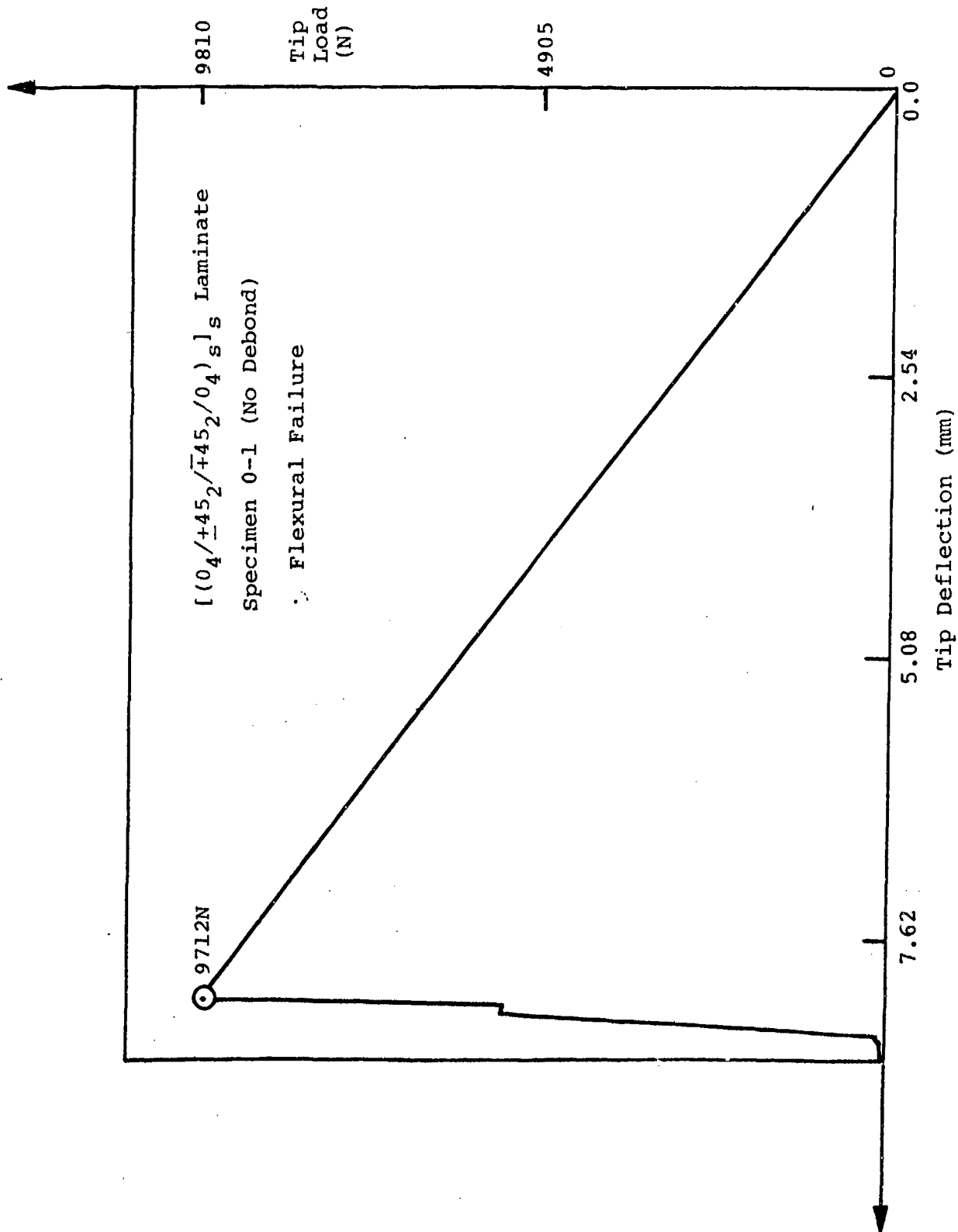
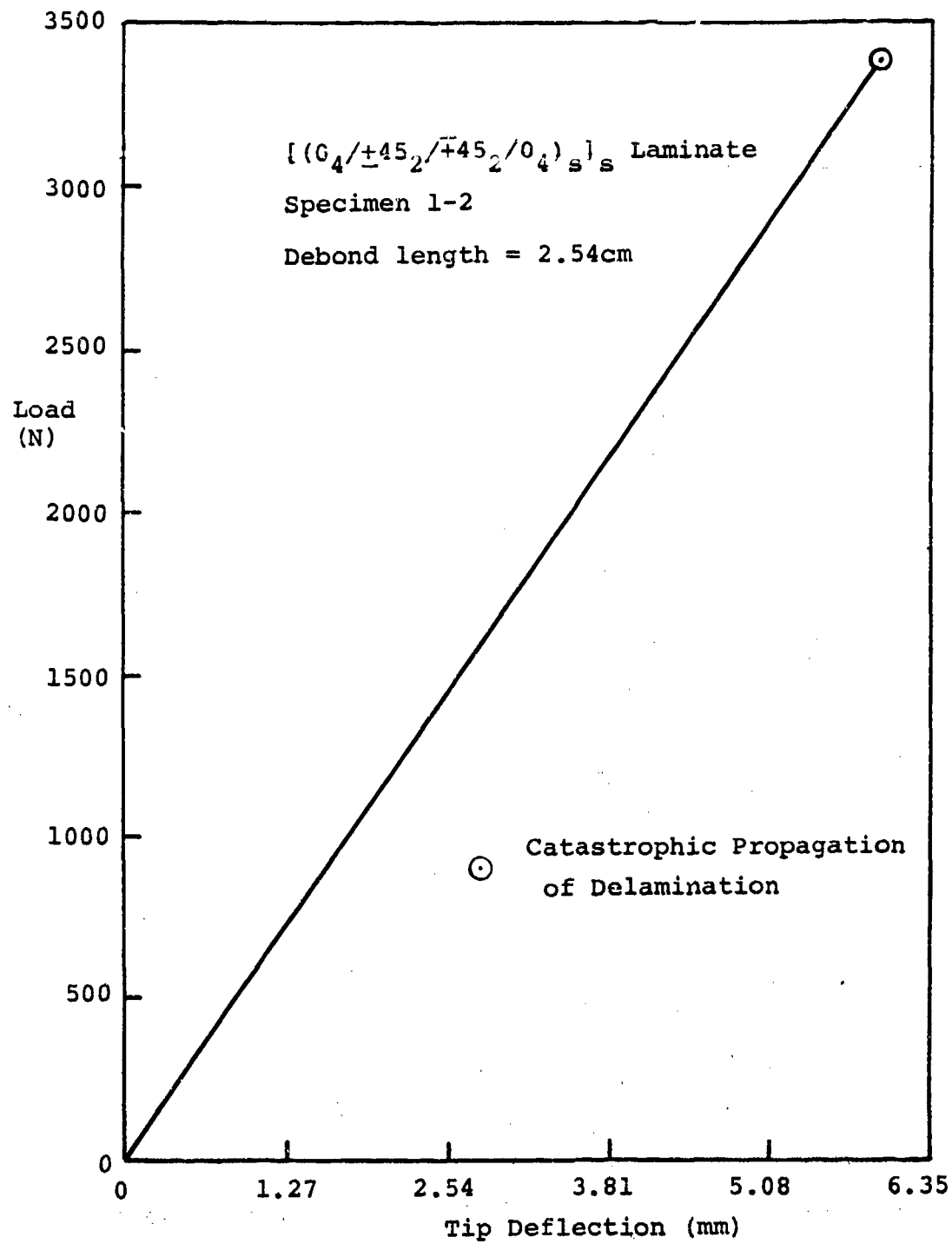Figure 32. Load-Deflection Behavior of a $[(0_4/\pm45_2/\mp45_2/0_4)_s]_s$ AS/3501 Beam with No Delamination

Figure 33. Variation of the $[(0_4/\pm45_2/\mp45_2/0_4)_s]_s$ AS/3501 Laminated Beam Tip Deflection with the Applied Tip Load
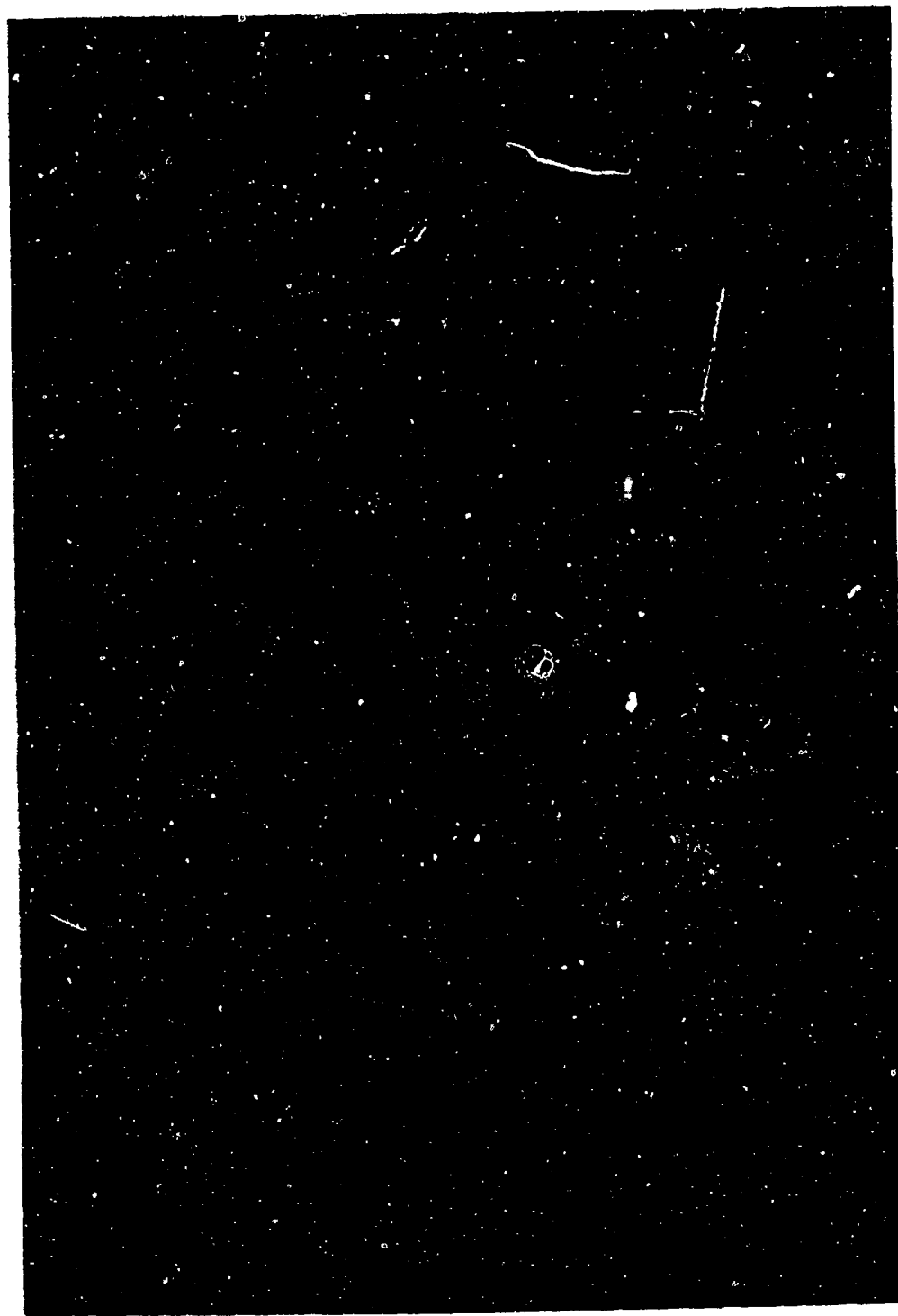
Figure 34. A Typical "C" Scan of a [45/0/-45/0]$_s$ AS/3501 Laminated Panel after Fabrication
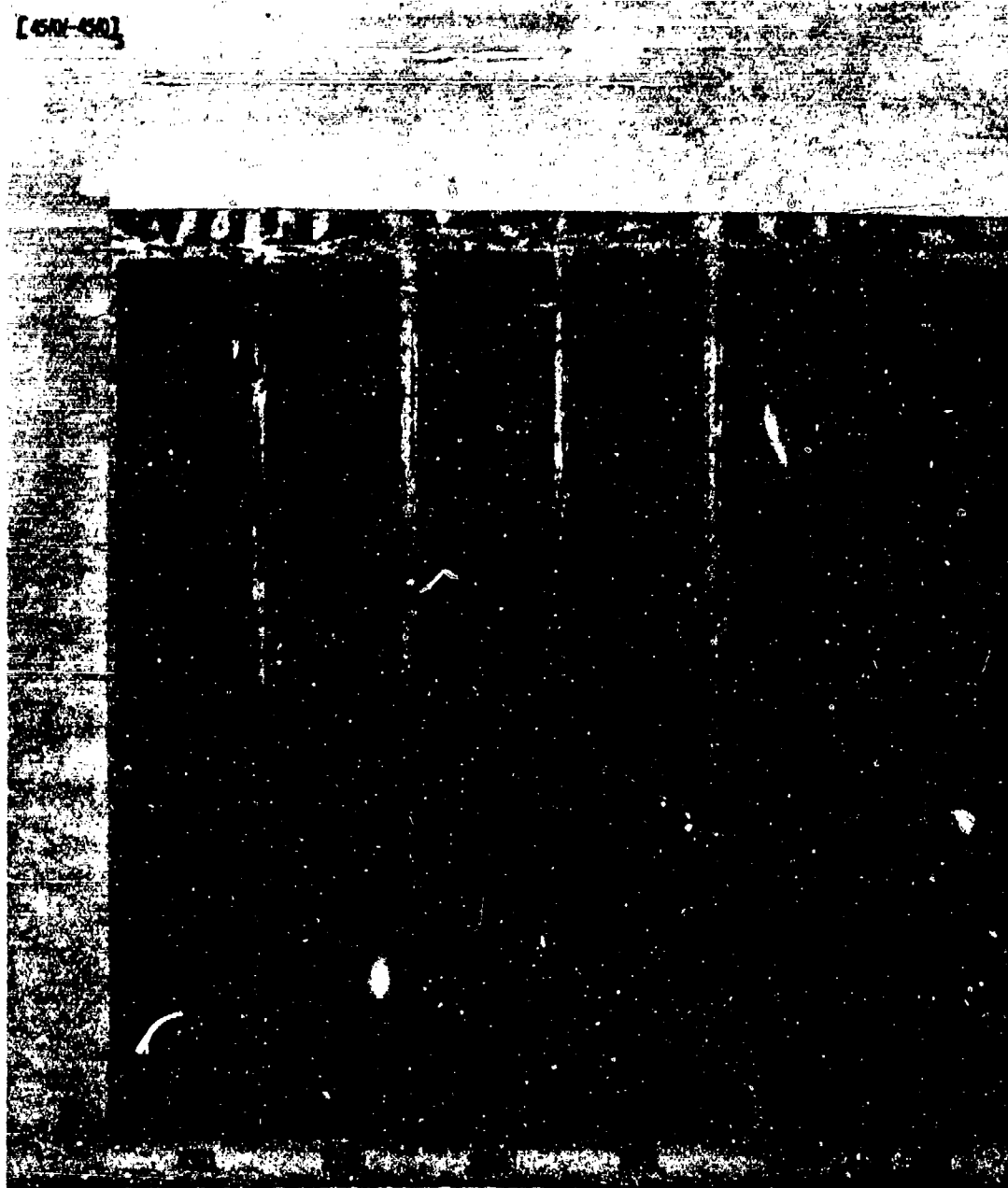
Figure 35. Typical "C" Scans of Unnotched $[45/0/-45/0]_s$
AS/3501 Specimens after Fabrication
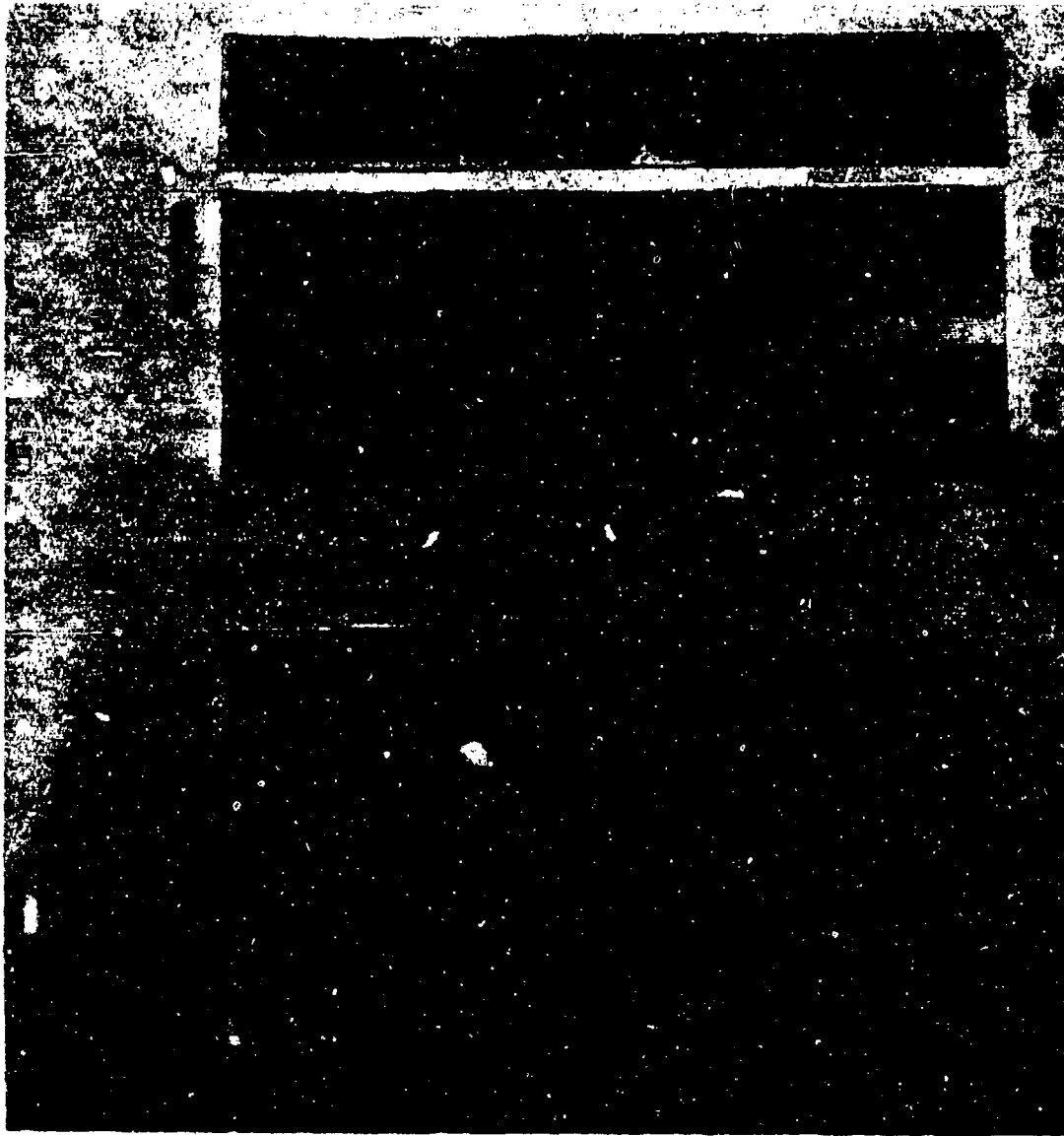
Figure 36. "C" Scans of $[\pm 45]_s$ AS/3501 Specimens Before and After Fatigue Loading ($S = 0.45$, $N = 10^4$ Cycles)
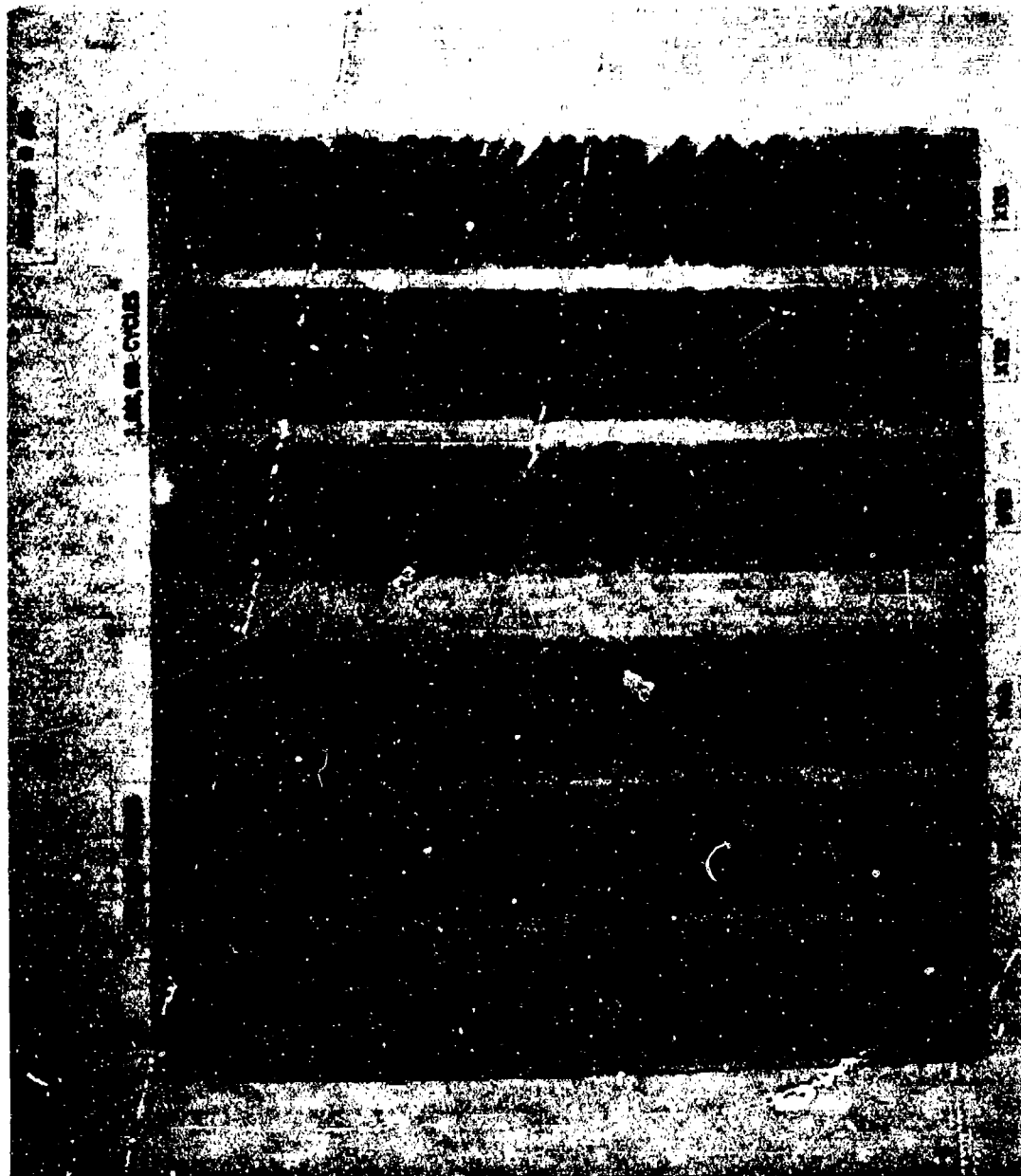
Figure 37. Accumulation of Edge Damage after 5×10^5 and 10^6 Cycles in $[45/0/-45/0]_s$ AS/3501 Specimens Fatigued at 30 Hertz with $S = 0.67$ and $R = 0.1$
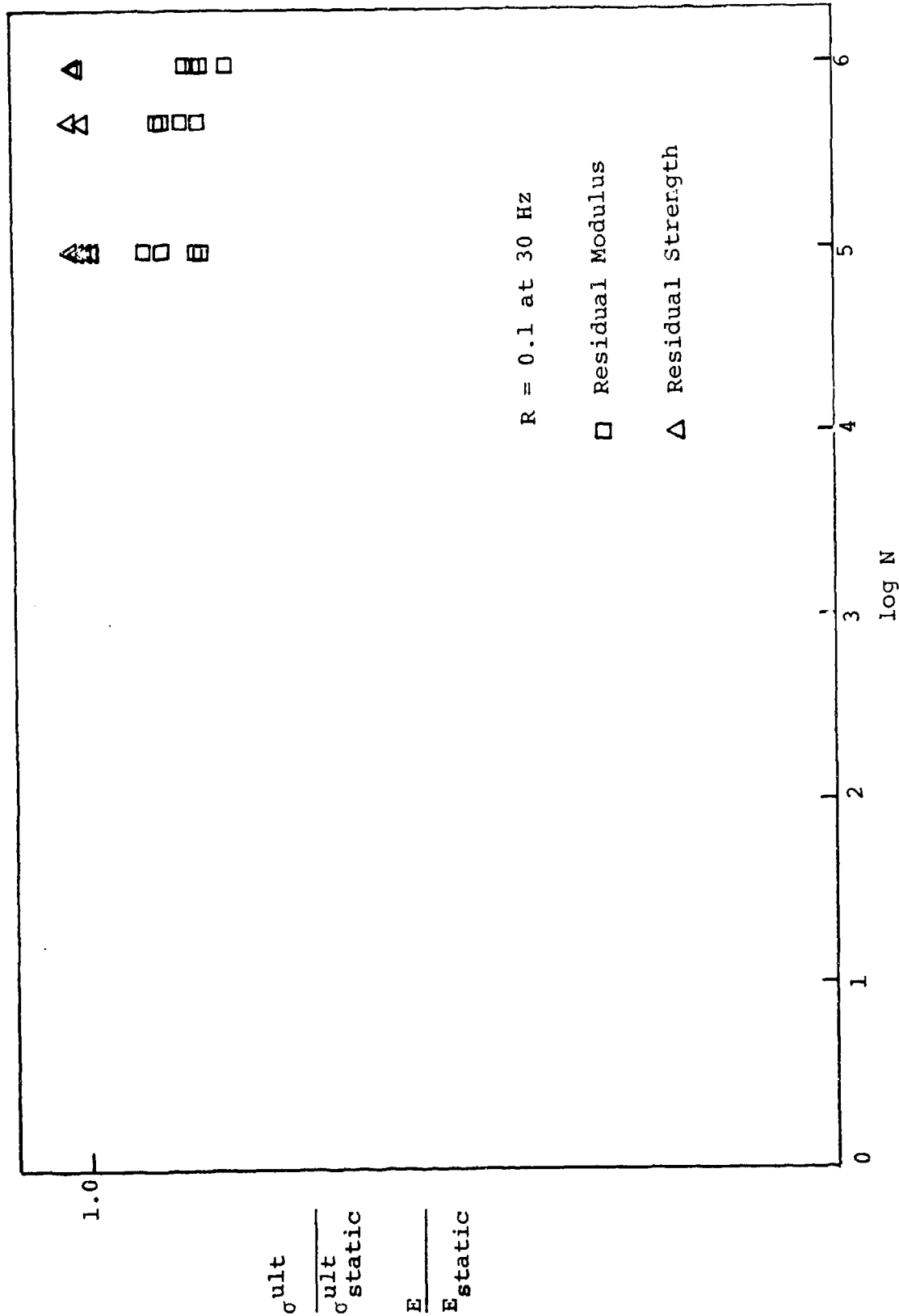
Figure 38. Variation of Residual Strength/Moduli of Unnotched $[45/0/-45/0]_s$ AS/3501 Laminates with N
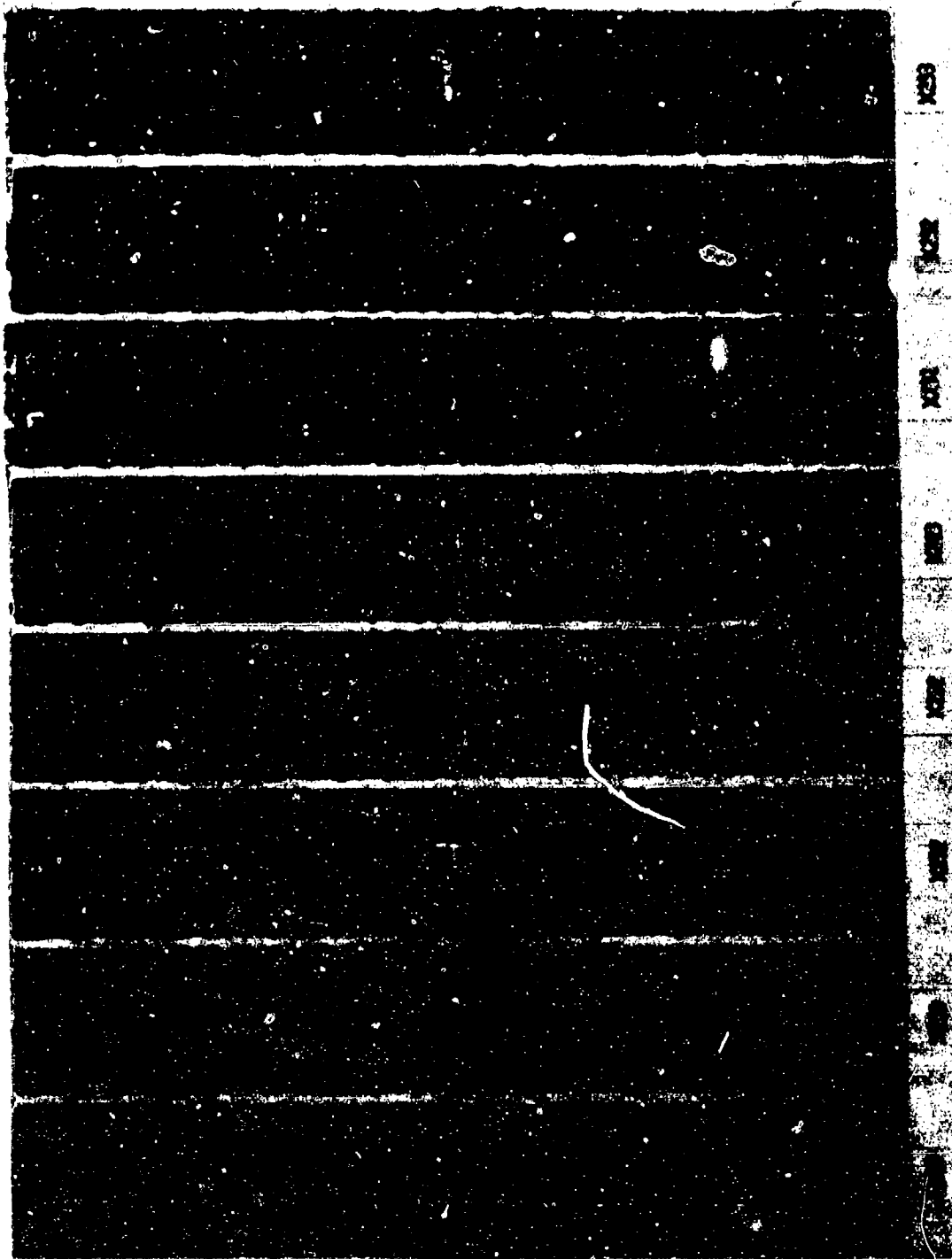
Figure 39. Ultrasonic "C" Scans of Pristine, Notched $[45/0/-45/0]_s$ AS/3501 Specimens
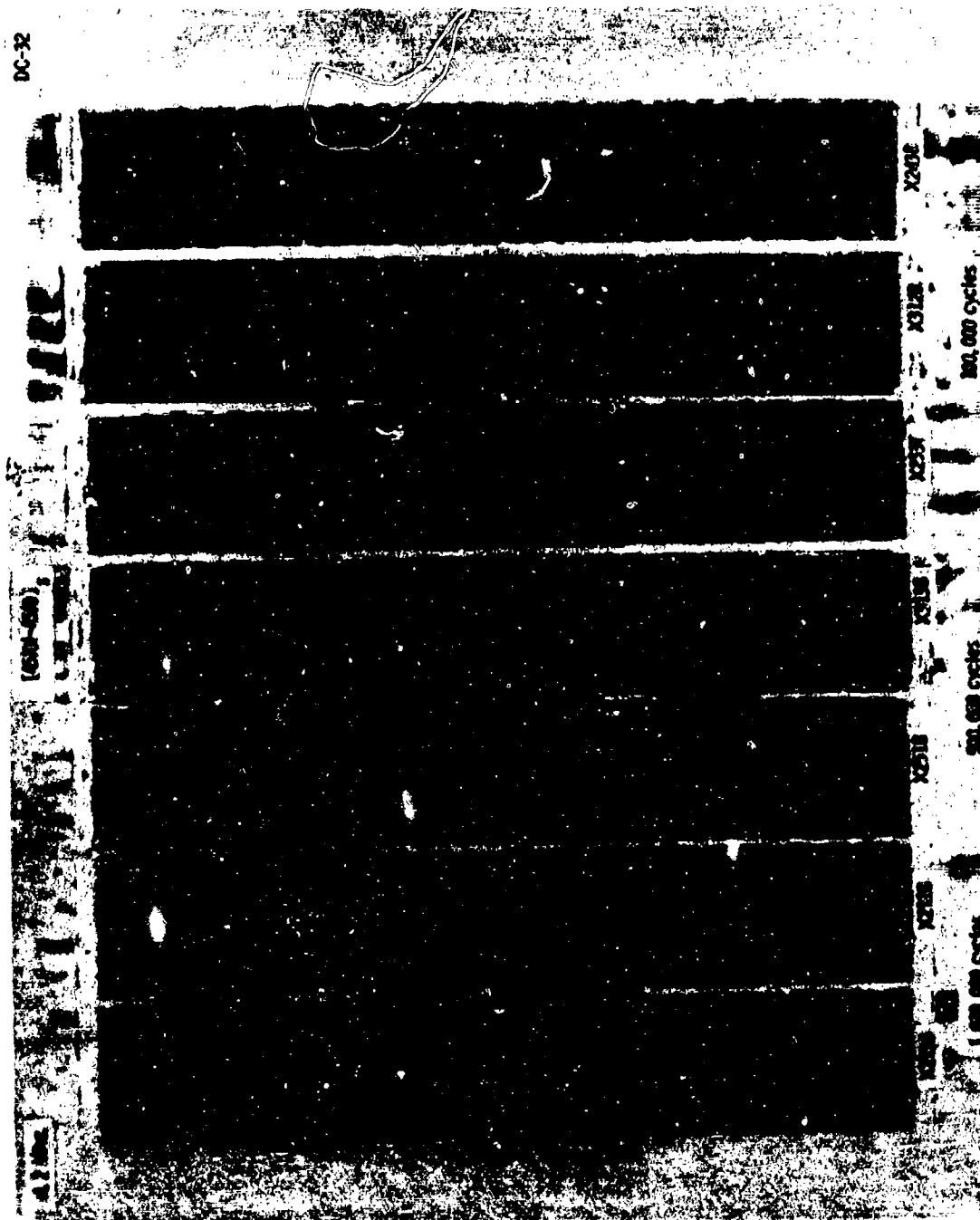
Figure 40. "C" Scans of Fatigued, Notched [45/0/-45/0]s AS/3501 Specimens at a Gate Frequency of 4.2 MHz

Figure 41. "C" Scans of Fatigued, Notched $[45/0/-45/0]_s$ AS/3501 Specimens at a Gate Frequency of 7.2 MHz

Figure 42. A Magnified View of the Fatigued, Notched $[45/0/-45/0]_s$ Specimen (X212B) after 10^6 Cycles
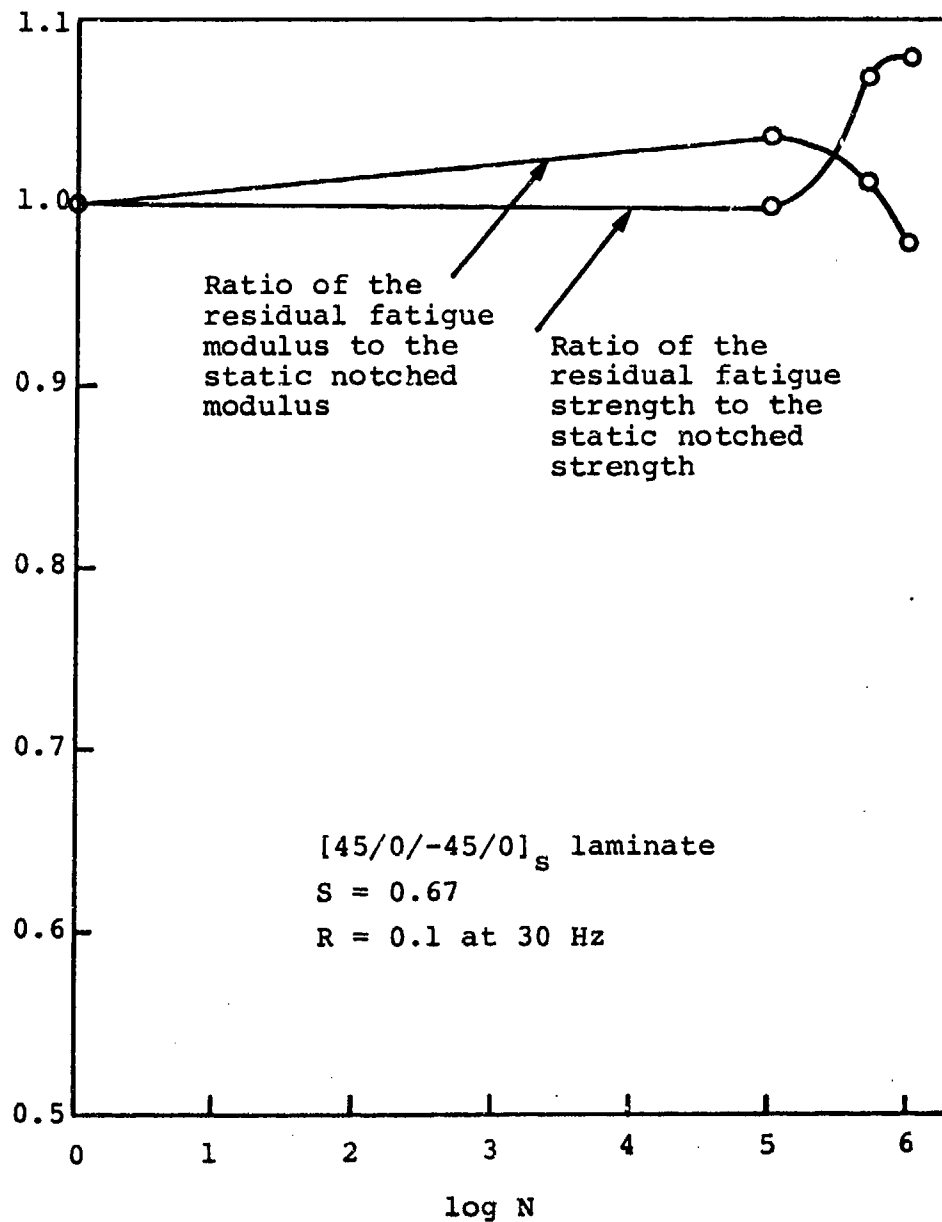
Figure 43. Residual Strength and Residual Modulus in a Notched [45/0/-45/0]$_s$ AS/3501 Laminate when S = 0.67
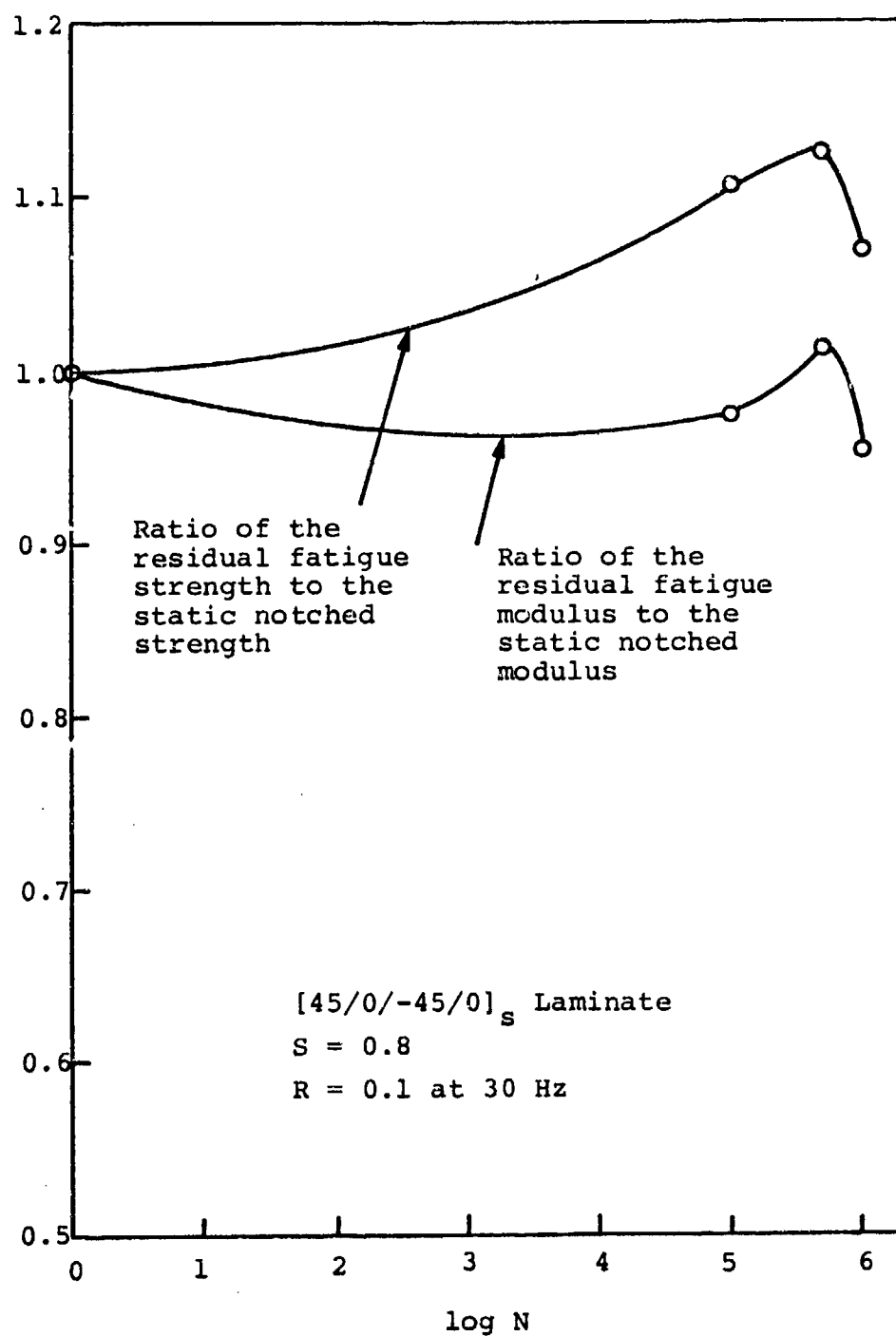
Figure 44. Residual Strength and Residual Modulus in a
            Notched [45/0/-45/0]$_s$ AS/3501 Laminate when
            S = 0.8
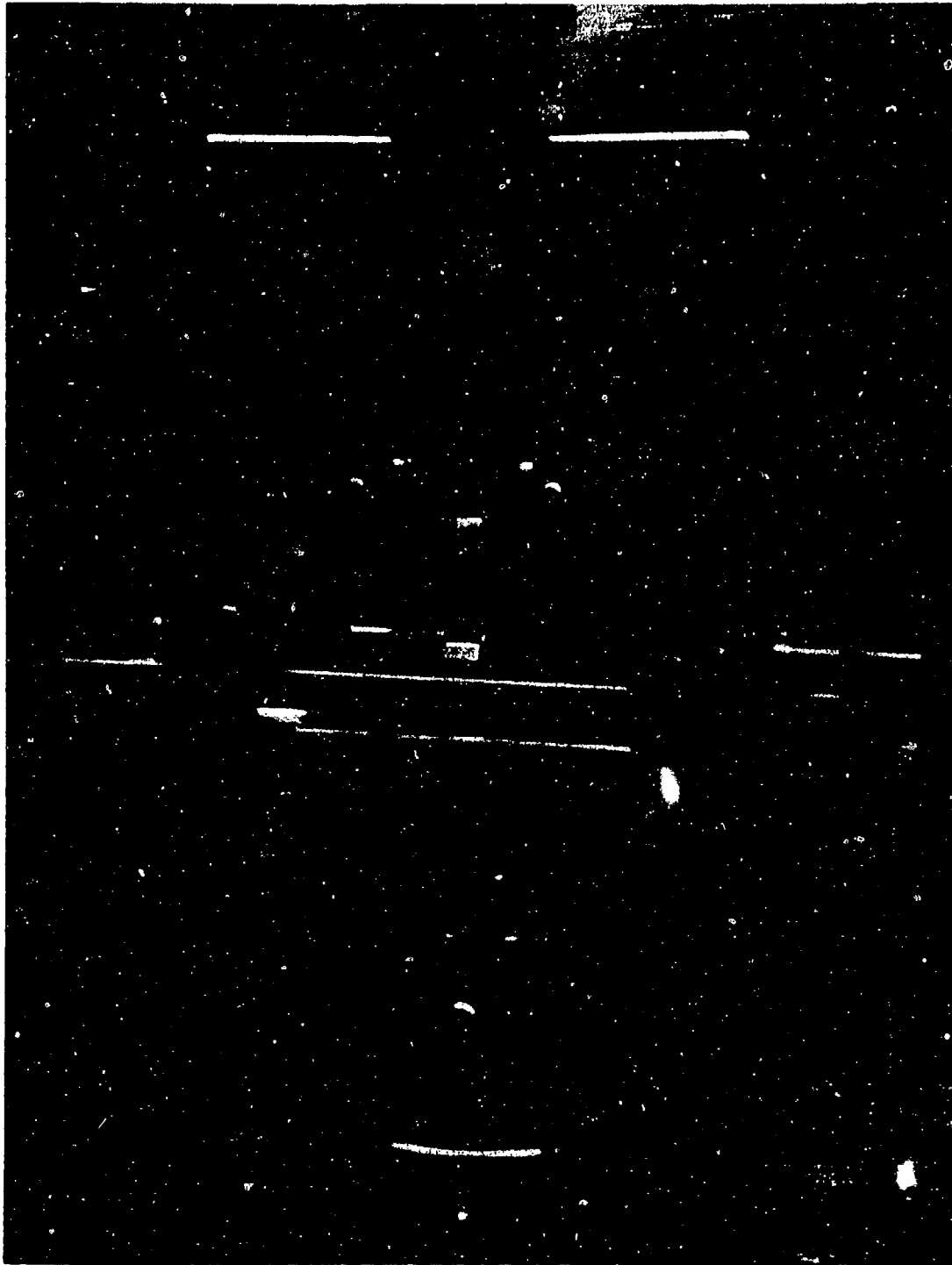
Figure 45.   Flexural Fatigue Apparatus

Figure 46. The Complete Setup for Flexural Fatigue Tests
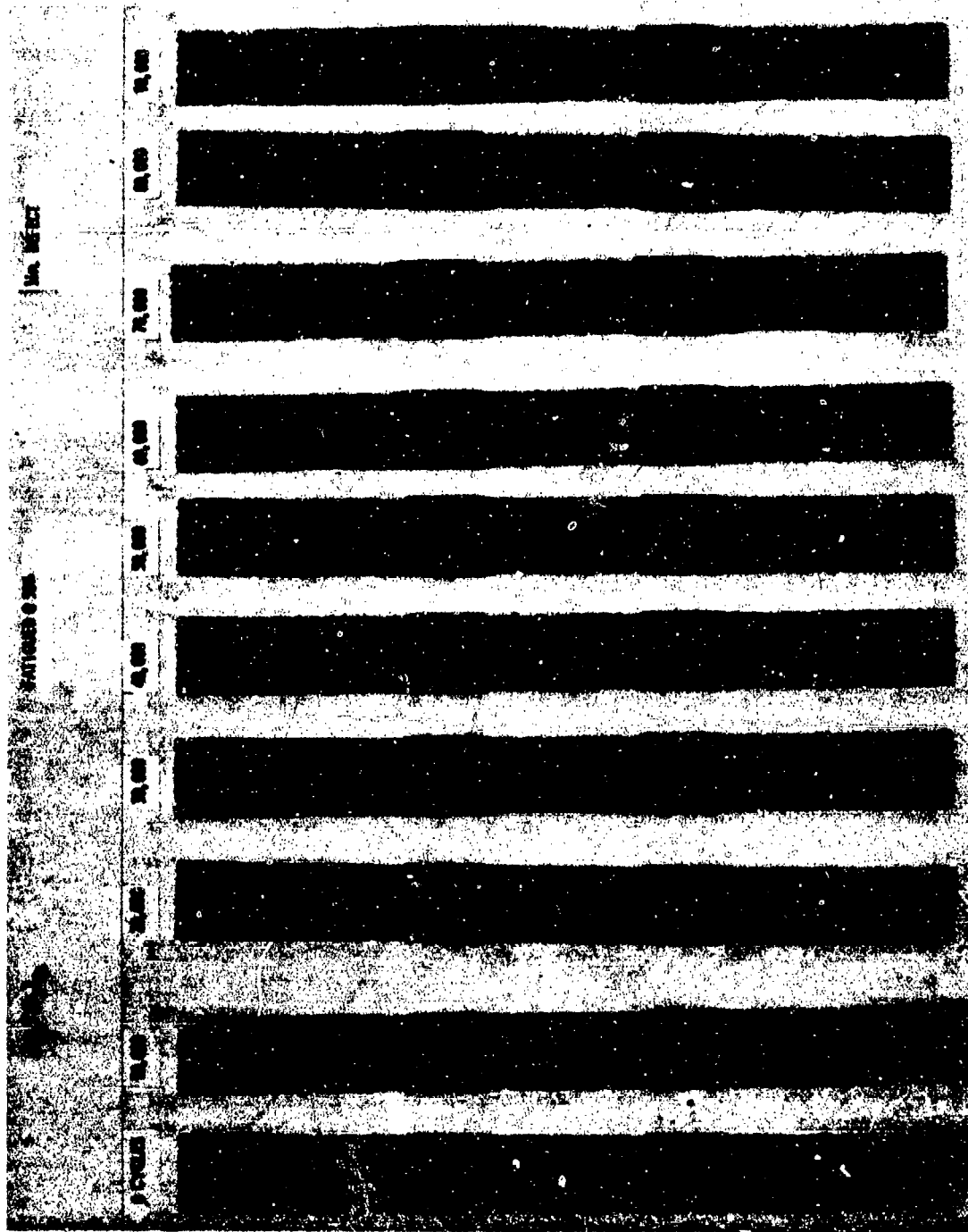
Figure 47. "C" Scans of $[0_4/\pm45_2]_{2s}$ AS/3501 Specimens, with Implanted 2.54 cm Debonds, after Various Cycles of Flexural Fatigue Loading at S = 0.5
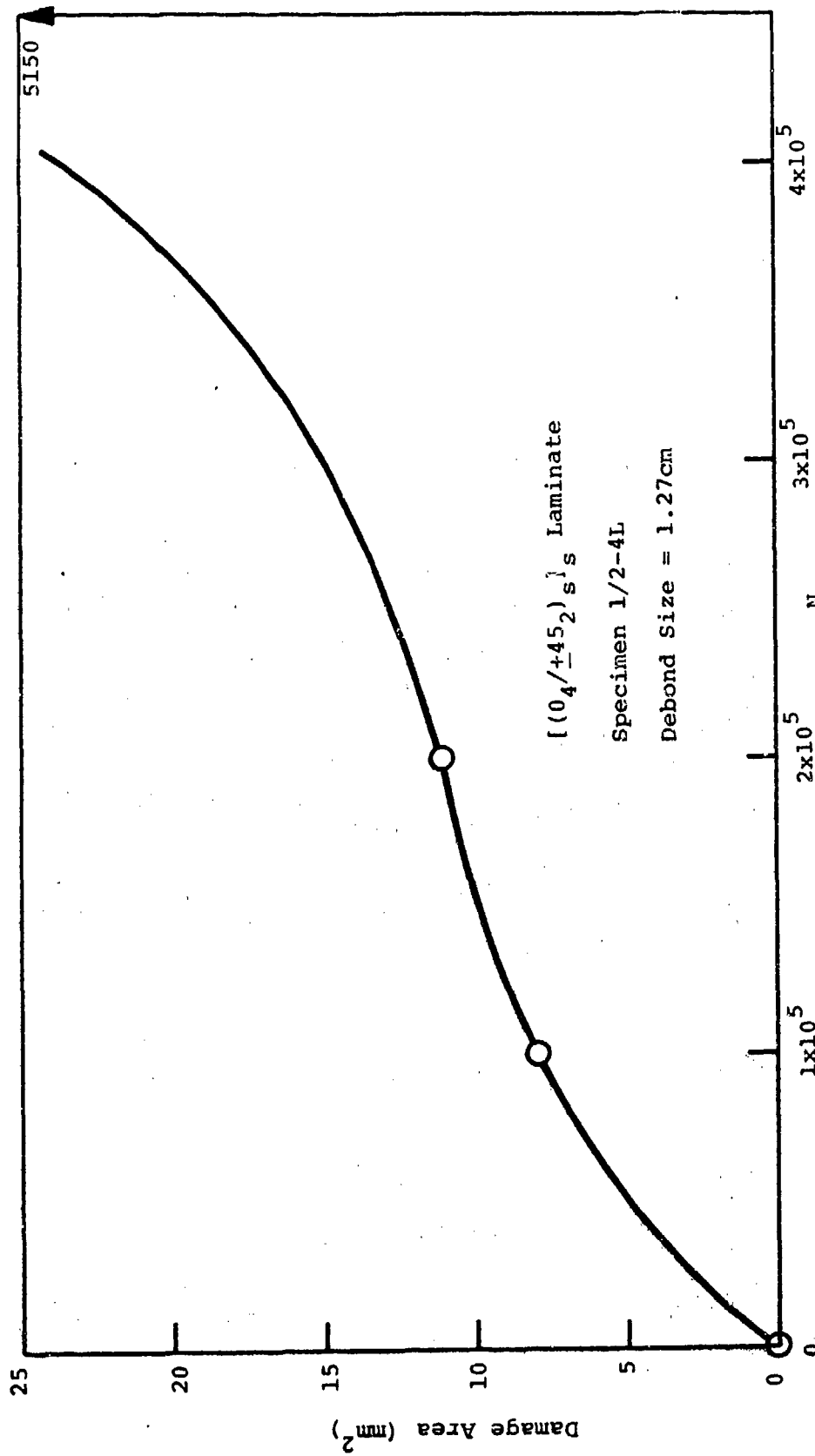
Figure 48. Growth of Damage Area at the Failure Site with N for a $[(0_4/\pm45_2)_s]_s$ Laminate with a 1.27cm Debond
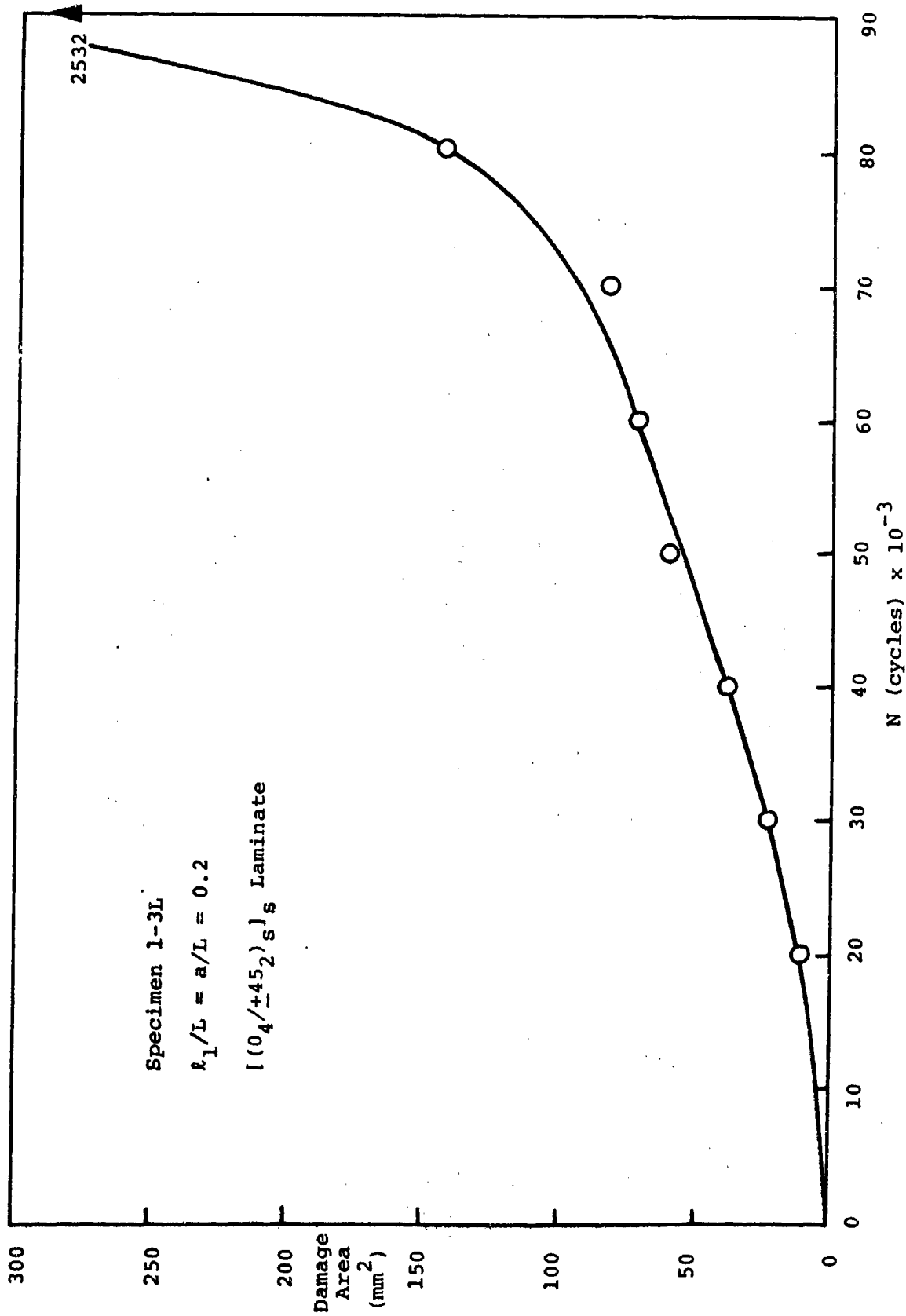
Figure 49. Growth of Damage Area at the Failure Site with N for a $[(0_4/\pm45_2)_s]_s$ Laminate with a 2.54cm Debond

Figure 50. The Vibration Apparatus with a $[0_4/\pm45_2]_{2s}$ AS/3501 Specimen at Its Third Mode

Figure 51. The Fourth Mode Shape of a $[0_4/\pm45_2]_{2s}$ AS/3501 Specimen
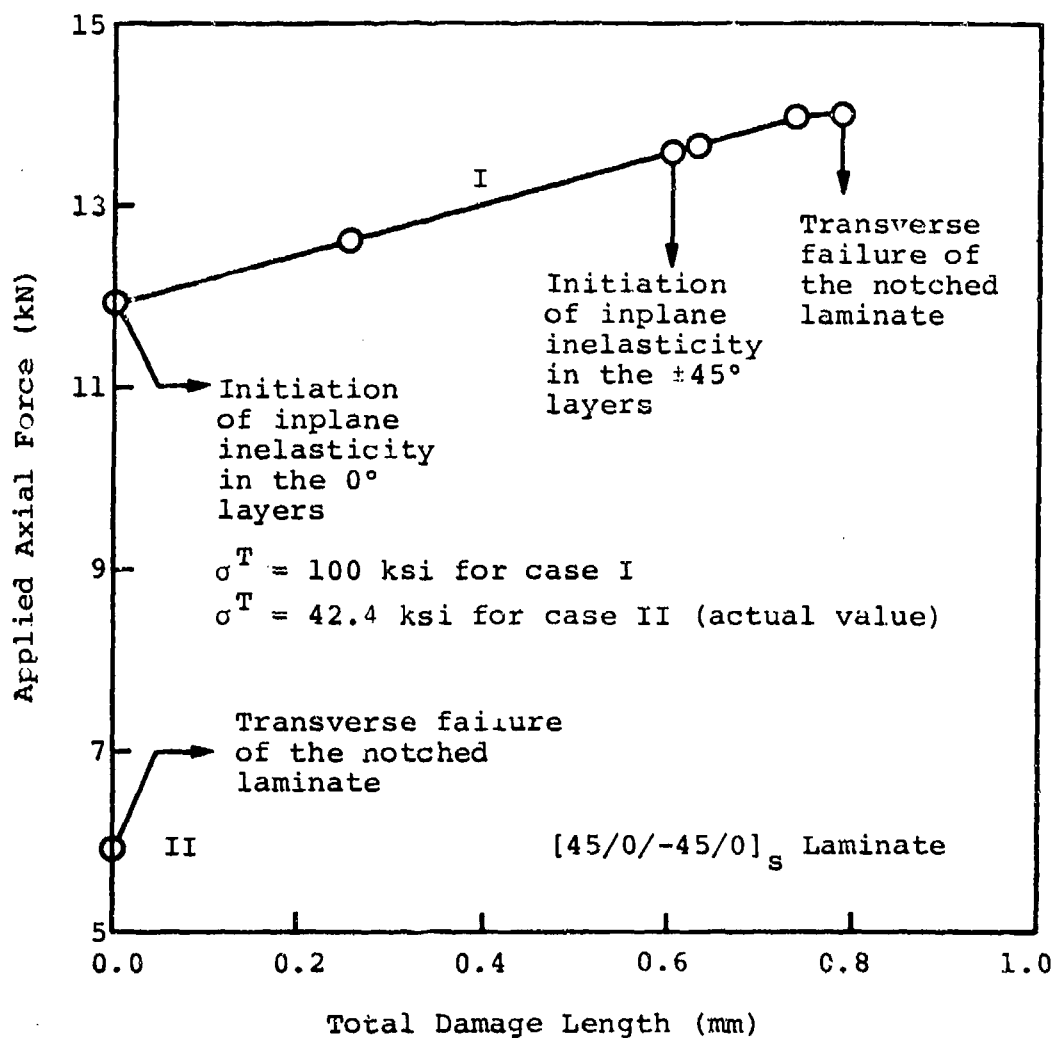
Figure 52. A Static Failure Analysis of the Notched
[45/0/-45/0]ₛ Laminate for Two Values of the
Transverse Failure Stress, σ^T
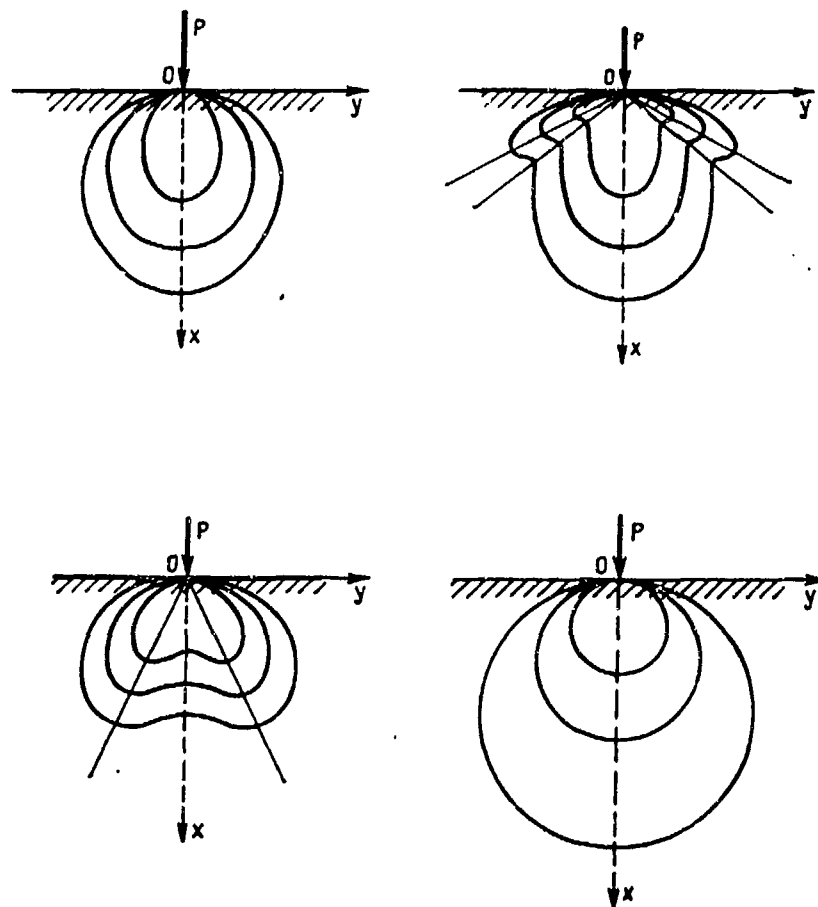
Figure 53. Lines of Constant Stresses for Different
Elastic, Orthotropic Half Planes (Reproduced
from "Anisotropic Plates" by S. G. Lekhnitskii)

APPENDIX A
CRITICALITY OF INTERLAMINAR DELAMINATIONS
IN LAMINATED BEAMS

A simplified analysis is presented here to estimate the criticality of an interlaminar delamination in a laminated beam. The debond may be a birth defect that occurs during the fabrication process or a service defect that is a result of cyclic loading, impact, etc. Considering a typical practical application to be an aircraft wing, the structural element is modeled as a cantilevered laminated beam. The delamination, through the width, is assumed to exist at any axial location along the length of the beam, and between any two laminae through the thickness (fig. 2). The flawed beam is then analyzed as four different beams that are joined together, with appropriate boundary and matching conditions imposed to realize the true response of the debonded beam.

The two Euler equations for a beam, using Timoshenko beam theory to include shear deformation effects, are (ref.19):

$$\frac{\partial}{\partial x} \left(EI \frac{\partial \psi}{\partial x} \right) + k \left(\frac{\partial y}{\partial x} - \psi \right) - I_\rho \frac{\partial^2 \psi}{\partial t^2} = 0 \tag{A1}$$

and

$$\frac{m \partial^2 y}{\partial t^2} - \frac{\partial}{\partial x} \left[k \left(\frac{\partial y}{\partial x} - \psi \right) \right] - p = 0 \tag{A2}$$

The deflected beam geometry, its coordinates, the loading, and transverse shear force conventions are shown in figure 12. ψ is the slope of the deflection curve neglecting shear deformation and β is the angle of shear at the neutral axis. The total slope is

$$\frac{\partial y}{\partial x} = \psi + \beta \tag{A3}$$

E is the Young's modulus of the beam material, and I is the cross-sectional moment of inertia. m is the mass per unit length of the beam and I_ρ is the mass moment of inertia

about the neutral axis per unit length of the beam. $p(x,t)$ is the instantaneous lateral load intensity per unit length at time t, and

$$k = k' \, A \, G \qquad\qquad (A4)$$

where A is the cross-sectional area of the beam, G is the shear modulus of elasticity, and k' is a numerical constant depending on the geometry of the cross section. For a rectangular cross-section, $k' = 2/3$. For a uniform beam, $m = \rho A$ and

$$I_\rho = \rho A R^2, \qquad\qquad (A5)$$

where ρ is the mass density of the beam material and R is the radius of gyration of the cross section about an axis perpendicular to the plane of motion and through the neutral axis.

The static analysis considers a tip-loaded uniform cantilever beam (fig. 2). The Euler equations, for this case, reduce to:

$$EI \, \frac{d^2\psi}{dx^2} + k \, \left(\frac{dy}{dx} - \psi\right) = 0 \qquad\qquad (A6)$$

$$\frac{d}{dx} \, [k \, (\frac{dy}{dx}) - \psi)] = 0 \qquad\qquad (A7)$$

The bending moment, M, and the transverse shear force, Q, at any section of the beam, are given by:

$$M = EI \, \frac{d\psi}{dx}, \qquad\qquad (A8)$$

and

$$Q = -k \, (\frac{dy}{dx} - \psi) \qquad\qquad (A9)$$

The deflections, slopes and material properties of the four different beams are identified by the use of proper subscripts. The axial coordinate x_i for the ith beam has its origin at the left end of that beam (fig. 2). Equations (A6) and (A7) may be combined to give a third order, ordinary

ordinary differential equation for $y_i(x)$. This results in twelve constants of integration when all the four beam elements are considered. In addition, the transverse shear force division between the elements above and below the crack of length a (fig. 2) leads to an extra unknown to be solved for. If the applied tip load is P and the beam element above the crack (i=3) carries a transverse shear force of $\hat{P}$, the element below the crack (i=4) carries a shear force of $(P-\hat{P})$.

The thirteen boundary and matching conditions used in obtaining the deflection solution at any axial location of the debonded beam are:

$$y_1(x_1=0)=0, \text{ or, } y_1=0 \text{ at } x_1=0 \tag{A10}$$

$$\psi_1(x_1=0) = 0 \tag{A11}$$

$$M_2(x_2=\ell_2) = 0 \tag{A12}$$

$$M_1(x_1=\ell_1) = -P(\ell_2+a) \tag{A13}$$

$$\psi_3(x_3=0) = \psi_1(x_1=\ell_1) \tag{A14}$$

$$\psi_3(x_3=0) = \psi_4(x_4=0) \tag{A15}$$

$$y_3(x_3=0) = y_1(x_1=\ell_1) \tag{A16}$$

$$y_3(x_3=0) = y_4(x_4=0) \tag{A17}$$

$$y_2(x_2=0) = y_3(x_3=a) \tag{A18}$$

$$y_2(x_2=0) = y_4(x_4=a) \tag{A19}$$

$$\psi_2(x_2=0) = \psi_3(x_3=a) \tag{A20}$$

$$\psi_2(x_2=0) = \psi_4(x_4=a) \tag{A21}$$

$$M_1(x_1=\ell_1) = M_3(x_3=0) + M_4(x_4=0) + M_{axial} \tag{A22}$$

M_{axial} is the bending moment due to the couple created by the horizontal or axial force reactions H_3 and H_4 in beam elements 3 and 4, respectively. The axial forces are a result

A-3

of an elongation of element 3 and a corresponding contraction
of element 4 in order to ensure compatibility of displacements
and slopes. The axial elongation in element 3, u_3, is given by:

$$u_3 = -\Delta\psi \frac{d_4}{2} + u_o \tag{A23}$$

where

$$\Delta\psi = \psi_2(x_2=0) - \psi_1(x_1=\ell_1) \tag{A24}$$

$$d_4/2 = d/2 - d_3/2 \tag{A25}$$

and u_o is the axial rigid body displacement in elements 3 and 4.
$d = d_1 = d_2$ is the total thickness of the debonded beam, and d_3
and d_4 are the thicknesses of elements 3 and 4, respectively.
It follows that the axial contraction, u_4, in element 4 is:

$$u_4 = u_0 + \Delta\psi \frac{d_3}{2}. \tag{A26}$$

Since

$$u_3 = \frac{H_3 a}{A_3 E_3} \quad \text{and} \quad u_4 = \frac{H_4 a}{A_4 E_4} , \tag{A27}$$

the axial force equilibrium equation at the crack tip locations,

$$H_3 + H_4 = 0, \tag{A28}$$

yields a solution for the rigid body displacement:

$$u_o = \frac{\Delta\psi}{2(A_3 E_3 + A_4 E_4)} \; (A_3 E_3 d_4 - A_4 E_4 d_3) \tag{A29}$$

if b is the width of the beam, $A_3 = bd_3$ and $A_4 = bd_4$. This simpli-
fies equation (A29) to:

$$u_o = \frac{d_3 d_4 (E_3 - E_4)}{2(d_3 E_3 + d_4 E_4)} \; \Delta\psi \tag{A30}$$

An interesting inference from the above equation is that
a rigid body translation takes place only when E_3 is not equal
to E_4. If the beam material is isotropic or if the delamination

in a midplane-symmetric, laminated, anisotropic beam is in the midplane, there will be no rigid body axial displacements. When the debond occurs between two layers such that E_3 and E_4 have different magnitudes, a rigid body translation in elements 3 and 4 is essential for displacement and slope compatibility.

With the above expressions for the axial forces in elements 3 and 4, half the total beam thickness apart, M_{axial} may be written as:

$$M_{axial} = - H_3 d/2 = -A_3 E_3 u_3 d/2a \tag{A31}$$

Using the boundary and matching conditions, (A10) through (A22), in the general solutions to the beam equations (A6) and (A7) for all the four elements, the deflection function for the tip-loaded delaminated beam is obtained. Computing the tip deflection from this solution, Clapeyron's theorem is used to obtain the total strain energy, U, in the beam:

$$U = - \frac{1}{2} P \, y_2(x_2 = \ell_2). \tag{A32}$$

or,

$$2U/P^2 = - \frac{y_2(x_2 = \ell_2)}{P} \tag{A33}$$

Carrying out the aforementioned substitutions, one obtains:

$$\frac{2U}{P^2} = \frac{\ell_2^3}{3(EI)_2} - \frac{C_2}{P} \, \ell_2 - \frac{C_3}{P} + \frac{\ell_2}{k_2} \tag{A34}$$

where

$$\frac{C_2}{P} = \frac{C_8}{P} - \frac{a(\ell_2 + 0.5a)}{\phi_2} \tag{A35}$$

$$\frac{C_3}{P} = [\frac{a^3}{6(EI)_3} - \frac{a}{k_3}] \, \frac{\gamma}{P} + \frac{C_7}{P} \, \frac{a^2}{2} + \frac{C_8}{P} \, a + \frac{C_9}{P} \tag{A36}$$

$$\frac{C_7}{P} = -\frac{a}{2(EI)_3}\frac{\tilde{P}}{P} - \frac{(\ell_2 + 0.5a)}{\phi_2} \tag{A37}$$

$$\frac{C_8}{P} = \frac{\ell_1(\ell_1 - 2L)}{2(EI)_1} \tag{A38}$$

$$\frac{C_9}{P} = \frac{\ell_1^2(\ell_1 - 3L)}{6(EI)_1} - \frac{\ell_1}{k_1} \tag{A39}$$

$$\frac{\tilde{P}}{P} = \frac{a_1}{a_1 + a_2} \tag{A40}$$

$$a_1 = \frac{a^2}{12(EI)_4} + \frac{1}{k_4} \tag{A41}$$

$$a_2 = \frac{a^2}{12(EI)_3} + \frac{1}{k_3} \tag{A42}$$

$$\phi_2 = \phi_1 + (EI)_3 + (EI)_4 \tag{A43}$$

$$\phi_1 = \frac{A_3 E_3 E_4 d_4 d^2}{4(d_3 E_3 + d_4 E_4)} = \frac{a M_{axial}}{\Delta \psi} \tag{A44}$$

Griffith's energy balance criterion is used to determine the criticality of the delamination. Let γ_a be the specific adhesive surface fracture energy that is required to create unit surface area through the propagation of the delamination. The energy balance criterion states that the loss in the total strain energy due to an incremental change in the crack length is equal to the surface fracture energy that is necessary to create the corresponding surface area. Expressed mathematically, the Griffith energy balance criterion is:

$$\frac{\partial U}{\partial a} = 2b\gamma_a \tag{A45}$$

Substituting equation (A34) into equation (A45):

$$\frac{2(\partial U/da)}{P_{cr}^2} = \frac{4b\gamma_a}{P_{cr}^2} = \frac{\ell_2^2}{(EI)_2} \frac{d\ell_2}{da} - \frac{C_2}{P} \frac{d\ell_2}{da} - \ell_2 \frac{d(C_2/P)}{da} -$$

$$\frac{d(C_3/P)}{da} + \frac{1}{k_2} \frac{d\ell_2}{da} = \phi_3 \qquad (A46)$$

or,

$$P_{cr}/\sqrt{\gamma_a} = 2\sqrt{b/\phi_3} \qquad (A47)$$

P_{cr} is the magnitude of the critical load at which propagation of delamination is imminent. The derivatives that appear in the expression for ϕ_3, equation (A46), are:

$$\frac{d(C_2/P)}{da} = \frac{a}{(EI)_3} \frac{\overset{\circ}{P}}{P} + \frac{a^2}{2(EI)_3} \frac{d(\overset{\circ}{P}/P)}{da} + \frac{C_7}{P} + a\frac{d(C_7/P)}{da} +$$

$$\frac{d(C_8/P)}{da} \qquad (A48)$$

$$\frac{d(C_3/P)}{da} = -\frac{1}{k_3} \frac{\overset{\circ}{P}}{P} - \frac{a}{k_3} \frac{d(\overset{\circ}{P}/P)}{da} + \frac{a^2}{2(EI)_3} \frac{\overset{\circ}{P}}{P} + \frac{a^3}{6(EI)_3}$$

$$\frac{d(\overset{\circ}{P}/P)}{da} + a\frac{C_7}{P} + \frac{a^2}{2} \frac{d(C_7/P)}{da} + \frac{C_8}{P} + a\frac{d(C_8/P)}{da} + \frac{d(C_9/P)}{da} \qquad (A49)$$

$$\frac{d(C_7/P)}{da} \approx -\frac{[d\ell_2/da+0.5]}{\phi_2} - \frac{1}{2(EI)_3}[\overset{\gamma}{P}/P + a\frac{d(\overset{\gamma}{P}/P)}{da}] \qquad (A50)$$

$$\frac{d(C_8/P)}{da} = -\frac{(L-\ell_1)}{(EI)_1}\frac{d\ell_1}{da} \qquad (A51)$$

$$\frac{d(C_9/P)}{da} = -\frac{(L-0.5\ell_1)}{(EI)_1}\ell_1\frac{d\ell_1}{da} - \frac{1}{k_1}\frac{d\ell_1}{da} \qquad (A52)$$

$$\frac{d(\overset{\gamma}{P}/P)}{da} = \frac{a}{6(EI)_4(a_1+a_2)}[1-\frac{\overset{\gamma}{P}}{P}\{1+\frac{(EI)_4}{(EI)_3}\}] \qquad (A53)$$

It is seen from equation (A47) that the critical value of the tip load is a function of the location and length of delamination, the material and geometric properties of the beam, and the specific adhesive surface fracture energy for the given adherend-adhesive combination. The propagation of the delamination, along the interface, may take place in any of the following ways depending on the material and geometric data:

(i) propagation of the delamination into element 1; in this case, $d\ell_1 = -da$ and $d\ell_2 = 0$;

(ii) propagation of the delamination into element 2; in this case, $d\ell_2 = -da$ and $d\ell_1 = 0$;

(iii) propagation of the delamination into elements 1 and 2 simultaneously; in this case, $d\ell_1 = d\ell_2 = -\frac{da}{2}$.

The critical load for each case is obtained by substituting the appropriate values of $d\ell_1/da$ and $d\ell_2/da$ into equation (A47). The direction in which the delamination propagates is governed by the least of the three P_{cr} values.

The variation of $P_{cr}/\overline{\gamma_a}$ with the crack length a is plotted for different sets of beam data. One experimental data point on this curve would suffice to evaluate $\hat{\gamma}_a$.

APPENDIX B
VIBRATION ANALYSIS OF LAYERED BEAMS
WITH DELAMINATIONS

The vibration analysis of a laminated beam is carried out by eliminating ψ from equations (A1) and (A2) to obtain the well-known Timoshenko equation for lateral vibration of prismatic beams (ref. 19):

$$EI \frac{\partial^4 y}{\partial x^4} + m \frac{\partial^2 y}{\partial t^2} - (I_\rho + \frac{EIm}{k}) \frac{\partial^4 y}{\partial x^2 \partial t^2} + I_\rho \frac{m}{k} \frac{\partial^4 y}{\partial t^4} = p +$$

$$\frac{I_\rho}{k} \frac{\partial^2 p}{\partial t^2} - \frac{EI}{k} \frac{\partial^2 p}{\partial x^2} \tag{B1}$$

Setting p=0 in the above equation, the Timoshenko equation for lateral, free vibration is obtained:

$$EI \frac{\partial^4 y}{\partial x^4} + m \frac{\partial^2 y}{\partial t^2} - (I_\rho + \frac{EIm}{k}) \frac{\partial^4 y}{\partial x^2 \partial t^2} + I_\rho \frac{m}{k} \frac{\partial^4 y}{\partial t^4} = 0 \tag{B2}$$

Assuming

$$y(x,t) = y(x) \, e^{i\omega t} \tag{B3}$$

equation (B2) is rewritten as:

$$EI \frac{d^4 y}{dx^4} - m\omega^2 y + \omega^2 (I_\rho + \frac{EIm}{k}) \frac{d^2 y}{dx^2} + I_\rho \frac{m}{k} \omega^4 y = 0 \tag{B4}$$

or,

$$\frac{d^4 y}{dx^4} + \omega^2 (\frac{1}{C_o^2} + \frac{1}{C_q^2}) \frac{d^2 y}{dx^2} + (\frac{\omega^4}{C_o^2 C_q^2} - \frac{\omega^2}{C_o^2 R^2}) y = 0 \tag{B5}$$

where

$$C_o^2 = E/\rho, \quad C_q^2 = k'G/\rho \quad \text{and} \quad R^2 = I/A \tag{B6}$$

A general form of the solution to equation (B5) is:

$$y(x) = B \sin \alpha x + C \cos \alpha x + D \sinh \beta x + E \cosh \beta x \tag{B7}$$

where B,C,D and E are constants. If

$$\gamma = \omega^2 \left(\frac{1}{C_o^2} + \frac{1}{C_q^2}\right) \tag{B8}$$

and

$$\delta = \frac{\omega^4}{C_o^2 C_q^2} - \frac{\omega^2}{C_o^2 R^2} \tag{B9}$$

α and β are the solutions to the following quartic equations:

$$\alpha^4 - \gamma \alpha^2 + \delta = 0 \tag{B10}$$

$$\beta^4 + \gamma \beta^2 + \delta = 0 \tag{B11}$$

The four constants in equation (B7) are evaluated through the application of the proper boundary conditions. As discussed in Appendix A, the delaminated beam is treated analytically as four beam elements joined together with the appropriate boundary and matching conditions (fig. 2). Subscripts (i=1,4) on the various quantities identify the elements they correspond to. Sixteen conditions are specified to evaluate the free vibration frequencies that yield nontrivial solutions for the constants B_i, C_i, D_i and E_i:

$$y_1(x_1=0) = 0 \tag{B12}$$

$$\psi_1(x_1=0) = 0 \tag{B13}$$

$$Q_2(x_2=\ell_2) = 0 \tag{B14}$$

$$M_2(x_2=\ell_2) = 0 \tag{B15}$$

$$y_1(x_1=\ell_1) = y_3(x_3=0) \tag{B16}$$

$$y_1(x_1=\ell_1) = y_4(x_4=0) \tag{B17}$$

$$\psi_1(x_1=\ell_1) = \psi_3(x_3=0) \tag{B18}$$

$$\psi_1(x_1=\ell_1) = \psi_4(x_4=0) \tag{B19}$$

$$y_3(x_3=a) = y_2(x_2=0) \tag{B20}$$

$$y_4(x_4=a) = y_2(x_2=0) \tag{B21}$$

$$\psi_3(x_3=a) = \psi_2(x_2=0) \tag{B22}$$

$$\psi_4(x_4=a) = \psi_2(x_2=0) \tag{B23}$$

$$Q_1(x_1=\ell_1) = Q_3(x_3=0) + Q_4(x_4=0) \tag{B24}$$

$$M_1(x_1=\ell_1) = M_3(x_3=0) + M_4(x_4=0) + M_{axial} \tag{B25}$$

$$Q_2(x_2=0) = Q_3(x_3=a) + Q_4(x_4=a) \tag{B26}$$

$$M_2(x_2=0) = M_3(x_3=a) + M_4(x_4=a) + M_{axial} \tag{B27}$$

In imposing boundary conditions that involve the bending slopes, the general form of the bending slope solution (ref.20) is used:

$$\psi(x) = \frac{(k'G/E)p^2 + \beta^2}{\beta} [D \cosh \beta x + E \sinh \beta x] +$$
$$\frac{(k'G/E)p^2 - \alpha^2}{\alpha} [-B \cos \alpha x + C \sin \alpha x] \tag{B28}$$

where

$$p^2 = \omega^2/C_o^2 \tag{B29}$$

Equations (B12) to (B27) and the solutions (B7) and (B28) yield sixteen homogeneous equations for the four sets of constants B_i, C_i, D_i and E_i (i-1,4). These equations, when written in matrix form, yield non-trivial solutions for the constants when the determinant of the matrix vanishes.

The free vibration frequencies are obtained numerically by computing the determinant of the 16x16 matrix for different values of frequencies and finding the frequencies corresponding to a null determinant by interpolation. These frequencies may be normalized with respect to the fundamental frequency of

vibration of the same beam without delamination. This will give a measure of the drop in frequency due to the presence and growth of delaminations in layered beams.

D I S T R I B U T I O N   L I S T

Commander
Naval Air Systems Command (AIR-954)   2 COPIES
Department of the Navy
Washington, DC 20361

Commander
Naval Air Systems Command (AIR-320)   1 COPY
Department of the Navy
Washington, DC 20361

Commander
Naval Air Systems Command (AIR-4114C)   1 COPY
Department of the Navy
Washington, DC 20361

Commander
Naval Air Systems Command (AIR-5203)   1 COPY
Department of the Navy
Washington, DC 20361

Commander
Naval Air Systems Command (AIR-52031B)   1 COPY
Department of the Navy
Washington, DC 20361

Commander
Naval Air Systems Command (AIR-52032)   1 COPY
Department of the Navy
Washington, DC 20361

Commander
Naval Air Systems Command (AIR-52032D)   1 COPY
Department of the Navy
Washington, DC 20361

Dr. Robert Crane (AFML/LLP)   1 COPY
Wright-Patterson Air Force Base
Air Force Materials Laboratory
Dayton, OH 45433

Mr. N. Tideswell (Code 2823)   1 COPY
David W. Taylor Naval Ship R&D Center
Annapolis, MD 21402

Mr. S. Friedman (Code 2823)   1 COPY
David W. Taylor Naval Ship R&D Center
Annapolis, MD 21402

DISTRIBUTION LIST

Mr. D. Polansky   1 COPY
Naval Surface Weapons Center
White Oak
Silver Spring, MD 20910

Mr. J. R. Gleim   1 COPY
Naval Ship Engineering Center
Washington, DC 20362

Mr. J. F. Goff   1 COPY
Naval Surface Weapons Center
White Oak
Silver Spring, MD 20910

Mr. J. R. Lowney   1 COPY
Naval Surface Weapons Center
White Oak
Silver Spring, MD 20910

Mr. G. V. Blessing   1 COPY
Naval Surface Weapons Center
White Oak
Silver Spring, MD 20910

Dr. M. I. Jacobson
Lockheed Missles & Space Company, Inc.   1 COPY
Sunnyvale, CA 94088

Mr. S. D. Hart(Code 8435)   1 COPY
Naval Research Laboratory
Washington, DC 20375

Mr. I. Wolock (Code 8433)   1 COPY
Naval Research Laboratory
Washington, DC 20375

Mr. C. Anderson   1 COPY
Naval Surface Weapons Center
Dahlgren, VA 22448

Mr. D. Nesterok (Code 92713)   1 COPY
Naval Air Engineering Center
Lakehurst, NJ 08723

DISTRIBUTION LIST

Mr. R. Deitrich (Code 92713) Naval Air Engineering Center Lakehurst, NJ 08723	1 COPY
Mr. J. M. Warren Naval Surface Weapons Center White Oak Silver Spring, MD 20910	1 COPY
Dr. W. J. Renton Manager - Advanced Composites Vought Corporation Post Office Box 6144 Dallas, TX 75222	1 COPY
Dr. C. Sanday (Code 6370) Naval Research Laboratory Washington, DC 20375	1 COPY
Dr. R. Weimer (Code 6370) Naval Research Laboratory Washington, DC 20375	1 COPY
Administrator Defense Documentation Center for Scientific and Technical Information (DDC) Bldg. #5, Cameron Station Alexandria, VA 22314	12 COPIES